

Numerical Simulation Schemes for Inhomogeneous Convection-Diffusion Systems Modeling Fluidized Beds

Dissertation

zur Erlangung des akademischen Grades

**doctor rerum naturalium
(Dr. rer. nat.)**

von **Yaser Alkurdi, B. Sc.**

geb. am 25.10.1981 in Damaskus, Syrien

genehmigt durch die Fakultät für Mathematik
der Otto-von-Guericke-Universität Magdeburg

Gutachter:

Prof. Dr. rer. nat. habil. Gerald Warnecke
Jun.-Prof. Dr. Andreas Bück

Eingereicht am: 16.11.2016

Verteidigung am: 24.05.2017

Acknowledgements

Firstly, I would like to express my thankfulness and my deep gratitude to my supervisor **Prof. Dr. Gerald Warnecke**, without his support and his guidance it was impossible to complete this work. I really appreciate his help and his friendly discussions. I will be forever thankful for his kindness.

I am also very grateful to **Jun.-Prof. Dr. Andreas Bück** who really helped me so much and gave me the idea of this work and supervised the work from the beginning to the end with a very lovely patience.

I wish to thank **Prof. Dr. Lothar Mörl** for his unlimited help and his very useful lectures which explained many things related to my work.

I also like to thank the staff in the faculty for mathematics and the Institute for Analysis and Numerics, as well as the staff in the Institute for Process engineering.

I would like also to thank my supervisor in Syria **Dr. Muntajab Alhasan** for his support.

A special thank is for my wife **Inaam Alshami** for her unconditional love and support. Last but not least, my deep gratitude to my family for their unlimited encouragement and love throughout my life.

Abstract

In a typical fluidized bed, liquid to be granulated is atomized into small droplets by an atomizer located at the top of the chamber. These droplets adhere and spread on the surface of the solid particles which are suspended in the air and form a film on their surface. This liquid film starts to evaporate leaving a hard crust on the particles surface. A model that describes the temperature and humidity inside a fluidized bed was introduced by Heinrich [32].

During the flight of the droplets before they adhere on the surface of the particles, the droplets can be carried away by the gas flow, or they turn into the solid state after the volatile liquid evaporates. These two cases disable the process. Here we consider the third case where these droplets hit the particle surfaces. In this work we take into consideration that these droplets loose some of their mass before hitting the surface of the particles.

The aim of this thesis is to reformulate and extend this model to make it more general and closer to the reality. The model introduced by Heinrich [32] is modified, two new equations related to the temperature of the air and humidity in the empty space between the nozzle and the particles were added and finally the model equation for the nozzle spray is also reformulated to be convenient to the new model. This is achieved for the 1D and 2D cases.

The next step is to find an efficient numerical solution for the new model. Our model consists of coupled partial differential equations (PDE's), in essence, hyperbolic and parabolic equations. To solve this model, discontinuous Galerkin method (DG) was adapted for the spatial discretization, where the domain is discretized into smaller cells, then we look for an approximate solution in every cell. In order to determine the approximate solution we look for the weak formulation. This can be achieved by multiplying the partial differential equation by a test function belongs to the finite dimensional space and then we integrate over every cell. After some manipulations we get a system of ordinary differential equations.

The resulting ordinary differential equations (ODE's) are solved employing numerical differentiation formulas (NDF).

The numerical results agree with the theoretical consideration for the one and two dimensional cases.

Moreover, another study has been conducted to describe another process related to the spray drying. In this process, we study the change of the temperature and the concentration of the droplets, in addition to the population balance model for drying of droplets containing aggregating nanoparticles.

Zusammenfassung

In einer typischen Wirbelschicht wird die zu granulierende Flüssigkeit mithilfe eines auf der Kammer fixierten Zerstäubers in Tröpfchen verdüst. Diese kleinen Tröpfchen haften und verteilen sich auf die Oberfläche der soliden Partikel, die sich in der Luft befinden, und bilden eine dünne Schicht auf der Oberfläche. Die Schicht fängt an zu verdampfen und lässt eine harte Schicht auf der Partikeloberfläche. Heinrich [32] stellte ein Modell vor, welches die Temperatur und Feuchtigkeit in einer Wirbelschicht darstellt. Bevor die Tröpfchen während ihres Fluges die Partikel erreichen, können sie durch den Gasströmungsweg abgetragen werden. Außerdem werden sie evtl. nach Ausdünstung der verdampfbaren Flüssigkeit zum Festkörper. Diese zwei Fälle verhindern den Prozess. Wir berücksichtigen hier den dritten Fall, bei dem die Tröpfchen die Partikeloberfläche erreichen. In dieser Arbeit berücksichtigen wir auch einen möglichen Massenverlust der Tröpfchen, bevor sie auf der Oberfläche landen. Das Ziel dieser Dissertation ist es, dieses Modell neu zu formulieren und so zu erweitern, dass es allgemeiner wird und die Realität besser annähert.

Das von Heinrich [32] vorgestellte Modell wird in dieser Arbeit modifiziert. Im Wesentlichen werden zwei Gleichungen hinzugefügt, die die Temperatur und Feuchtigkeit im Leerraum zwischen der Sprühdüse und den Partikeln beschreiben. Anschließend wird eine Modellgleichung des Sprays zur Anpassung an das neue Modell, sowohl für den ein- als auch zweidimensionalen Fall, dargelegt. Im zweiten Schritt soll eine effiziente numerische Lösung für das neue Modell beschrieben werden.

Unser Modell setzt sich aus gekoppelten partiellen Differentialgleichungen (PDE's), nämlich hyperbolischen und parabolischen Differentialgleichungen, zusammen. Für die Lösung dieses Modells wurde die unstetige Galerkin-Methode zur räumlichen Diskretisierung eingesetzt. Dabei wird das Gebiet in kleinen Zellen zerlegt und für jede Zelle eine approximierete Lösung gesucht. Dafür wird schwache Formulierung eingesetzt. Die partielle Differentialgleichung wird mit einer dem finiten dimensional Raum zugehörigen Testfunktion multipliziert. Danach wird über jeder Zelle integriert. Nach einigen Manipulationen bekommen wir ein System von gewöhnlichen Differentialgleichungen. Die daraus entstehenden gewöhnlichen Differentialgleichungen (ODE's) wurden anschließend durch Formeln der numerischen Differentiation (NDF) gelöst. Die numerischen Ergebnisse stimmen mit der theoretischen Betrachtung der ein- und zweidimensionalen Fälle überein. In einer zweiten Studie beschreiben wir darüber hinaus einen mit der Sprühtrocknung zusammenhängenden Prozess. Untersucht werden dabei im Wesentlichen die Veränderung der Temperatur und Konzentration der Tröpfchen. Weiter betrachten wir das Populationsbilanzmodell der Trocknung von Tröpfchen, die aggregierende Nanoteilchen beinhalten.

Contents

1	Introduction	1
2	A New Mathematical Modeling of Heat and Mass Transfer in Fluidized Beds	5
2.1	Fundamental assumptions and variables	5
2.2	Derivation of the balance equations	13
2.2.1	Total balance equations	26
2.3	Boundary conditions	26
2.4	Two dimensional model for the liquid deposition into the fluidized bed . .	29
2.4.1	Liquid deposition on a single particle surface	29
2.4.2	Mass balance of spraying	35
2.5	Invariant regions	35
3	Spray Drying Process	43
3.1	Introduction	43
3.2	Mechanism of the process	44
3.3	Mathematical models of the process	45
3.3.1	Basic variables	46
3.3.2	Change of the water mass fraction	47
3.3.3	Temperature of the droplet	49
3.3.4	Study of a population balance model of nano-suspension droplets .	50
3.4	Numerical results	51
3.5	Velocity distribution and droplet movement within the nozzle spray cone .	55
4	Numerical Scheme and Discretization of Hyperbolic and Parabolic Systems	61
4.1	Introduction	61
4.2	Spatial discretization of a scalar conservation law in one space dimension .	62
4.2.1	The weak formulation	62
4.2.2	Diagonalizing the mass matrix	63
4.2.3	Numerical flux	66
4.2.4	Error estimation	68

CONTENTS

4.3	The local discontinuous Galerkin method for one dimensional second order diffusion problems	68
4.3.1	The weak formulation	69
4.3.2	Error estimation	72
4.4	Discontinuous Galerkin method for two dimensional hyperbolic problems .	73
4.4.1	Spatial discretization and weak formulation	73
4.5	The local discontinuous Galerkin method for two dimensional second order diffusion problems	79
4.5.1	The weak formulation	81
4.6	Numerical solution of ordinary differential equations	89
4.6.1	Runge-Kutta method	89
4.6.2	Adaptive Runge-Kutta methods	90
4.6.3	Backward and Numerical Differentiation Formulas	92
4.6.4	Newton and Simplified Newton's Iteration	94
4.7	Numerical integration	95
4.8	The L^2 error and the experimental order of convergence EOC	98
4.9	Numerical examples	99
4.9.1	1D hyperbolic partial differential equation example	99
4.9.2	1D parabolic partial differential equation example	100
4.9.3	2D hyperbolic partial differential equation example	100
4.9.4	2D parabolic partial differential equation example	101
5	Numerical Results	103
5.1	Numerical results in 1D	103
5.2	Numerical results in 2D	106
6	Summary	126
A	Notations	127
A.0.1	Dimensionless numbers	129
B	Parameters for Heat and Mass Transfer in Fluidized Beds	130
B.0.2	Constants	130
B.0.3	Values of parameters	131
B.0.4	Parameters calculations	133
B.1	Parameters	135
	Bibliography	137
	Curriculum Vitae	145

Chapter 1

Introduction

A fluidized bed is a situation in an apparatus of process engineering in which some solid or liquid particles are suspended against gravity due to a strong upward flow of surrounding gas. This situation is then used for treatment of the particles, e.g. they may be dried, burned or coated.

Due to the wide applications of fluidized beds for industrial purposes, the need to study the mechanics of fluidized beds became more and more important. This comes from the fact that important products of the chemical industries are particles.

The technology of fluidized beds was initiated in 1922 by the German engineer Fritz Winkler [89] who made the first application of fluidization in a reactor for coal gasification. Many different constructions of fluidized beds were then developed for various industrial requirements.

Fluidized beds are also used to produce particles with required properties such as dust free, dry, free flowing, low attrition, etc. One such process is fluidized bed spray granulation. For it several technologies are available such as

- **Aggregation:** Powders are suspended and then agglomerated due to a binder suspension or solution which forms liquid bridges between the powder particles.
- **Blending:** Gas flows through bulk solids causing optimized blending and reducing blending time.
- **Encapsulation:** Solids liquids or gaseous material are packaged in capsules.
- **Drying:** Hot air dries powder particles, where small particles leave the fluid bed and the bigger are transported into the subsequent section.
- **Coating (Layering):** Dense particles are produced, where suspension, solution or emulsion leaves a solid film on the surfaces of the particles.

Fluidized beds are widely used due to the high rate of mass and heat transfer between the gas and the particles. By convention the heat is transferred from the bulk phase to the surface of the particles and then into the particles by conduction, while the humidity is transferred in a form of vapor to the bulk phase by convection [39].

Considerable research was done to predict the particle formation in fluidized beds using

CHAPTER 1. INTRODUCTION

population balance equations. These population balance equations (PBEs) predict the temporal change of particle-property distributions [51], [56], [60].

In our work we shall focus on the coating process, where particles in this process are growing in layers. Agglomeration can take place without a binding agent by molecular forces (e.g. van der Waals forces, ionic and hydrogen bonds), electrostatic or magnetic interparticle forces, as well as by thermal effects and chemical reaction, see [7]. To avoid the agglomerates bounded by molecular forces, a mechanical stress is applied to increase the distance between the particles above a critical threshold. The electrostatic and the magnetic forces are short-range forces affect only the very small particles and they are neglected in our work. The thermal effects which include sintering, partial melting and glass transition are also neglected here because of the nature of this work. To avoid agglomeration due to the binder liquid, some parameters have to be chosen in a right way, e.g. particles below $100\ \mu\text{m}$ in diameter tend to agglomerate because of the binder liquid. Several studies have been done to investigate the phenomena inside the chamber, see e.g. [53] [87], [51], [70], [50], [61], [88], [38]. Various models were studied, see Heinrich et al. [34, 33, 35], Heinrich [32], Reppmann [66], Trojosky [84], Blumschein [4] and Henneberg [36]. Nagaiah [54] used an improved model. This model is mesh independent in order to be more flexible with different meshes. Also he reformulated the model equation for the nozzle spray in two and three dimensions.

This work is motivated to study the pneumatic behavior of the heat and the mass transfer beside some other phenomena which take place inside the chamber of the apparatus. Some possible applications can be found in [1] and [87]. Several researches have been done to study the behavior of the particles, the wetting efficiency, the humidity of air, the temperature of air, the temperature of particles, the temperature of the liquid film, the growth of the particles, the agglomeration, etc.

In the process of the fluidized beds, liquid to be granulated is atomized into small droplet by an atomizer. These droplets adhere on the surface of the particles. The hot gas which flows through the distributor at the bottom of the fluidized beds causes the water to evaporate. Due to this, the initial values of each of the air humidity, the degree of wetting, the temperature of the air, the particles as well as the temperature of the liquid film will change. The previous model introduced by Heinrich [32] gave a system of partial differential equations which find the change of the values of the previous quantities. The solution of this system satisfies the balance equations.

In this work we modify the model which was introduced by Heinrich [32] and Nagaiah [52], where we assume that the droplets sprayed from the nozzle loose some of their mass due to evaporation. Because of that, the apparatus is divided into two regions. The upper region includes just the sprayed droplets, while the lower region includes the solid particles wetted by collision with the droplets. We assume that the partial evaporation of the droplets takes place in the upper region only. In addition to this modification we

introduce a new model related to the upper region. The model equation for the nozzle spray is also reformulated to be convenient with the new model. The results that we got fulfil the balance equations and show the change of the studied quantities in both regions. The difference between the old and the new model can be noticed in the numerical results. Due to the evaporation of the sprayed droplets in region (1), less amount of the liquid will enter region (2). Consequently, less humidity will be observed at the outlet of region (2). The new model is completely explained in Chapter 2.

In Chapter 3 we study another process called *the spray drying process* which has a very wide usage in the drying technology. In this chapter we study the change of the temperature and the concentration of the droplet, as well as the shrinkage of the droplet radius due to the evaporation at the surface of the droplet. The aggregation of the nano-particles inside a single droplet is also studied briefly in this chapter. At the end of Chapter 3, some numerical results are presented. These numerical results are supported by some experiments.

Chapter 4 focuses on the discretization of the partial differential equations in space and time for hyperbolic and parabolic systems in the $1D$ and the $2D$ cases. Due to the high complexity of the nature of the equations which describe the fluidized bed, the exact solution is unknown. For this purpose, some numerical methods can be introduced to find an approximate solution for the partial differential equations. In our work we use a high order numerical method called *discontinuous Galerkin method*. In this method, the domain is discretized into cells, then we integrate the equations over every cell. Finally we get a system of ordinary differential equation related to time. The result system can be solved using a type of implicit numerical methods called *the numerical differentiation formulas* (NDF) which are a modification of backward differentiation formulas (BDF). To see the validity of the used numerical methods we introduce some examples of certain problems related to convection and diffusion equations with the exact solutions.

In Chapter 5 we introduce the numerical results in $1D$ and in $2D$ case of each of the humidity of air, the degree of wetting, the temperature of air, the temperature of particles, as well as the temperature of the liquid film.

Finally, Chapter 6 presents a brief summary and conclusions regarding this work.

At the end, an appendix is given including the relations and the formulas which are needed to find some parameters.

Chapter 2

A New Mathematical Modeling of Heat and Mass Transfer in Fluidized Beds

A typical fluidized bed granulation device is a cylindrical apparatus provided with a nozzle positioned at the top, bottom, or side of the chamber as shown in Figure 2.1. A hot gas passes through a porous plate at the bottom which is penetrable to the gas but not to the particles. This gas flows through the voids among the particles to be granulated. The process starts when the minimal fluidization point is achieved. At this point the fluidization starts and then these particles are suspended in the heated air. The nozzle starts spraying a granulation liquid which contains a volatile liquid like water. This liquid, sprayed as droplets, hits and then is distributed on the surface of the particles. The volatile liquid evaporates due to the hot, unsaturated fluidizing gas, leaving a thin solid film on the particle surface. The process of enlarging the particles by layers is called layering or coating.

Here we consider a batch operation (particle side) where the number of particles in this process stays constant during the process while the size of the particles increases.

2.1 Fundamental assumptions and variables

In order to model these processes we have to consider balance of mass, momentum, and energy. Their derivation is explained below. Some of the assumptions that we make and the formulas have been used in a number of previous publications, such as [33, 4].

Geometric configuration: In our work we divide the chamber into two regions as it is explained in Figure 2.3.

Region (1): This region extends from the height where the particles arrive to the top of

CHAPTER 2. A NEW MATHEMATICAL MODELING OF HEAT AND MASS TRANSFER IN FLUIDIZED BEDS

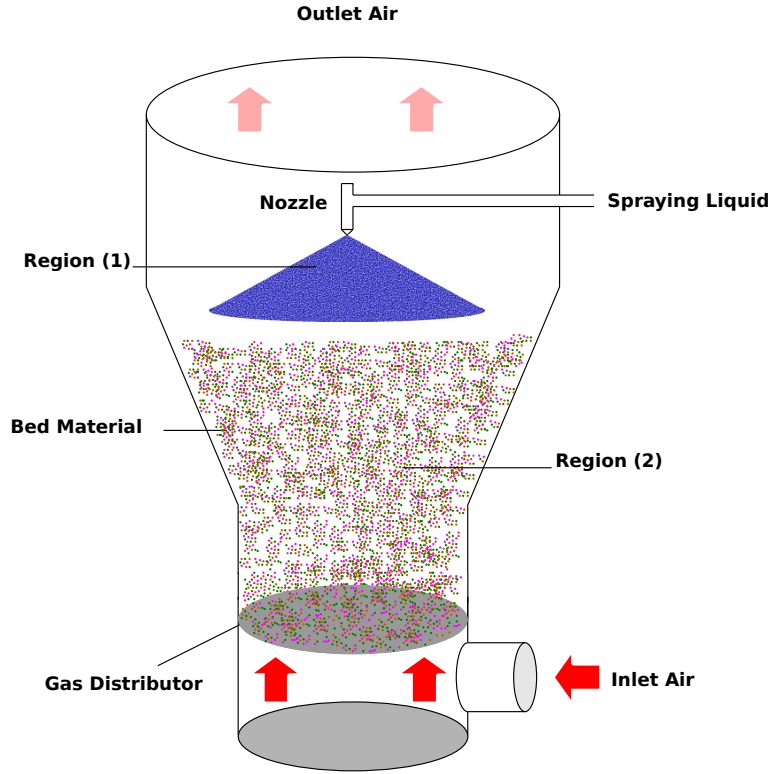


Figure 2.1: Top-spray fluidized bed granulator

the chamber where the nozzle is located.

Region (2): This region extends from the bottom of the chamber to the highest point where the particles arrive.

Now we introduce some fundamental variables and assumptions which are needed for the work, then we shall conclude our new model considering the both regions.

In the following, we denote by d_p the diameter of the particle, ρ_p the density of the particle, ξ_p the drag coefficient, ρ_A density of air, V_A velocity of air, ν_A the kinematic viscosity and g the gravitational acceleration. A freely floating single particle is affected by some forces [51] as shown in Figure 2.2. These forces are known as gravity force F_{gr}

$$F_{gr} = \frac{\pi}{6} d_p^3 \rho_p g,$$

lifting force F_{li}

$$F_{li} = \frac{\pi}{6} d_p^3 \rho_A g,$$

drag force F_{dr}

2.1. FUNDAMENTAL ASSUMPTIONS AND VARIABLES

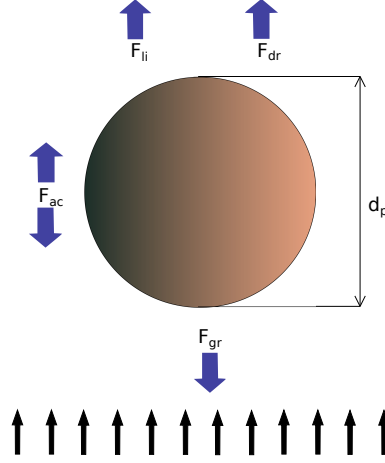


Figure 2.2: Forces affect a freely floating single particle

$$F_{dr} = \frac{1}{2} \xi_p \frac{\pi}{4} d_p^2 \rho_A V_A^2,$$

and accelerating force F_{ac}

$$F_{ac} = \frac{\pi}{6} d_p^3 \rho_p \frac{dV_A}{dt}.$$

At a balance point, the sum of these forces is zero due to Newton's law, i.e.

$$\sum \underline{F} = 0$$

or

$$\underline{F}_{gr} + \underline{F}_{li} + \underline{F}_{dr} + \underline{F}_{ac} = 0.$$

Projecting these force vectors onto the z-axis leads to

$$-\frac{\pi}{6} d_p^3 \rho_p g + \frac{\pi}{6} d_p^3 \rho_A g + \frac{1}{2} \xi_p \frac{\pi}{4} d_p^2 \rho_A V_A^2 = 0.$$

After some cancellations and dividing the both sides by $\rho_A \nu_A^2$ we get the following relation

$$\frac{4}{3} \frac{d_p^3 g (\rho_p - \rho_A)}{\rho_A \nu_A^2} = \xi_p \left(\frac{d_p V_A}{\nu_A} \right)^2.$$

This can be written also as

$$\frac{4}{3} Ar = \xi_p Re^2,$$

where Ar and Re are the Archimedes number and the Reynolds number respectively, see Appendix A.

Specific surface area of a particle: The surface area of the particles plays a very important role to determine the heat transfer and the amount of evaporation of the liquid

CHAPTER 2. A NEW MATHEMATICAL MODELING OF HEAT AND MASS TRANSFER IN FLUIDIZED BEDS

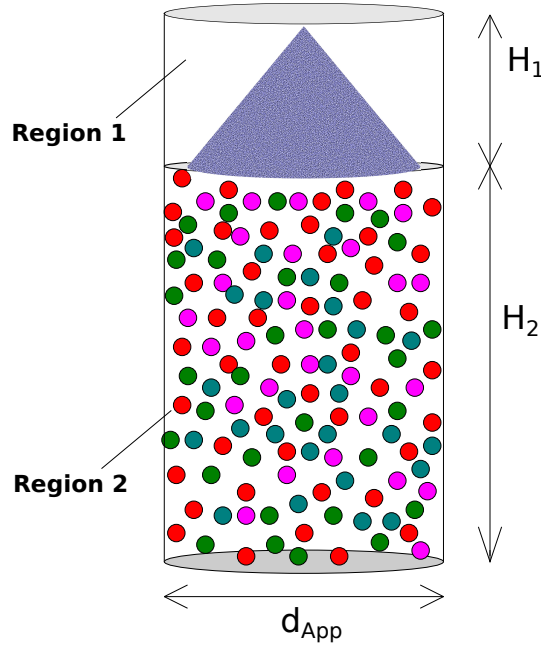


Figure 2.3: The two regions

spread on the surface of these particles. The specific surface area A^* of a particle is given as

$$A^* = \frac{dA}{dV}$$

where dA and dV are the incremental surface area and the incremental volume of the particle respectively.

For monodisperse particles with d_p as a diameter, the previous relation can be written as

$$A^* = \frac{dA}{dV} = \frac{\pi d_p^2}{\frac{1}{6}\pi d_p^3} = \frac{6}{d_p}.$$

Concentration: The concentration κ_i of a component i in a mixed phase of substances is given as the mass m_i of this component per unit volume

$$\kappa_i = \frac{dm_i}{dV}.$$

Porosity: The ratio of the volume of the voids to the total volume is denoted by the porosity ε . It has values between 0 and 1, or is taken as a percentage between 0 and 100%. It can be calculated either from the following formula

$$\varepsilon = \frac{V_{voids}}{V_{total}}$$

or as a function of Archimedes number and Reynolds number [28]

$$\varepsilon = \left(\frac{18Re + 0.36Re^2}{Ar} \right)^{0.21}.$$

2.1. FUNDAMENTAL ASSUMPTIONS AND VARIABLES

In fluidized beds the porosity grows from its minimum value $\varepsilon_{mf} = 0.4$ at the minimal fluidization point and reach its maximum value $\varepsilon = 1$ at the elutriation point.

Wetting efficiency: The Wetting efficiency ϕ or the degree of wetting is given as the ratio of wetted particle surface area A_{wetted} to the total particle surface area $A_{wetted} + A_{unwetted}$

$$\phi = \frac{A_{wetted}}{A_{wetted} + A_{unwetted}} = \frac{A_{wetted}}{\sum A_{p,single}} = \frac{A_{wetted}}{A_p}$$

where $A_{p,single}$ is the surface area of a single particle and A_p is the surface area of all particles.

Supposing that the particles are completely wetted with a film thickness F that has the density ρ_L we get the maximum concentration $\kappa_{L,max}$ to be

$$\kappa_{L,max} = A^*(1 - \varepsilon)F\rho_L.$$

In this case the degree of wetting can be given for $i = L$ as

$$\phi = \frac{\kappa_L}{\kappa_{L,max}}.$$

Density of air: Using the ideal gas law, the density of dry air can be written as a function of gas pressure P_A and gas temperature T as follows

$$\rho_A = \frac{P_A}{\tilde{R}_A T}$$

while the density ρ_V of vapour is

$$\rho_V = \frac{P_V}{\tilde{R}_V T},$$

where $\tilde{R}_A = 287.22 \text{ J}/(\text{kgK})$ is the specific gas constant for dry air, $\tilde{R}_V = 461.5 \text{ J}/(\text{kgK})$ the individual gas constant water vapor and P_V the pressure water vapor.

Partial pressure: In a mixture of ideal gases, the partial pressure of an ideal gas is equal to the pressure of the same gas if it occupies the same volume at the same temperature. We denote by P_i the pressure of the i^{th} component. According to Dalton's law of partial pressures, the total pressure P of the mixture is equal to the sum of the pressures P_i of the components in the mixture, i.e.

$$P = \sum_{i=1}^n P_i,$$

where n is the number of the components in the mixture. In the case of humid air, the total pressure is

$$P = P_A + P_V.$$

Specific gas constant: For dry air, the specific gas constant R_A is given as

$$R_A = \frac{\kappa_B N_A}{M_A},$$

CHAPTER 2. A NEW MATHEMATICAL MODELING OF HEAT AND MASS TRANSFER IN FLUIDIZED BEDS

where κ_B is Boltzmann constant, $M_A = 0.02896 \text{ kg/mol}$ is the molecular mass of air and N_A is Avogadro constant. For water vapor it is given as

$$R_V = \frac{\kappa_B N_A}{M_V},$$

where $M_V = 0.01802 \text{ kg/mol}$ is the molecular mass of vapor.

Humidity of air Y_A :

$$\begin{aligned} Y_A &= \frac{\rho_V}{\rho_A} = \frac{P_V/(\tilde{R}_V T)}{P_A/(\tilde{R}_A T)} = \frac{\tilde{R}_A P_V}{\tilde{R}_V P_A} \\ &= \frac{(\kappa_B/M_V) P_V}{(\kappa_B/M_A) P_A} = \frac{M_V P_V}{M_A P_A} = \frac{M_V}{M_A} \frac{P_V}{P - P_V}. \end{aligned} \quad (2.1)$$

Latent enthalpy of vaporization Δh_{ev} : It describes the enthalpy change that is needed to transform a quantity of a substance from liquid to gas at a specific pressure.

Enthalpy of humid air: The enthalpy of humid air h_{st} per volume element is the sum of the enthalpy of dry air h_A per volume element and the enthalpy of vapor h_V per volume element, i.e.

$$h_{st} = h_A + h_V.$$

The enthalpy of dry air per volume element is given as

$$\begin{aligned} h_A &= \rho_A C_{pA} \theta_A dV \\ &= m_A C_{pA} \theta_A \end{aligned}$$

where C_{pA} is the specific heat capacity of the air, m_A the mass of the air and θ_A the temperature of the air. The enthalpy of vapor per volume element is

$$\begin{aligned} h_V &= \rho_A Y_A (C_{pV} \theta_A + \Delta h_{V,0}) dV \\ &= m_A Y_A (C_{pV} \theta_A + \Delta h_{V,0}) \end{aligned}$$

where C_{pV} is the specific heat capacity of the vapor.

Saturation vapor pressure P_{sat} : The pressure at the point where the number of water molecules which are escaping from the water surface due to evaporation is equal to the number of molecules which are returning to the liquid is called saturation vapor pressure. It is a function of the temperature where increasing the temperature leads to an increase in the saturation vapor pressure. Saturation vapor pressure can be approximated through

2.1. FUNDAMENTAL ASSUMPTIONS AND VARIABLES

the ‘‘Antoine equation’’ as a function of the temperature θ_{sat} , see Schlünder and Tsotsas [71]

$$P_{sat}(\theta_{sat}) = \exp\left(23.462 - \frac{3978.205}{233.349 + \theta_{sat}}\right).$$

Adiabatic saturation humidity Y_{sat} :

$$Y_{sat}(\theta_{sat}) = \frac{M_V}{M_A} \frac{P_{sat}}{P - P_{sat}}. \quad (2.2)$$

The mass transfer coefficient β : This coefficient is used to predict the process of the transport of masses across an interface or a bulk phase. This coefficient can be found using the Sherwood number, see Appendix A.

Mass flow rate of evaporation \dot{m}_{ev} : If a droplet of the sprayed liquid hits a particle before it evaporates and returns into solid, it spreads on the surface of this particle covering the partial area A of the total surface area of this particle. After adhering, the liquid evaporates at the interface A between the liquid and the humid air. The evaporation flow can be written as a function of the vapor pressure and the saturated vapor pressure as follows

$$\dot{m}_{ev} = \beta A \frac{P}{RT} M_V \ln\left(\frac{P - P_V}{P - P_{sat}}\right), \quad (2.3)$$

where R is the ideal gas constant.

From (2.1) we can write

$$P_V = \frac{P Y_A}{(M_V/M_A) + Y_A}.$$

Similarly from (2.2)

$$P_{sat} = \frac{P Y_{sat}}{(M_V/M_A) + Y_{sat}}.$$

Substituting into (2.3) the evaporation flow can be written as

$$\begin{aligned} \dot{m}_{ev} &= \beta A \frac{P M_A}{RT} \frac{M_V}{M_A} \ln\left(\frac{(M_V/M_A) + Y_{sat}}{(M_V/M_A) + Y_A}\right) \\ &= \beta A \rho_A K_s (Y_{sat} - Y_A), \end{aligned}$$

where we set

$$K_s = \frac{(M_V/M_A)}{Y_{sat} - Y_A} \ln\left(\frac{(M_V/M_A) + Y_{sat}}{(M_V/M_A) + Y_A}\right),$$

which is known as Stefan correction. Here we consider the case that the partial pressure of the vapor is too small in comparison with the total pressure of the system, i.e. $P_V \ll P$. In this case, the corrector K_s can be taken to be 1. Now the evaporation flow is determined by the formula

$$\dot{m}_{ev} = \beta \rho_A A (Y_{sat} - Y_A). \quad (2.4)$$

CHAPTER 2. A NEW MATHEMATICAL MODELING OF HEAT AND MASS TRANSFER IN FLUIDIZED BEDS

For droplets, A is the surface area of the droplet given as

$$A = 4\pi d_{dr}^2.$$

Here d_{dr} is the radius of the droplet, and the evaporation mass for a single droplet is

$$\dot{m}_{ev} = 4\beta\rho_A\pi d_{dr}^2(Y_{sat} - Y_A).$$

Enthalpy flow of the evaporated water \dot{q}_{ev} : Here we assume that the heat needed for evaporation is taken from the liquid film, while the heat needed for raising the temperature from θ_L to θ_A comes from the air. The volume-based heat flow of the evaporation \dot{q}_{ev} is given as

$$\dot{q}_{ev} = \beta\rho_AA^*(1 - \epsilon)\phi(Y_{sat} - Y_A)(\Delta h_{V,0} + C_{pV}\theta_A).$$

The heat transfer coefficient α : This coefficient is defined as a proportionality coefficient which is used to find the heat transfer between two surfaces. This coefficient can be calculated using Nusselt number, see Appendix A

Figure 2.4 shows the enthalpy flow of evaporated water \dot{h}_{ev} , the enthalpy flow between the wetted part of the particle and the air \dot{q}_{AL} , between the unwetted part and the air \dot{q}_{AP} , as well as between the film and the particle \dot{q}_{PL} . Heat is transported between interfaces through conduction, convection and radiation.

In the following, we denote by θ_A the temperature of the air, θ_P the temperature of the

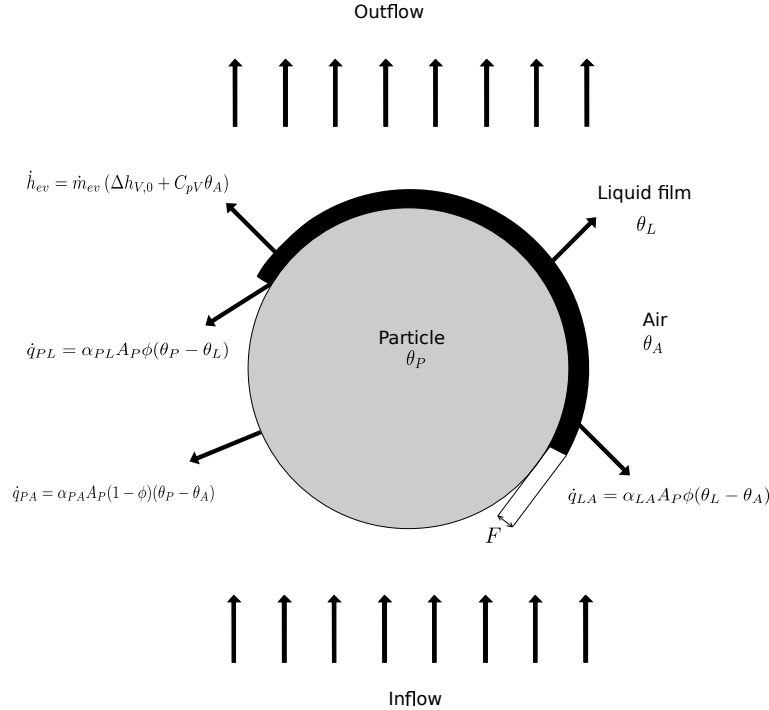


Figure 2.4: Heat and mass transfer on a wetted particle

2.2. DERIVATION OF THE BALANCE EQUATIONS

particles and θ_L the temperature of the liquid.

The volume based heat flow from the particle to the film \dot{q}_{PL} is given as

$$\dot{q}_{PL} = (1 - \epsilon)A^*\phi\alpha_{PL}(\theta_P - \theta_L), \quad (2.5)$$

while for the heat flow from the air to the film \dot{q}_{AL} is

$$\dot{q}_{AL} = (1 - \epsilon)A^*\phi\alpha_{AL}(\theta_A - \theta_L), \quad (2.6)$$

and from the air to the particle \dot{q}_{AP} is modeled as

$$\dot{q}_{AP} = (1 - \epsilon)A^*(1 - \phi)\alpha_{AP}(\theta_A - \theta_P). \quad (2.7)$$

During the flight of the droplets in region (1), three different cases are available.

Elutriation takes place when some droplets are carried away by the gas flow before entering region (2).

Rebound describes the case when droplets turn into the solid state after the volatile liquid is evaporated. In this case these minute particles rebound from the surface of the larger solid particles. These dried fines are elutriated if they are light or they remain in the bed if they are heavy enough.

Adhesion happens when droplets hit and deposit on the surface of the particles. The first two cases disable the process, while the third case is the required case.

2.2 Derivation of the balance equations

To find the model we follow Nagaiah [54] and Heinrich et al. [33]. A general balance equation can be written in the following expression

$$\frac{d}{dt} \int_V u dV = - \int_S s(u) \cdot \vec{n} ds + \int_V v dV. \quad (2.8)$$

This form represents the conservation of some quantities u in a closed region with a volume V and a surface area S over a closed interval $[0, T]$. The function u here is a continuous and differentiable vector valued function defined as $u : \Omega \times [0, T] \rightarrow \mathbb{R}^\ell$. This function contains the variables which are conserved. The function $s : \mathbb{R}^\ell \rightarrow \mathbb{R}^3$ is a vector valued flux, \vec{n} is the outward pointing normal vector on the surface S , and v is the rate of production of u . The vector flux $s(u)$ can be chosen to model different mechanisms such as advection, convection or dispersion.

On the left hand side of equation (2.8) it is possible to move the derivative inside the integral, and by applying the Gauss's theorem to the first term of the right hand side of (2.8) we get

$$\int_V \frac{\partial u}{\partial t} dV = - \int_V \nabla \cdot s(u) dV + \int_V v dV. \quad (2.9)$$

CHAPTER 2. A NEW MATHEMATICAL MODELING OF HEAT AND MASS TRANSFER IN FLUIDIZED BEDS

We will denote the first term on the right hand side as the transport term and the second term the source term, which actually may be a sink term for a negative source.

The following model is given in Cartesian coordinates.

Assumptions for region (1).

- All droplets are spherical.
- All droplets have the same radius d_{dr} , i.e. the droplets are monodisperse.
- The hot air flows as ideal plug through the fluidized bed, i.e. we have a plug flow tube reactor (PFTR) behavior. The flow velocity is constant everywhere.
- The droplet temperature θ_d is uniform throughout each droplet, i.e. $Bi < 0.1$, where Bi is the Biot number which gives an index of the heat transfer resistances inside of and at the surface of the droplet. See Appendix A.
- All droplets hit the particles before they turn into the solid state, i.e. no overspray.

Temperature of the droplet θ_d

The temperature of the droplet increases due to the hot air, consequently the mass and the outer radius of every droplet decreases because of the evaporation flow. The evaporation flow can be calculated from the formula

$$\begin{aligned}\dot{m}_{ev1} &= \beta_1 \rho_{A1} A_{sd} (Y_{sat1} - Y_{A1}) \\ &= 4\beta_1 \rho_{A1} \pi d_{dr}^2 (Y_{sat1} - Y_{A1}).\end{aligned}\tag{2.10}$$

The temperature of a single droplet is given by the following ordinary differential equation

$$\frac{d\theta_d}{dt} = \frac{1}{C_{pL1}m_w + C_{pS}m_S} [\alpha_{AL}(\theta_{A1} - \theta_d)4\pi d_{dr}^2 - \dot{m}_{ev1}(-C_{pL1}\theta_d + \Delta h_{V,0} + C_{pV1}\theta_{A1})]\tag{2.11}$$

where C_{pL1} and C_{pS} are the specific heat capacity of the liquid and the specific heat capacity of the solid in the droplet respectively. The quantities m_w and m_S are the mass of liquid in a single droplet and the mass of the solids inside this droplet.

The radius of the droplet d_{dr} in the above equation is not constant. It is changing with

2.2. DERIVATION OF THE BALANCE EQUATIONS

respect to time. To find the change of the radius of a single droplet we start with the change of the mass m_1 of a single droplet with respect to time t given by

$$\frac{dm_1}{dt} = -\dot{m}_{ev1}. \quad (2.12)$$

We have

$$m_1 = V_{dr}\rho_{L1} = \frac{4}{3}\pi\rho_{L1}d_{dr}^3$$

where V_{dr} is the volume of a single droplet. Replacing m_1 and \dot{m}_{ev1} in (2.12) we get

$$\frac{4}{3}3\pi\rho_{L1}d_{dr}^2 \frac{dd_{dr}}{dt} = -4\beta_1\rho_{A1}\pi d_{dr}^2 (Y_{sat1} - Y_{A1}).$$

After some cancellations we obtain

$$\frac{dd_{dr}}{dt} = -\frac{\beta_1(Sh)\rho_{A1}}{\rho_{L1}}(Y_{sat1} - Y_{A1}). \quad (2.13)$$

Therefore equations (2.11) and (2.13) are coupled.

Mass balance of air in region (1)

Figure 2.5 illustrates the enthalpy flow of evaporated water alongside with the enthalpy flow between the droplet and the air.

The humidity of air which enters region (1) is increasing due to the evaporation flow which comes from the surface of the droplets. By convection the humidity is transferred in a form of vapor to the bulk phase.

Source term: In (2.9) the source v is taken to be the evaporation flow \dot{m}_{ev1} from 2.10.

Transport term: The convection in the plug flow which is given by $s(u) = \dot{m}_{st1}$ can be taken as the transport term.

Balance equation:

The humidity Y_{A1} is given as the ratio of the vapor mass m_{st1} to the mass of air m_{A1} . Consequently we find that $m_{st1} = Y_{A1}m_{A1}$ and $\dot{m}_{st1} = Y_{A1}\dot{m}_{A1}$ where \dot{m}_A is the mass flow rate of the air. Inserting these terms to the balance equation (2.9) leads to

$$\int_{V_1} \frac{\partial m_{st1}}{\partial t} dV_1 = - \int_{V_1} \frac{\partial \dot{m}_{st1}}{\partial z} H_1 dV_1 + \int_{V_1} \dot{m}_{ev1} dV_1.$$

Here H_1 represents the height of region (1). For more details about deriving such an equation the reader is referred to Heinrich [32]. Using equation (2.10) we can write

$$\int_{V_1} \frac{\partial(Y_{A1}m_{A1})}{\partial t} dV_1 = - \int_{V_1} \frac{\partial(Y_{A1}\dot{m}_A)}{\partial z} H_1 dV_1 + \int_{V_1} \beta_1\rho_{A1}A_{droplets}(Y_{sat1} - Y_{A1}) dV_1.$$

CHAPTER 2. A NEW MATHEMATICAL MODELING OF HEAT AND MASS TRANSFER IN FLUIDIZED BEDS

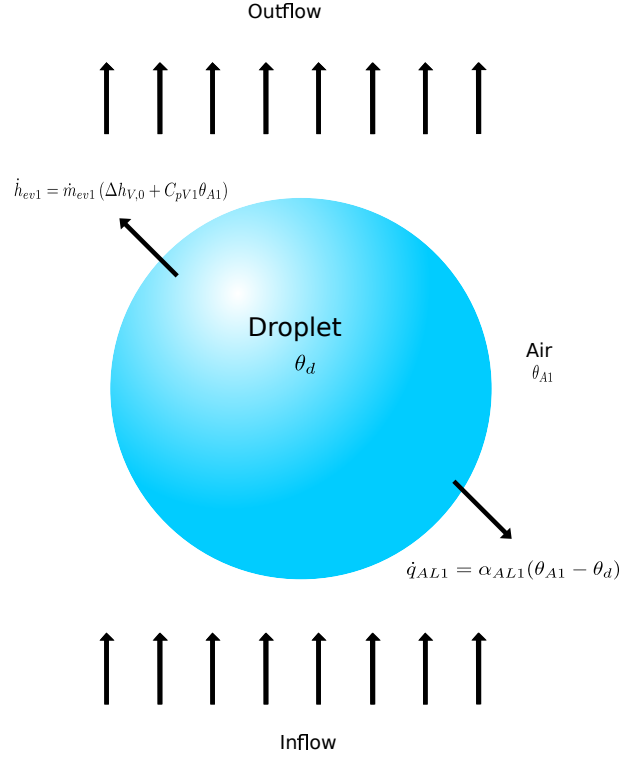


Figure 2.5: Heat and mass transfer on a droplet

Here $A_{droplets}$ represents the surface area of all droplets. Since the integral balance holds for arbitrary volume V_1 we obtain the differential equation

$$m_{A1} \frac{\partial Y_{A1}}{\partial t} = -\dot{m}_A H_1 \frac{\partial Y_{A1}}{\partial z} + \beta_1 \rho_{A1} A_{droplets} (Y_{sat1} - Y_{A1}).$$

Dividing both sides by m_{A1} gives

$$\frac{\partial Y_{A1}}{\partial t} = -Q_1 \frac{\partial Y_{A1}}{\partial z} + Q_2 (Y_{sat1} - Y_{A1}), \quad (2.14)$$

where

$$Q_1 = \frac{\dot{m}_A}{m_{A1}} H_1.$$

$$Q_2 = \frac{\beta_1 \rho_{A1} A_{droplets}}{m_{A1}}.$$

Energy balance of air in region (1)

Figure (2.5) shows the heat flow which occurs between the droplet and air beside the enthalpy flow of evaporated water. The heat transfer coefficient is calculated according to Gnielinski [26].

2.2. DERIVATION OF THE BALANCE EQUATIONS

Source term: Here it can be taken to be the enthalpy of the evaporation flow \dot{h}_{ev1} given by $\dot{h}_{ev1} = \dot{m}_{ev1} (\Delta h_{V,0} + C_{pV1} \theta_{A1})$.

Sink: The sink term is the enthalpy flow between the droplet and air \dot{q}_{AL1} which can be calculated from equation (2.6).

Transport term: In equation (2.9) the transport term is the convection in the plug flow $s(u) = \dot{h}_{st1}$.

Balance equation:

We have

$$\begin{aligned} h_{st1} &= h_{A1} + h_{V1} \\ &= m_{A1} C_{pA1} \theta_{A1} + m_{A1} Y_{A1} \Delta h_{V,0} + m_{A1} Y_{A1} C_{pV1} \theta_{A1}, \end{aligned}$$

Taking the derivative of the above formula with respect to time leads to the following equation

$$\begin{aligned} \frac{\partial h_{st1}}{\partial t} &= m_{A1} C_{pA1} \frac{\partial \theta_{A1}}{\partial t} + m_{A1} \Delta h_{V,0} \frac{\partial Y_{A1}}{\partial t} + m_{A1} C_{pV1} \left(Y_{A1} \frac{\partial \theta_{A1}}{\partial t} + \theta_{A1} \frac{\partial Y_{A1}}{\partial t} \right) \\ &= m_{A1} (C_{pA1} + C_{pV1} Y_{A1}) \frac{\partial \theta_{A1}}{\partial t} + m_{A1} (\Delta h_{V,0} + C_{pV1} \theta_{A1}) \frac{\partial Y_{A1}}{\partial t}. \end{aligned}$$

Similarly we find

$$\frac{\partial \dot{h}_{st1}}{\partial z} = \dot{m}_A (C_{pA1} + C_{pV1} Y_{A1}) \frac{\partial \theta_{A1}}{\partial z} + \dot{m}_A (\Delta h_{V,0} + C_{pV1} \theta_{A1}) \frac{\partial Y_{A1}}{\partial z}.$$

Again, making use of equation (2.9) gives

$$\int_{V_1} \frac{\partial h_{st1}}{\partial t} dV_1 = - \int_{V_1} \frac{\partial \dot{h}_{st1}}{\partial z} H_1 dV_1 - \int_{V_1} \dot{q}_{AL1} dV_1 + \int_{V_1} \dot{h}_{ev1} dV_1. \quad (2.15)$$

Substituting $\frac{\partial h_{st1}}{\partial t}$ and $\frac{\partial \dot{h}_{st1}}{\partial z}$ in (2.15) leads to

$$\begin{aligned} &\int_{V_1} \left(m_{A1} (C_{pA1} + C_{pV1} Y_{A1}) \frac{\partial \theta_{A1}}{\partial t} + m_{A1} (\Delta h_{V,0} + C_{pV1} \theta_{A1}) \frac{\partial Y_{A1}}{\partial t} \right) dV_1 \\ &= - \int_{V_1} \left(\dot{m}_A (C_{pA1} + C_{pV1} Y_{A1}) H_1 \frac{\partial \theta_{A1}}{\partial z} - \dot{m}_A (\Delta h_{V,0} + C_{pV1} \theta_{A1}) H_1 \frac{\partial Y_{A1}}{\partial z} \right) dV_1 \end{aligned}$$

CHAPTER 2. A NEW MATHEMATICAL MODELING OF HEAT AND MASS TRANSFER IN FLUIDIZED BEDS

$$- \int_{V_1} \alpha_{AL1} A_{droplets} (\theta_{A1} - \theta_d) dV_1 + \int_{V_1} \dot{m}_{ev1} (\Delta h_{V,0} + C_{pV1} \theta_{A1}) dV_1.$$

Replacing $\frac{\partial Y_{A1}}{\partial t}$ from (2.14) we find

$$\begin{aligned} \int_{V_1} m_{A1} (C_{pA1} + C_{pV1} Y_{A1}) \frac{\partial \theta_{A1}}{\partial t} dV_1 &= \int_{V_1} m_{A1} (\Delta h_{V,0} + C_{pV1} \theta_{A1}) \left[\frac{\dot{m}_A}{m_{A1}} H_1 \frac{\partial Y_{A1}}{\partial z} - \frac{\dot{m}_{ev1}}{m_{A1}} \right] dV_1 \\ &- \int_{V_1} \dot{m}_A (C_{pA1} + C_{pV1} Y_{A1}) H_1 \frac{\partial \theta_{A1}}{\partial z} dV_1 - \int_{V_1} \dot{m}_A (\Delta h_{V,0} + C_{pV1} \theta_{A1}) H_1 \frac{\partial Y_{A1}}{\partial z} dV_1 \\ &- \int_{V_1} \alpha_{AL1} A_{droplets} (\theta_{A1} - \theta_d) dV_1 + \int_{V_1} \dot{m}_{ev1} (\Delta h_{V,0} + C_{pV1} \theta_{A1}) dV_1. \end{aligned}$$

After some cancellations we get

$$\begin{aligned} \int_{V_1} m_{A1} (C_{pA1} + C_{pV1} Y_{A1}) \frac{\partial \theta_{A1}}{\partial t} dV_1 &= - \int_{V_1} \dot{m}_A H_1 (C_{pA1} + C_{pV1} Y_{A1}) \frac{\partial \theta_{A1}}{\partial z} dV_1 \\ &- \int_{V_1} \alpha_{AL1} A_{droplets} (\theta_{A1} - \theta_d) dV_1. \end{aligned}$$

Since the integral equation is independent of the choice of volume we can write

$$m_{A1} (C_{pA1} + C_{pV1} Y_{A1}) \frac{\partial \theta_{A1}}{\partial t} = - \dot{m}_A H_1 (C_{pA1} + C_{pV1} Y_{A1}) \frac{\partial \theta_{A1}}{\partial z} - \alpha_{AL1} A_{droplets} (\theta_{A1} - \theta_d).$$

Finally, dividing both sides by $m_{A1} (C_{pA1} + C_{pV1} Y_{A1})$ leads us to

$$\frac{\partial \theta_{A1}}{\partial t} = -Q_1 \frac{\partial \theta_{A1}}{\partial z} - Q_3 (\theta_{A1} - \theta_d), \quad (2.16)$$

where

$$Q_3 = \frac{\alpha_{AL1} A_{droplets}}{m_{A1} (C_{pA1} + C_{pV1} Y_{A1})}.$$

2.2. DERIVATION OF THE BALANCE EQUATIONS

Assumptions for region (2)

- All particles are spheres.
- All particles have the same average diameter d_p , i.e. the particles are monodisperse.
- The fluidized bed has a constant porosity.
- The injected liquid is completely deposited onto the particles as a film with constant thickness F .
- A plug flow tube reactor (PFTR) behavior.
- The solid and liquid density are constants.
- The particles are ideally mixed, i.e. we have a continuous stirred-tank reactor (CSTR) with uniform wetted particles for the one-dimensional model.
- There is no agglomeration, overspray or breakage.
- We have a non-ideal mixing of particles for the two-dimensional model with non-uniform liquid distribution.
- Only the constant-rate period of drying (first drying period) is observed, i.e. drying from surface-wet particles.

Mass balance of the air in region (2)

The humidity which is carried with the inlet hot gas flow increases according to the evaporation of the liquid film on the particles. The vapor is transferred into the air as a function of mass transfer. In equation (2.9) we can take

the source term as the evaporation flow \dot{m}_{ev2} and

the transport term as the convection in the plug flow $s(u) = \dot{m}_{st2}$.

CHAPTER 2. A NEW MATHEMATICAL MODELING OF HEAT AND MASS TRANSFER IN FLUIDIZED BEDS

Balance equation

Taking H_2 as the height of region (2) and substituting the source term and the transport term in equation (2.9) gives

$$\int_{V_2} \frac{\partial m_{st2}}{\partial t} dV_2 = - \int_{V_2} \frac{\partial \dot{m}_{st2}}{\partial z} H_2 dV_2 + \int_{V_2} \dot{m}_{ev2} dV_2.$$

The usage of equation (2.4) beside the fact that $m_{st2} = Y_{A2}m_{A2}$ gives

$$\int_{V_2} \frac{\partial (Y_{A2}m_{A2})}{\partial t} dV_2 = - \int_{V_2} \frac{\partial (Y_{A2}\dot{m}_A)}{\partial z} H_2 dV_2 + \int_{V_2} \beta_2 \rho_{A2} A_p \phi (Y_{sat2} - Y_{A2}) dV_2.$$

This equation can be also written in the form

$$\frac{\partial (m_{A2}Y_{A2})}{\partial t} = -H_2 \frac{\partial (\dot{m}_A Y_{A2})}{\partial z} + \beta_2 \rho_{A2} A_p \phi (Y_{sat2} - Y_{A2}).$$

Since the mass of air is independent of time, and the mass flow rate of air is independent of space, it is possible to write

$$m_{A2} \frac{\partial Y_{A2}}{\partial t} = -\dot{m}_A H_2 \frac{\partial Y_{A2}}{\partial z} + \beta_2 \rho_{A2} A_p \phi (Y_{sat2} - Y_{A2}).$$

After dividing the both sides of the above equation by m_{A2} we get

$$\frac{\partial Y_{A2}}{\partial t} = -Q_4 \frac{\partial Y_{A2}}{\partial z} + Q_5 \phi (Y_{sat2} - Y_{A2}), \quad (2.17)$$

$$Q_4 = \frac{\dot{m}_A}{m_{A2}} H_2.$$

$$Q_5 = \frac{\beta_2 \rho_{A2} A_p}{m_{A2}}.$$

Energy balance of the air in region (2)

Several studies have been done to study the distribution of the temperature of air inside the fluidized bed during the layering process, see e.g. Nienow and Rowe [56], Smith and Nienow [80] and Wnukowski [91]. Here we follow Heinrich et al. [33].

As it is seen in Figure 2.4, the inlet gas comes in contact with the wetted and the unwetted part of the particles. Due to this contact, a heat flow takes place between the unwetted portion of the particle and air beside the heat flow which occurs between the wetted part (liquid film) of the particle and air. The enthalpy of the evaporated water also increases the energy of air. In equation (2.9)

the source term is the enthalpy of the evaporation flow $\dot{h}_{ev2} = \dot{m}_{ev2} (\Delta h_{V,0} + C_{pV2} \theta_{A2})$,

2.2. DERIVATION OF THE BALANCE EQUATIONS

the sink terms are the enthalpy flow between the liquid film and air \dot{q}_{AL2} , enthalpy flow between the unwetted portion and air \dot{q}_{AP} which can be calculated from equations (2.6) and (2.7) respectively, while

the transport term is the convection in the plug flow $s(u) = \dot{h}_{st2}$.

Balance equation:

We have

$$\begin{aligned} h_{st2} &= h_{A2} + h_{V2} \\ &= m_{A2}C_{pA2}\theta_{A2} + m_{A2}Y_{A2}\Delta h_{V,0} + m_{A2}Y_{A2}C_{pV2}\theta_{A2}. \end{aligned}$$

Taking the derivative of both sides with respect to time leads to

$$\frac{\partial h_{st2}}{\partial t} = m_{A2} (C_{pA2} + C_{pV2}Y_{A2}) \frac{\partial \theta_{A2}}{\partial t} + m_{A2} (\Delta h_{V,0} + C_{pV2}\theta_{A2}) \frac{\partial Y_{A2}}{\partial t}.$$

Similarly we can write

$$\frac{\partial \dot{h}_{st2}}{\partial z} = \dot{m}_A (C_{pA2} + C_{pV2}Y_{A2}) \frac{\partial \theta_{A2}}{\partial z} + \dot{m}_A (\Delta h_{V,0} + C_{pV2}\theta_{A2}) \frac{\partial Y_{A2}}{\partial z}.$$

When we substitute the source, the sink and the transport terms in the balance equation (2.9) we obtain the following balance

$$\int_{V_2} \frac{\partial h_{st2}}{\partial t} dV_2 = - \int_{V_2} \frac{\partial \dot{h}_{st2}}{\partial z} H_2 dV_2 - \int_{V_2} \dot{q}_{AL2} dV_2 - \int_{V_2} \dot{q}_{AP} dV_2 + \int_{V_2} \dot{h}_{ev2} dV_2, \quad (2.18)$$

Replacing the integrands in the above equation gives

$$\begin{aligned} & \int_{V_2} \left(m_{A2} (C_{pA2} + C_{pV2}Y_{A2}) \frac{\partial \theta_{A2}}{\partial t} + m_{A2} (\Delta h_{V,0} + C_{pV2}\theta_{A2}) \frac{\partial Y_{A2}}{\partial t} \right) dV_2 \\ &= - \int_{V_2} \left(\dot{m}_A (C_{pA2} + C_{pV2}Y_{A2}) H_2 \frac{\partial \theta_{A2}}{\partial z} - \dot{m}_A (\Delta h_{V,0} + C_{pV2}\theta_{A2}) H_2 \frac{\partial Y_{A2}}{\partial z} \right) dV_2 \\ & \quad - \int_{V_2} \alpha_{AL2} A_p \phi (\theta_{A2} - \theta_L) dV_2 - \int_{V_2} \alpha_{AP} A_p (1 - \phi) (\theta_{A2} - \theta_P) dV_2 \\ & \quad + \int_{V_2} \dot{m}_{ev2} (\Delta h_{V,0} + C_{pV2}\theta_{A2}) dV_2. \end{aligned}$$

Replacing $\frac{\partial Y_{A2}}{\partial t}$ from (2.17), and after some cancellations we get

$$\int_{V_2} m_{A2} (C_{pA2} + C_{pV2}Y_{A2}) \frac{\partial \theta_{A2}}{\partial t} dV_2 = - \int_{V_2} \dot{m}_A H_2 (C_{pA2} + C_{pV2}Y_{A2}) \frac{\partial \theta_{A2}}{\partial z} dV_2$$

CHAPTER 2. A NEW MATHEMATICAL MODELING OF HEAT AND MASS TRANSFER IN FLUIDIZED BEDS

$$- \int_{V_2} \alpha_{AL2} A_p \phi (\theta_{A2} - \theta_L) dV_2 - \int_{V_2} \alpha_{AP} A_p (1 - \phi) (\theta_{A2} - \theta_P) dV_2.$$

The heat transfer coefficient between air and the dry portion of the particle α_{AP} as well as between the liquid film and air α_{AL} are assumed to be equal as in Groenewold [29], i.e. $\alpha_{AP} = \alpha_{AL} = \alpha$.

Taking into consideration that the integral balance holds for arbitrary volume V_2 and after dividing the both sides by $m_{A2} (C_{pA2} + C_{pV2} Y_{A2})$ we obtain

$$\frac{\partial \theta_{A2}}{\partial t} = -Q_4 H_2 \frac{\partial \theta_{A2}}{\partial z} - Q_6 [\phi (\theta_{A2} - \theta_L) + (1 - \phi) (\theta_{A2} - \theta_P)], \quad (2.19)$$

where

$$Q_6 = \frac{\alpha A_p}{m_{A2} (C_{pA2} + C_{pV2} Y_{A2})}.$$

Energy balance of the particles

Assuming that the heat transfer coefficient between air and the dry portion of the particle is equal to the heat transfer coefficient between air and the liquid film, i.e. $\alpha_{AL} = \alpha_{AP} = \alpha$ we introduce a corrective factor f as follows

$$f = \frac{\alpha_{PL}}{\alpha}.$$

This dimensionless factor is known as the heat transfer ratio.

The heat flow which takes place between the particles and liquid film as well as between the unwetted part of the particles and air beside the intensity of dispersion cause a temporal change to the enthalpy of the particles. Making use of equation (2.9) we consider

the source term as the heat transfer between the unwetted portion of the particles and air \dot{q}_{AP} ,

the sink term as the heat transfer between the liquid film and the particles \dot{q}_{PL} which can be found from (2.5), while

the transport term as the particle conduction $s(u) = -D\nabla h_p$, where D is the conduction matrix.

Balance equation:

Substituting these terms in equation (2.9) we get

$$\int_{V_2} \frac{\partial h_p}{\partial t} dV_2 = \int_{V_2} \nabla \cdot (D\nabla h_p) dV_2 + \int_{V_2} \dot{q}_{AP} dV_2 - \int_{V_2} \dot{q}_{PL} dV_2,$$

where the enthalpy of the solids h_p is given as $h_p = m_p C_{pP} \theta_P$. Here C_{pP} and m_p are the specific heat capacity and the total mass of the particles respectively. Replacing the

2.2. DERIVATION OF THE BALANCE EQUATIONS

integrands in the above equation leads us to the following balance

$$\int_{V_2} \frac{\partial(m_p C_{pP} \theta_P)}{\partial t} dV_2 = \int_{V_2} \nabla \cdot (D \nabla (m_p C_{pP} \theta_P)) dV_2 + \int_{V_2} \alpha_{AP} A_p (1 - \phi) (\theta_{A2} - \theta_P) dV_2 - \int_{V_2} \alpha_{PL} A_p \phi (\theta_P - \theta_L) dV_2.$$

This equation can be also written in the form

$$m_p C_{pP} \frac{\partial \theta_P}{\partial t} = m_p C_{pP} \nabla \cdot (D \nabla \theta_P) + \alpha_{AP} A_p (1 - \phi) (\theta_{A2} - \theta_P) - \alpha_{PL} A_p \phi (\theta_P - \theta_L).$$

Dividing both sides by $m_p C_{pP}$ and the usage of the heat transfer ratio f leads to the following PDE

$$\frac{\partial \theta_P}{\partial t} = \nabla \cdot (D \nabla \theta_P) + Q_7 [(1 - \phi) (\theta_{A2} - \theta_P) - f \phi (\theta_P - \theta_L)], \quad (2.20)$$

where

$$Q_7 = \frac{\alpha A_p}{m_p C_{pP}}.$$

Mass balance of water

The maximal liquid mass inside the fluidized bed is reached when the surface areas of all particles are covered with liquid film, i.e. the particles are 100% wetted. In this case the maximum liquid concentration per volume element is given as

$$\rho_{L,max} = A_p^* (1 - \epsilon) F \rho_L.$$

It would be very effective from the energetic point of view if the particles are completely or almost completely wetted, but in fact this may leads to undesired results where small particles may tend to agglomerate. Therefore these wet conditions should be taken into account in experiments.

In our new model the sprayed liquid loses some of its amount due to the evaporation which takes place when the droplets pass through region (1). In equation (2.9) we can take

the source term to be the effective mass flow $\dot{M}_{LV,eff}$ which is given by $\dot{M}_{LV,eff} = \dot{M}_{LV} - \dot{m}_{ev1}$, where \dot{M}_{LV} is the mass flow of the drop deposition ,

the sink term to be the evaporation flow \dot{m}_{ev2} and

the transport term to be the particle conduction $s(u) = -D \nabla M_{LP}$, where $M_{LP} = A_p \phi F \rho_L$.

CHAPTER 2. A NEW MATHEMATICAL MODELING OF HEAT AND MASS TRANSFER IN FLUIDIZED BEDS

Balance equation:

Replacing these terms in equation (2.9) gives

$$\int_{V_2} \frac{\partial M_{LP}}{\partial t} dV_2 = \int_{V_2} \nabla \cdot (D \nabla M_{LP}) dV_2 - \int_{V_2} \dot{m}_{ev2} dV_2 + \int_{V_2} \dot{M}_{LV,eff} dV_2.$$

Substituting in the previous equation

$$\begin{aligned} \int_{V_2} \frac{\partial (A_p \phi F \rho_{L2})}{\partial t} dV_2 &= \int_{V_2} \nabla \cdot (D \nabla (A_p \phi F \rho_{L2})) dV_2 - \int_{V_2} \beta_2 \rho_{A2} A_p \phi (Y_{sat2} - Y_{A2}) dV_2 \\ &+ \int_{V_2} \dot{M}_{LV,eff} dV_2. \end{aligned}$$

It is also possible to write this equation in the following form

$$A_p F \rho_{L2} \frac{\partial \phi}{\partial t} = A_p F \rho_{L2} \nabla \cdot (D \nabla \phi) - \beta_2 \rho_{A2} A_p \phi (Y_{sat2} - Y_{A2}) + \dot{M}_{LV,eff}.$$

Dividing both sides by $A_p F \rho_{L2}$ leads to

$$\frac{\partial \phi}{\partial t} = \nabla \cdot (D \nabla \phi) - Q_8 \phi (Y_{sat2} - Y_{A2}) + Q_9 \dot{M}_{LV,eff}, \quad (2.21)$$

where

$$\begin{aligned} Q_8 &= \frac{\beta_2 \rho_{A2}}{F \rho_{L2}}, \\ Q_9 &= \frac{1}{A_p F \rho_{L2}}. \end{aligned}$$

Energy balance of Water

The sprayed liquid enters region (1) with a specific temperature and then it changes after passing through this region as we saw in equation (2.11) and enters region (2) with another temperature $\theta_{d,end}$. The droplets then hit and deposit on the surfaces of the particles as a film. The temperature of this liquid film is influenced by the dispersion of the particles, the heat flow between the liquid film and air \dot{q}_{AL} , the heat flow between the liquid film and the particle \dot{q}_{PL} , the enthalpy flow brought by the liquid into the bed \dot{h}_{dr} as well as the enthalpy of evaporation \dot{h}_{ev} . Again we replace the source term, the sink term and the transport term in the equation (2.9) where

the source terms here are \dot{h}_{dr} , \dot{q}_{PL} , \dot{q}_{AL} , where $\dot{h}_{dr} = \dot{M}_{LV,eff} C_{pL2} \theta_{d,end}$,

the sink term is the enthalpy of evaporation flow \dot{h}_{ev} , where

$$\dot{h}_{ev} = \dot{m}_{ev2} (\Delta h_{V,0} + C_{p,V2} \theta_{A2}) = \beta_2 \rho_{A2} A_p \phi (Y_{sat} - Y_{A2}) (\Delta h_{V,0} + C_{p,V2} \theta_{A2}) \text{ and}$$

2.2. DERIVATION OF THE BALANCE EQUATIONS

the transport term is the particle conduction $s(u) = -D\nabla h_L$, where $h_L = m_L C_{pL2} \theta_L = V_L \rho_{L2} C_{pL2} \theta_L = A_p \phi F \rho_{L2} C_{pL2} \theta_L$.

Balance equation:

Inserting these terms to the balance equation (2.9) leads us to

$$\int_{V_2} \frac{\partial h_L}{\partial t} dV_2 = \int_{V_2} \nabla \cdot (D\nabla h_L) dV_2 + \int_{V_2} \dot{q}_{AL} dV_2 + \int_{V_2} \dot{q}_{PL} dV_2 + \int_{V_2} \dot{h}_{dr} dV_2 - \int_{V_2} \dot{h}_{ev} dV_2,$$

Substituting the integrands in the above equation gives

$$\begin{aligned} \int_{V_2} \frac{\partial (A_p \phi F \rho_{L2} C_{pL2} \theta_L)}{\partial t} dV_2 &= \int_{V_2} \nabla \cdot (D\nabla (A_p \phi F \rho_{L2} C_{pL2} \theta_L)) dV_2 + \int_{V_2} \alpha_{AL} A_p \phi (\theta_{A2} - \theta_L) dV_2 \\ &+ \int_{V_2} \alpha_{PL} A_p \phi (\theta_P - \theta_L) dV_2 + \int_{V_2} \dot{M}_{LV,eff} C_{pL2} \theta_{d,end} dV_2 \\ &- \int_{V_2} \beta_2 \rho_{A2} A_p \phi (Y_{sat2} - Y_{A2}) (\Delta h_{V,0} + C_{pV2} \theta_{A2}) dV_2. \end{aligned}$$

The integral balance holds for arbitrary V_2 so we can write the previous equation in the form

$$\begin{aligned} A_p F \rho_{L2} C_{pL2} \frac{\partial (\phi \theta_L)}{\partial t} &= A_p F \rho_{L2} C_{pL2} \nabla \cdot (D\nabla (\phi \theta_L)) + \alpha_{AL} A_p \phi (\theta_{A2} - \theta_L) \\ &+ \alpha_{PL} A_p \phi (\theta_P - \theta_L) - \beta_2 \rho_{A2} A_p \phi (Y_{sat} - Y_{A2}) (\Delta h_{V,0} + C_{pV2} \theta_{A2}) + \dot{M}_{LV,eff} C_{pL2} \theta_{d,end}. \end{aligned}$$

Inserting the corrective factor f and dividing the both sides by the term $A_p F \rho_{L2} C_{pL2}$ leads to the partial differential equation for liquid film temperature

$$\begin{aligned} \frac{\partial (\phi \theta_L)}{\partial t} &= \nabla \cdot (D\nabla (\phi \theta_L)) + Q_{10} [\phi (\theta_{A2} - \theta_L) + f \phi (\theta_P - \theta_L)] \\ &- Q_{11} \phi (Y_{sat2} - Y_{A2}) (\Delta h_{V,0} + C_{pV2} \theta_{A2}) + Q_{12} \dot{M}_{LV,eff}, \end{aligned} \quad (2.22)$$

where

$$\begin{aligned} Q_{10} &= \frac{\alpha}{F \rho_{L2} C_{pL2}}, \\ Q_{11} &= \frac{\beta_2 \rho_{A2}}{F \rho_{L2} C_{pL2}}, \\ Q_{12} &= \frac{\theta_{d,end}}{A_p F \rho_{L2}}. \end{aligned}$$

2.2.1 Total balance equations

In fluidized beds it is possible to find the outlet humidity and the outlet temperature of air at the steady state through the total balance equations.

Humidity of air: The outlet air humidity can be found by knowing the values of the inlet air humidity, mass flow of the liquid and the mass flow of air as follows

$$Y_{A,out} = Y_{A,in} + \frac{\dot{M}_L}{\dot{m}_A}. \quad (2.23)$$

Temperature of air: The outlet temperature of air can be also found through the balance of the enthalpies inside the chamber. The balance equation for the temperature of air is

$$\theta_{A,out} = \frac{\dot{m}_A(C_{pA} + Y_{A,in}C_{pV})\theta_{A,in} + \dot{M}_L(C_{pL}\theta_{L,in} - \Delta h_{V,0})}{\dot{m}_A(C_{pA} + Y_{A,out}C_{pV})}. \quad (2.24)$$

These two balance equations are needed to check the numerical results at the steady state.

2.3 Boundary conditions

Region (1): As it is seen in Figure 2.6 the surface of the fluidized bed at region (1) is divided into 3 surfaces such that

$$\partial\Omega = \partial\Omega_1 + \partial\Omega_2 + \partial\Omega_3,$$

where

- $\partial\Omega_1$ represents the bottom surface,
- $\partial\Omega_2$ the side wall,
- $\partial\Omega_3$ the top surface.

The bottom surface: Here hot and humid air comes from region (2) to region (1) passing the surface $\partial\Omega_1$, so Dirichlet boundary conditions can be assumed for the bottom surface of region (1), i.e.

$$\begin{aligned} Y_{A1} &= Y_{A1,in} \text{ on } \partial\Omega_1, \\ \theta_{A1} &= \theta_{A1,in} \text{ on } \partial\Omega_1, \end{aligned}$$

where $Y_{A1,in}, \theta_{A1,in} \in \mathbb{R}$ are given constants.

The side wall: For simplicity we assume that the heat exchange between the bed and the

2.3. BOUNDARY CONDITIONS

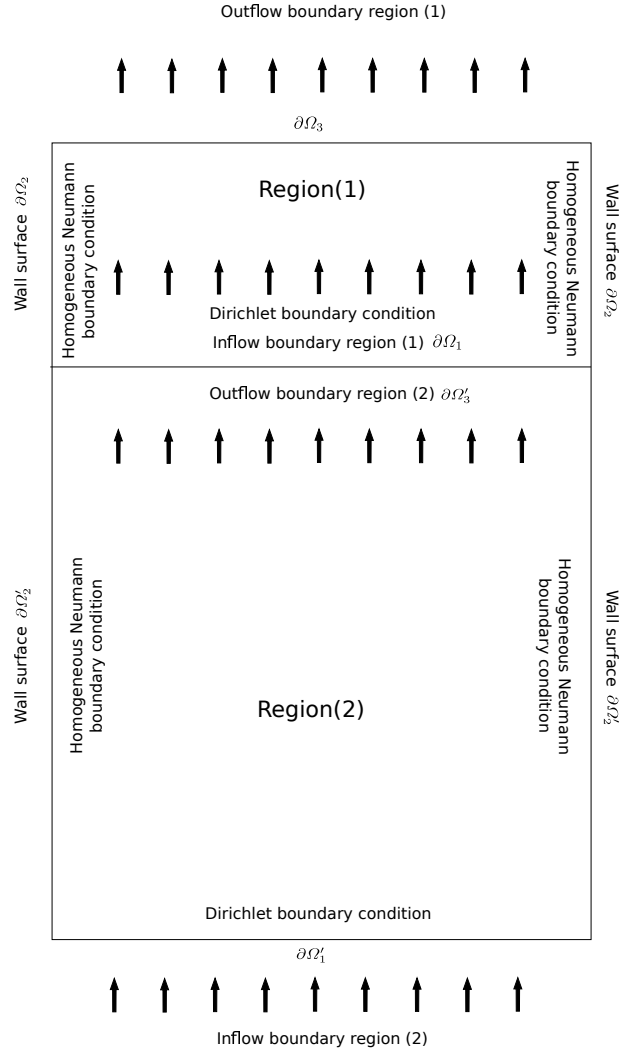


Figure 2.6: Initial and boundary conditions

wall of the apparatus is ignored, so it is possible to say that the gradient at the wall is zero.

The top surface: Since the boundary here is an outflow boundary, equations (2.14) and (2.16) have no boundary conditions.

Region (2): Similarly as it is seen in Figure 2.6 the surface of the fluidized bed at region (2) is also divided into 3 surfaces such that

$$\partial\Omega' = \partial\Omega'_1 + \partial\Omega'_2 + \partial\Omega'_3,$$

where

$\partial\Omega'_1$ represents the bottom surface,

CHAPTER 2. A NEW MATHEMATICAL MODELING OF HEAT AND MASS TRANSFER IN FLUIDIZED BEDS

$\partial\Omega'_2$ the side wall,
 $\partial\Omega'_3$ the top surface.

The bottom surface: The hot fluidizing gas passes the porous plate carrying vapour to the top of the bed, so again the boundary conditions for equations (2.17) and (2.19) are given as

$$\begin{aligned} Y_{A2} &= Y_{A2,in} \text{ on } \partial\Omega'_1, \\ \theta_{A2} &= \theta_{A2,in} \text{ on } \partial\Omega'_1. \end{aligned}$$

It is assumed that the heat transfer at the distributor plate is disregarded, so there is no flux for the degree of wetting, temperature of particles and temperature of liquid film, i.e.

$$\begin{aligned} \underline{n} \cdot D\nabla\phi &= 0 \text{ on } \partial\Omega'_1, \\ \underline{n} \cdot D\nabla\theta_P &= 0 \text{ on } \partial\Omega'_1, \\ \underline{n} \cdot D\nabla\theta_L &= 0 \text{ on } \partial\Omega'_1. \end{aligned}$$

The side wall: In general, the wall effects the temperature inside the bed, it can absorb temperature to increase its temperature or radiate temperature to decrease it. For our model we assume that the heat exchange between the wall and the bed is neglected, so we can write the boundary condition at the side wall as following

$$\begin{aligned} \underline{n} \cdot D\nabla\theta_P &= 0 \text{ on } \partial\Omega'_2, \\ \underline{n} \cdot D\nabla\theta_L &= 0 \text{ on } \partial\Omega'_2. \end{aligned}$$

The wall of the apparatus is impervious, so there is no flux of degree of wetting, i.e.

$$\underline{n} \cdot D\nabla\phi = 0 \text{ on } \partial\Omega'_2.$$

The top surface: This surface is described as the outflow surface, consequently equations (2.17) and (2.19) have no boundary condition. Also there is no flux for the degree of wetting, temperature of liquid and temperature of particles. The boundary conditions at the top surface for the equations (2.20), (2.21) and (2.22) are

$$\begin{aligned} \underline{n} \cdot D\nabla\phi &= 0 \text{ on } \partial\Omega'_3, \\ \underline{n} \cdot D\nabla\theta_P &= 0 \text{ on } \partial\Omega'_3, \\ \underline{n} \cdot D\nabla\theta_L &= 0 \text{ on } \partial\Omega'_3. \end{aligned}$$

2.4 Two dimensional model for the liquid deposition into the fluidized bed

In the sprayed region, droplets hit the particles and deposit on their surfaces. Practically particles close to the nozzle will be wetted more than those which are further from the nozzle orifice. The nearest particles to the distributor plate get the least amount of liquid in the sprayed region. This comes from the fact that particles close to the nozzle form a shelter allowing a lower amount of liquid to arrive on the particles that are further away [11]. Due to this fact, the temperature and the humidity are influenced by the spatial distribution of the sprayed liquid inside the chamber. The spraying area is influenced by both the impingement efficiency and the dispersion angle of the spray. The dispersion angle θ_{nozz} depends on the nozzle used. The impingement efficiency η_{im} refers to the ability of having contact between a droplet and a particle.

2.4.1 Liquid deposition on a single particle surface

At certain air velocities, droplets accelerated by the nozzle cannot follow the streamlines anymore and deposit on the surface of the particles when their trajectories intersect. After the collision between a droplet and a particle, the droplet can either be absorbed by the particle or rebound. The deposition efficiency ϕ_{dep} is given as the product of the impingement efficiency η_{im} and the adhesion probability h_{ad} , see Löffler [45],

$$\phi_{dep} = \eta_{im} h_{ad}. \quad (2.25)$$

Link and Schlünder [44] introduced a critical impingement velocity V_{crit} for horizontal, dry, non-porous surfaces given by

$$V_{crit} = \frac{4\eta_{dr} [3 \tan(\delta_s/2) + \tan^3(\delta_s/2)]^{2/3}}{d_{dr} \rho_{dr} \tan^2(\delta_s/2)}, \quad (2.26)$$

where δ_s is the contact angle. Contact angles with $\delta_s < 90^\circ$ lead to high wetting systems, while contact angles with $\delta_s > 90^\circ$ correspond to poorly wetting systems. Up to the critical velocity, droplets will adhere and spread on the particle surface, above this value droplets will rebound.

Impingement efficiency: For a single particle, the impingement efficiency is given as the ratio of the effective cross section, droplets will collide with the particle within this area, to the projection area of the particle, see Figure 2.7,

$$\eta_{im} = \left(\frac{d_{im}}{d_p} \right)^2. \quad (2.27)$$

In this equation d_{im} is unknown. However, Schuch [72] introduced an alternative formula using the Stokes number

$$\eta_{im} = \left(\frac{St}{St + 2a} \right)^b.$$

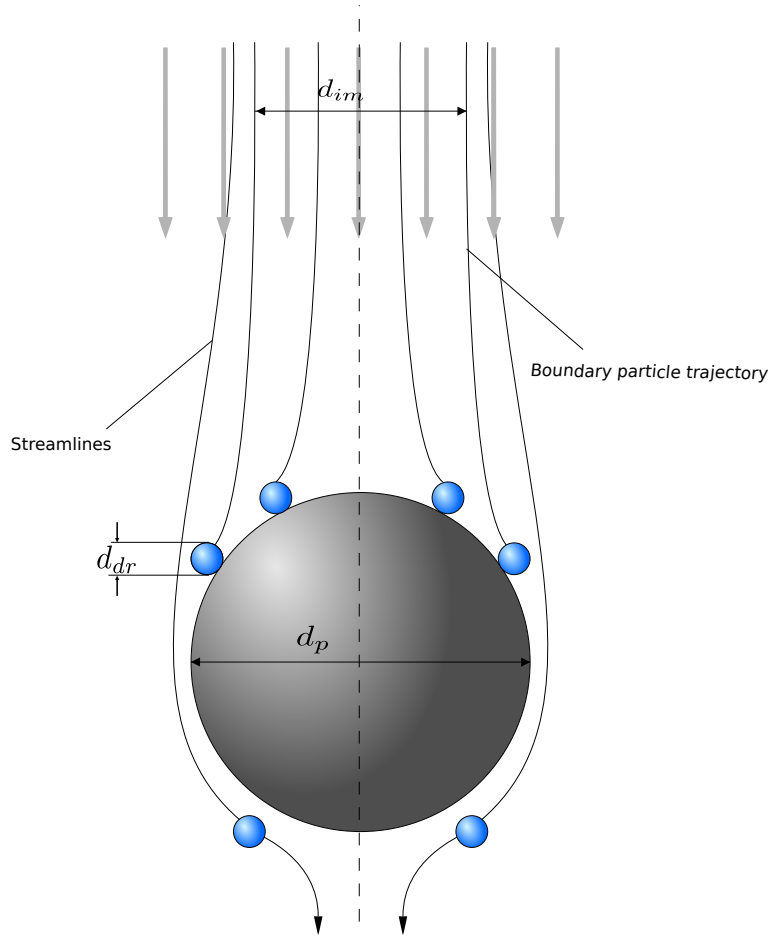


Figure 2.7: Collision of a droplet and a particle

The number St is the Stokes number given by

$$St = \frac{\rho_{dr} V_{gas} d_{dr}^2}{18 \eta_A d_p}. \quad (2.28)$$

The numbers a, b are parameters that can be found in [33]. From (2.27) and (2.28) it is obvious that increasing the size of the droplets leads to an increase in the impingement efficiency, as well as the increase of the atomizing air flow rate.

Adhesion probability: The ratio of droplets which collide with particles and are captured on the surfaces of these particles is referred to as the adhesion probability. Several factors affect the adhesion probability such as liquid properties, the structure of the particle surface, the kinetic energy of the droplets, wetting and spreading properties as well as the collision angle. Up to the critical impingement velocity, the adhesion probability can be assumed to be one. The adhesion probability decreases with the increase of the droplets size, the droplet temperature, as well as with increase of the droplet velocity above the critical impingement velocity at which droplets start to rebound. In this case

2.4. TWO DIMENSIONAL MODEL FOR THE LIQUID DEPOSITION INTO THE FLUIDIZED BED

the adhesion probability can be determined according to Link [43].

According to Löffler [45], the change of the concentration of droplets in fluidized beds with respect to the height of the bed is given by the following formula

$$-\frac{d\kappa}{\kappa} = 1.5 \frac{\epsilon}{1-\epsilon} \frac{\phi_{dep}}{d_p} dH_{Nd}$$

or

$$C_{dr} = \frac{\kappa}{\kappa_0} = \exp\left(-1.5 \frac{\epsilon}{1-\epsilon} \frac{\phi_{dep}}{d_p} H_{Nd}\right).$$

Here κ_0 is the initial concentration and H_{Nd} is the distance from the nozzle.

As seen in Figure 2.8, most of the injected liquid droplets deposit on the particles surfaces which are very close to the nozzle, while particles which are further away get a very small amount of liquid because the closed particles form a shelter preventing a large amount of liquid to reach the further particles. It is also obvious that increasing the porosity of the bed leads to an increase in the concentration. Figure 2.9 illustrates that the droplet concentration rises when the diameter of particles increases.

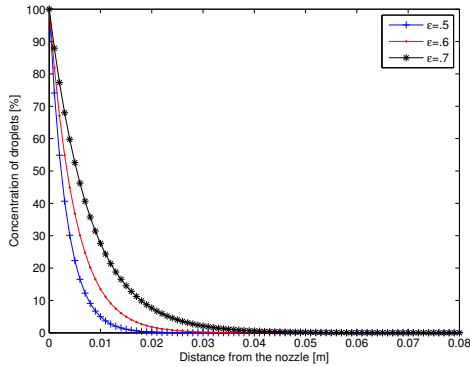


Figure 2.8: Influence of porosity on the droplet concentration

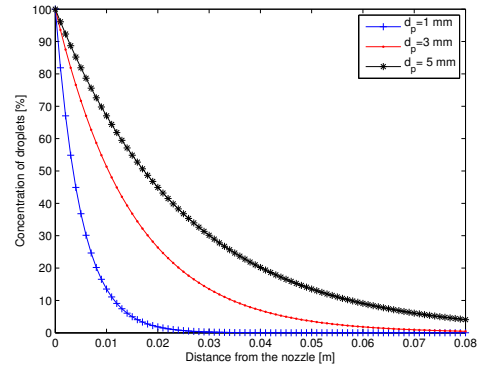


Figure 2.9: Influence of particle diameter on the droplet concentration

Assumptions:

- The spraying region forms a right circular cone.
- The velocity of droplets u_{dr} is considered to be constant until the droplets adhere to the particles surfaces.
- The liquid within the spraying region is assumed to be evenly distributed. Out of the spraying region the concentration is taken to be zero.

CHAPTER 2. A NEW MATHEMATICAL MODELING OF HEAT AND MASS TRANSFER IN FLUIDIZED BEDS

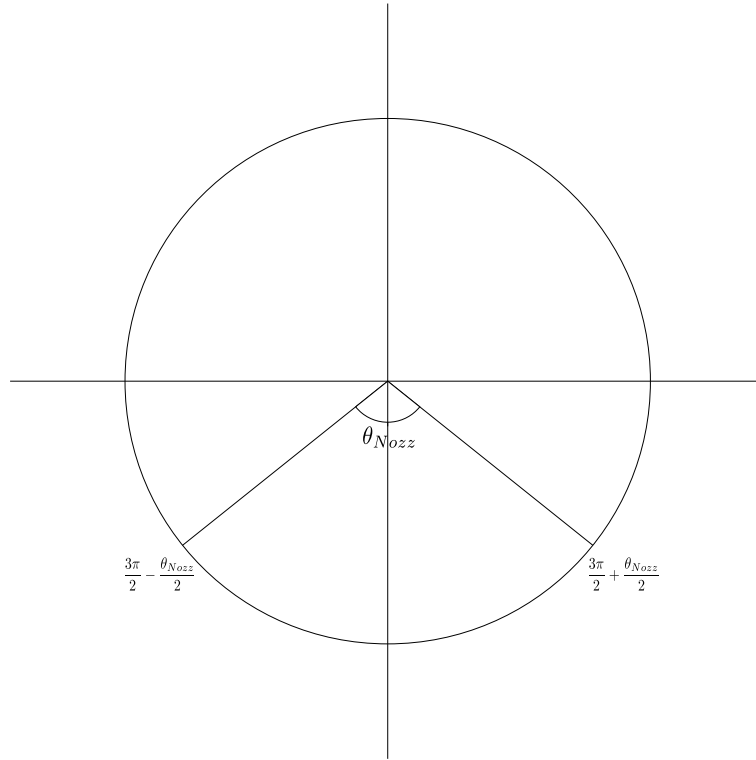


Figure 2.10: Polar coordinate of the nozzle

- The particles and the droplets are spheres.
- The deposition efficiency ϕ_{dep} is considered to be constant.
- The polar coordinates (r, θ) are taken in order to find the spatial drop concentration distribution. Here θ represents the angle of the cone, see Figure 2.10.

The average drop path length can be taken as

$$S_{Nd} = \frac{2}{3} \frac{\epsilon}{1 - \epsilon} \frac{d_p}{\phi_{dep}}, \quad (2.29)$$

see [33]. The drop concentration flow can be expressed as

$$\dot{\kappa}(x) = \begin{cases} \dot{\kappa}(r, \theta) & \text{if } R < r, \quad \frac{3\pi}{2} - \frac{\theta_{Nozz}}{2} \leq \theta \leq \frac{3\pi}{2} + \frac{\theta_{Nozz}}{2}, \\ 0 & \text{otherwise.} \end{cases} \quad (2.30)$$

Here R is the radius of the circle centered at the nozzle position. We assume for the

2.4. TWO DIMENSIONAL MODEL FOR THE LIQUID DEPOSITION INTO THE FLUIDIZED BED

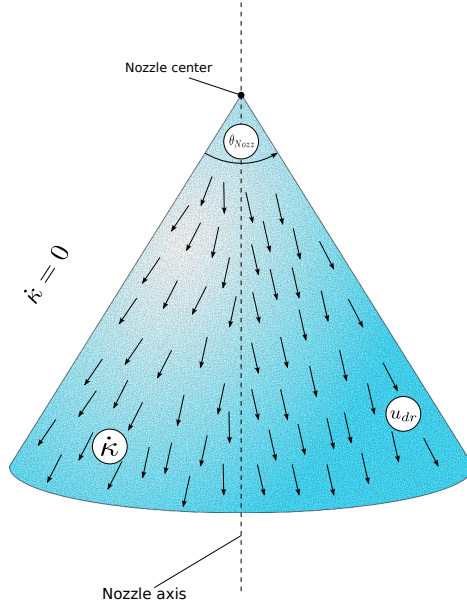


Figure 2.11: The nozzle spray

modeling that this circle does not contain any particles. The balance equation of the drop concentration in the polar coordinates is

$$\frac{\partial \kappa}{\partial t} = -\nabla \cdot (\kappa \underline{u}_{dr}) - \dot{\kappa}, \quad (2.31)$$

where $\dot{\kappa}$ is the lost drop concentration flow due to the deposition of particles surfaces and $\underline{u}_{dr} = u_{dr} \underline{e}_r$ is the velocity of droplets, where \underline{e}_r is the unit vector in the radial direction. For the divergence $\nabla \cdot (\kappa \underline{u}_{dr})$ we can write

$$\begin{aligned} \nabla \cdot (\kappa \underline{u}_{dr}) &= \nabla \cdot (\kappa u_{dr} \underline{e}_r) \\ &= u_{dr} (\underline{e}_r \cdot \nabla \kappa + \kappa \nabla \cdot \underline{e}_r). \end{aligned} \quad (2.32)$$

We have the relation

$$\begin{aligned} \underline{e}_r \cdot \nabla \kappa &= \underline{e}_r \cdot \left(\underline{e}_r \frac{\partial \kappa}{\partial r} + \underline{e}_\theta \frac{1}{r} \frac{\partial \kappa}{\partial \theta} \right) \\ &= (\underline{e}_r \cdot \underline{e}_r) \frac{\partial \kappa}{\partial r} + (\underline{e}_r \cdot \underline{e}_\theta) \frac{1}{r} \frac{\partial \kappa}{\partial \theta} \\ &= \frac{\partial \kappa}{\partial r}. \end{aligned}$$

CHAPTER 2. A NEW MATHEMATICAL MODELING OF HEAT AND MASS TRANSFER IN FLUIDIZED BEDS

Similarly, we obtain,

$$\begin{aligned}\kappa \cdot \nabla \underline{e}_r &= \kappa \cdot \left(\underline{e}_r \cdot \frac{\partial \underline{e}_r}{\partial r} + \frac{1}{r} \underline{e}_\theta \cdot \frac{\partial \underline{e}_r}{\partial \theta} \right) \\ &= \kappa \cdot \left(\underline{e}_r \cdot 0 + \frac{1}{r} \underline{e}_\theta \cdot \underline{e}_\theta \right) \\ &= \frac{\kappa}{r}.\end{aligned}$$

Substituting in equation (2.32) leads to

$$\nabla \cdot (\kappa \underline{u}_{dr}) = u_{dr} \left(\frac{\partial \kappa}{\partial r} + \frac{\kappa}{r} \right).$$

The balance equation (2.31) can be written now as

$$\frac{\partial \kappa}{\partial t} = -u_{dr} \left(\frac{\partial \kappa}{\partial r} + \frac{\kappa}{r} \right) - \dot{\kappa}. \quad (2.33)$$

Due to equation (2.29) the following holds

$$\dot{\kappa} = \frac{u_{dr}}{S_{Nd}} \kappa. \quad (2.34)$$

Substituting in the balance equation gives

$$\frac{\partial \kappa}{\partial t} = -u_{dr} \left(\frac{\partial \kappa}{\partial r} + \frac{\kappa}{r} \right) - \frac{u_{dr}}{S_{Nd}} \kappa. \quad (2.35)$$

Here we solve the above equation in the stationary case where $\frac{\partial \kappa}{\partial t} = 0$. This leads after canceling the velocity to the following ODE

$$\frac{d\kappa}{dr} = - \left(\frac{1}{r} + \frac{1}{S_{Nd}} \right) \kappa. \quad (2.36)$$

The general solution of this ODE is given as

$$\kappa = C(\theta) \frac{\exp\left(-\frac{r}{S_{Nd}}\right)}{r}, \quad (2.37)$$

where $C(\theta) \in \mathbb{R}$.

2.4.2 Mass balance of spraying

The mission here is to determine the constant $C(\theta)$. The liquid flow $\dot{m}_{dr}(r)$ passes through the spraying region, this flow can be found as following.

$$\begin{aligned}\dot{m}_{dr}(r) &= \int_S \kappa(\underline{x}) \underline{u}_{dr} d\underline{n} \\ &= \int_{\frac{3\pi}{2} - \frac{\theta_{Nozz}}{2}}^{\frac{3\pi}{2} + \frac{\theta_{Nozz}}{2}} C(\theta) \frac{\exp(-\frac{r}{S_{Nd}})}{r} u_{dr} r d\theta \\ &= C(\theta) u_{dr} \theta_{Nozz} \exp(-\frac{r}{S_{Nd}})\end{aligned}$$

The liquid mass flow \dot{M}_L can be determined by taking the limit of both sides when $r \rightarrow R$.

$$\dot{M}_L = \lim_{r \rightarrow R} \dot{m}_{dr}(r) = C(\theta) u_{dr} \theta_{Nozz} \exp(-\frac{R}{S_{Nd}}).$$

Consequently we get

$$C(\theta) = \frac{\dot{M}_L}{u_{dr} \theta_{Nozz} \exp(-\frac{R}{S_{Nd}})}.$$

Substituting in (2.37)

$$\kappa = \frac{\dot{M}_L}{u_{dr} \theta_{Nozz} \exp(-\frac{R}{S_{Nd}})} \frac{\exp(-\frac{r}{S_{Nd}})}{r}.$$

Replacing in(2.34) we get

$$\dot{\kappa} = \frac{\dot{M}_L}{\theta_{Nozz} S_{Nd}} \frac{\exp(-\frac{r-R}{S_{Nd}})}{r}, \quad (2.38)$$

where

$$\dot{M}_L = \int_{\mathbb{R}^2} \dot{\kappa} dX \quad (2.39)$$

2.5 Invariant regions

In this section we follow the analysis in Nagaiah [52] which was based on Smoller [81]. Note that our model has the following difference in comparison to the one in Nagaiah [52]. In our model the mass flow rate \dot{M}_L is not constant unlike in Nagaiah [52] where the mass flow rate is supposed to be constant and not influenced by the heat. Also in our model the temperature of the inlet liquid $\theta_{d,end}$ is influenced by the humidity and the temperature of air.

CHAPTER 2. A NEW MATHEMATICAL MODELING OF HEAT AND MASS TRANSFER IN FLUIDIZED BEDS

Invariant regions are very useful to study dynamical systems in order to determine properties such as the large time behavior of trajectories (solutions) as well as stability.

Definition 1. A set \mathcal{O} is called **invariant set** if every solution of the differential equation $\dot{x} = f(x)$ passing through any point of \mathcal{O} lies completely in \mathcal{O} , in another word, a subset $\mathcal{O} \subseteq \mathbb{E}$ is invariant set under the mapping $\Psi_t : \mathbb{E} \rightarrow \mathbb{E}$ if for all $x \in \mathbb{E}$, $\Psi_t(x) \in \mathcal{O}$, i.e. $\Psi_t(\mathcal{O}) \subseteq \mathcal{O}$ for all t . If this condition holds for $t \geq 0$ then \mathcal{O} is called a **positively (forwardly) invariant region**.

Here we consider an invariant region of the form

$$\prod = \bigcap_{i=1}^{i=n} \{v \in \mathcal{Q} : Z_i(v) \leq 0\}, \quad (2.40)$$

where $\mathcal{Q} \subseteq \mathbb{R}^m$, Z_i are smooth real valued functions defined on open subsets of \mathcal{Q} and for each i , the gradient ∇Z_i does not vanish, see Smoller [81].

Definition 2. The smooth function $Z : \mathbb{R}^n \rightarrow \mathbb{R}$ is called **quasi-convex** at v if whenever $\nabla Z_v \cdot \zeta = 0$, then the Hessian \mathcal{H} of Z is positive, i.e. $\mathcal{H}Z_v(\zeta, \zeta) \geq 0$.

Now we take an open interval Ω in \mathbb{R} , the $n \times n$ matrix-valued functions $\mathcal{D} = \mathcal{D}(v, x)$, $\mathcal{M} = \mathcal{M}(v, x)$ defined on an open subset in $\mathbb{R}^n \times \Omega$ and the smooth n -vector function \mathcal{F} .

Consider the system

$$\frac{\partial v}{\partial t} = \mathcal{D}v_{xx} + \mathcal{M}v_x + \mathcal{F}(v) \quad (x, t) \in \Omega \times \mathbb{R}^+, \quad (2.41)$$

together with the initial condition

$$v(x, 0) = v_0(x), \quad x \in \Omega. \quad (2.42)$$

Our model in region (2) can be written in the matrix form as above as follows

$$\begin{pmatrix} Y_{A2} \\ \theta_{A2} \\ \theta_P \\ \phi \\ \phi\theta_L \end{pmatrix}_t = \begin{pmatrix} 0 & 0 & 0 & 0 & 0 \\ 0 & 0 & 0 & 0 & 0 \\ 0 & 0 & D & 0 & 0 \\ 0 & 0 & 0 & D & 0 \\ 0 & 0 & 0 & 0 & D \end{pmatrix} \begin{pmatrix} Y_{A2} \\ \theta_{A2} \\ \theta_P \\ \phi \\ \phi\theta_L \end{pmatrix}_{xx} + \begin{pmatrix} -Q_4 & 0 & 0 & 0 & 0 \\ 0 & -Q_4 & 0 & 0 & 0 \\ 0 & 0 & 0 & 0 & 0 \\ 0 & 0 & 0 & 0 & 0 \\ 0 & 0 & 0 & 0 & 0 \end{pmatrix} \begin{pmatrix} Y_{A2} \\ \theta_{A2} \\ \theta_P \\ \phi \\ \phi\theta_L \end{pmatrix}_x + \begin{pmatrix} +Q_5\phi(Y_{sat2} - Y_{A2}) \\ -Q_6[\phi(\theta_{A2} - \theta_L) + (1 - \phi)(\theta_{A2} - \theta_P)] \\ +Q_7[(1 - \phi)(\theta_{A2} - \theta_P) - f\phi(\theta_P - \theta_L)] \\ -Q_8\phi(Y_{sat2} - Y_{A2}) + Q_9\dot{M}_{LV,eff} \\ +Q_{10}[\phi(\theta_{A2} - \theta_L) + f\phi(\theta_P - \theta_L)] - Q_{11}\phi(Y_{sat2} - Y_{A2})(\Delta h_{V,0} + C_{pV2}\theta_{A2}) + Q_{12}\dot{M}_{LV,eff} \end{pmatrix}.$$

In comparison between the previous two forms we see that

2.5. INVARIANT REGIONS

$$v = (Y_{A2}, \theta_{A2}, \theta_P, \phi, \phi\theta_L)$$

$$\mathcal{D} = \text{diag}(0, 0, D, D, D)$$

$$\mathcal{M} = \text{diag}(-Q_4, -Q_4, 0, 0, 0)$$

$$\mathcal{F}(v) = \begin{pmatrix} Q_5\phi(Y_{sat2} - Y_{A2}), \\ -Q_6[\phi(\theta_{A2} - \theta_L) + (1 - \phi)(\theta_{A2} - \theta_P)] \\ Q_7[(1 - \phi)(\theta_{A2} - \theta_P) - f\phi(\theta_P - \theta_L)] \\ -Q_8\phi(Y_{sat2} - Y_{A2}) + Q_9\dot{M}_{LV,eff} \\ Q_{10}[\phi(\theta_{A2} - \theta_L) + f\phi(\theta_P - \theta_L)] - Q_{11}\phi(Y_{sat2} - Y_{A2})(\Delta h_{V,0} + C_{pV2}\theta_{A2}) + Q_{12}\dot{M}_{LV,eff} \end{pmatrix}$$

It is obvious that $Q_5, Q_6, Q_7, Q_8, Q_9, Q_{10}, Q_{11}, Q_{12}, f, \dot{M}_{LV,eff}, \Delta h_{V,0}, C_{pV2} > 0$,

also $0 \leq Y_{A2} \leq Y_{sat2}$, $0 \leq \theta_{A2} \leq X$, $0 \leq \theta_P \leq X$, $0 \leq \phi \leq 1$, $0 \leq \theta_L \leq X$, where

X represents the inlet air temperature.

Theorem 2.5.1. *Let \prod be defined by (2.40), and suppose that for all $t \in \mathbb{R}^+$ and for every $v_0 \in \partial\prod$, so $Z_i(v) = 0$ for some i , the following conditions hold:*

1. ∇Z_i at v_0 is a left eigenvector of $\mathcal{D}(v_0, x)$, and $\mathcal{M}(v_0, x)$, for all $x \in \mathbb{R}$.
2. If $\nabla Z_i \mathcal{D}(v_0, x) = \mu \nabla Z_i$, with $\mu \neq 0$, then Z_i is quasi-convex at v_0 .
3. $\nabla Z_i \cdot \mathcal{F} \leq 0$ at v_0 , for all $t \in \mathbb{R}^+$.

Then \prod is invariant for (2.41).

Proof. See Smoller [81]. □

Since the process in region (1) is completely dependent on the process in region (2), it is enough to study the invariant region for the process in region (2).

Lemma 2.5.2. *Let \prod be defined as follows*

$$\prod = \{Y_{A2}, \theta_{A2}, \theta_P, \phi, \theta_L : 0 \leq Y_{A2} \leq Y_{sat2}, \quad 0 \leq \theta_{A2}, \theta_P, \theta_L \leq X, \quad 0 \leq \phi \leq 1\}.$$

Under the conditions

$$Y_{A2} \geq Y_{sat2} - \frac{1}{Q_{11}\phi(\Delta h_{V,0} + C_{pV2}\theta_{A2})} \left\{ Q_{10} \{ \phi\theta_{A2} + f\phi\theta_P \} + Q_{12}\dot{M}_{LV,eff} \right\} \text{ at } \theta_L = 0,$$

$$\theta_L \leq X - \frac{1}{f\phi}(1 - \phi)(\theta_{A2} - X) \text{ at } \theta_P = X.$$

CHAPTER 2. A NEW MATHEMATICAL MODELING OF HEAT AND MASS TRANSFER IN FLUIDIZED BEDS

$$Y_{A2} \leq Y_{sat2} - \frac{Q_9}{Q_8} \dot{M}_{LV,eff} \quad \text{at } \phi = 1$$

$$Y_{A2} \leq Y_{sat2} - \frac{1}{Q_{11}\phi(\Delta h_{V,0} + C_{pV2}\theta_{A2})} \left\{ Q_{10} \{ \phi(\theta_{A2} - X) + f\phi(\theta_P - X) \} + Q_{12} \dot{M}_{LV,eff} \right\}$$

at $\theta_L = X$, the system (2.41) has an invariant region.

Proof. Let

$$Z_1(u) = -Y_{A2}, \quad Z_2(u) = -\theta_{A2}, \quad Z_3(u) = -\theta_P, \quad Z_4(u) = -\phi,$$

$$Z_5(u) = -\theta_L, \quad Z_6(u) = Y_{A2} - Y_{sat2}, \quad Z_7(u) = \theta_{A2} - X,$$

$$Z_8(u) = \theta_P - X, \quad Z_9(u) = \phi - 1, \quad , Z_{10}(u) = \theta_L - X.$$

In this case the gradients are

$$\nabla Z_1 = \begin{pmatrix} -1 \\ 0 \\ 0 \\ 0 \\ 0 \end{pmatrix}, \nabla Z_2 = \begin{pmatrix} 0 \\ -1 \\ 0 \\ 0 \\ 0 \end{pmatrix}, \nabla Z_3 = \begin{pmatrix} 0 \\ 0 \\ -1 \\ 0 \\ 0 \end{pmatrix}, \nabla Z_4 = \begin{pmatrix} 0 \\ 0 \\ 0 \\ -1 \\ 0 \end{pmatrix}, \nabla Z_5 = \begin{pmatrix} 0 \\ 0 \\ 0 \\ 0 \\ -1 \end{pmatrix},$$

$$\nabla Z_6 = \begin{pmatrix} 1 \\ 0 \\ 0 \\ 0 \\ 0 \end{pmatrix}, \nabla Z_7 = \begin{pmatrix} 0 \\ 1 \\ 0 \\ 0 \\ 0 \end{pmatrix}, \nabla Z_8 = \begin{pmatrix} 0 \\ 0 \\ 1 \\ 0 \\ 0 \end{pmatrix}, \nabla Z_9 = \begin{pmatrix} 0 \\ 0 \\ 0 \\ 1 \\ 0 \end{pmatrix}, \nabla Z_{10} = \begin{pmatrix} 0 \\ 0 \\ 0 \\ 0 \\ 1 \end{pmatrix}.$$

In order to prove that Π is an invariant region we need to verify the three conditions of the Theorem 2.5.1. The eigenvalues of the diagonal matrix $\mathcal{D}(v_0, x)$ are $\{0, D\}$. The eigenspace corresponding to $\lambda = 0$ is given by

$$span \left[\begin{pmatrix} 1 \\ 0 \\ 0 \\ 0 \\ 0 \end{pmatrix}, \begin{pmatrix} 0 \\ 1 \\ 0 \\ 0 \\ 0 \end{pmatrix} \right],$$

while the eigenspace corresponding to $\lambda = D$ is given by

$$span \left[\begin{pmatrix} 0 \\ 0 \\ 1 \\ 0 \\ 0 \end{pmatrix}, \begin{pmatrix} 0 \\ 0 \\ 0 \\ 1 \\ 0 \end{pmatrix}, \begin{pmatrix} 0 \\ 0 \\ 0 \\ 0 \\ 1 \end{pmatrix} \right].$$

2.5. INVARIANT REGIONS

From above we find that all ∇Z_i for $i = 1, \dots, 10$ are left eigenvectors of $\mathcal{D}(v_0, x)$. Similarly we find that the eigenvalues of the matrix $\mathcal{M}(v_0, x)$ are $\{0, -Q_4\}$. The eigenvectors corresponding to $\lambda = 0$ are

$$\begin{pmatrix} 0 \\ 0 \\ 1 \\ 0 \\ 0 \end{pmatrix}, \begin{pmatrix} 0 \\ 0 \\ 0 \\ 1 \\ 0 \end{pmatrix}, \begin{pmatrix} 0 \\ 0 \\ 0 \\ 0 \\ 1 \end{pmatrix},$$

while the eigenvectors corresponding to $\lambda = -Q_4$ are

$$\begin{pmatrix} 1 \\ 0 \\ 0 \\ 0 \\ 0 \end{pmatrix}, \begin{pmatrix} 0 \\ 1 \\ 0 \\ 0 \\ 0 \end{pmatrix}.$$

This means again that the vectors ∇Z_i are left eigenvectors of $\mathcal{M}(v_0, x)$. The second condition of Theorem 2.5.1 holds automatically. Now we need to check the last condition. The equality $Z_1(v) = -Y_{A2}$ implies that

$$\nabla Z_1 \cdot \mathcal{F} |_{Y_{A2}=0} = -Q_5 \phi (Y_{sat2} - Y_{A2}) |_{Y_{A2}=0} = -Q_5 \phi Y_{sat2} \leq 0.$$

Similarly $Z_2(v) = -\theta_{A2}$ implies

$$\begin{aligned} \nabla Z_2 \cdot \mathcal{F} |_{\theta_{A2}=0} &= (-1) \{-Q_6 \{\phi (\theta_{A2} - \theta_L) + (1 - \phi) (\theta_{A2} - \theta_P)\}\} |_{\theta_{A2}=0} \\ &= Q_6 \{\phi (-\theta_L) + (1 - \phi) (-\theta_P)\} \leq 0. \end{aligned}$$

For $Z_3(v) = -\theta_P$ we obtain

$$\begin{aligned} \nabla Z_3 \cdot \mathcal{F} |_{\theta_P=0} &= (-1) \{Q_7 [(1 - \phi) (\theta_{A2} - \theta_P) - f \phi (\theta_P - \theta_L)]\} |_{\theta_P=0} \\ &= (-1) \{Q_7 [(1 - \phi) \theta_{A2} - f \phi (-\theta_L)]\} \leq 0. \end{aligned}$$

Again for $Z_4(v) = -\phi$ we have

$$\begin{aligned} \nabla Z_4 \cdot \mathcal{F} |_{\phi=0} &= (-1) \left\{ -Q_8 \phi (Y_{sat2} - Y_{A2}) + Q_9 \dot{M}_{LV,eff} \right\} |_{\phi=0} \\ &= (-1) \left\{ Q_9 \dot{M}_{LV,eff} \right\} \leq 0. \end{aligned}$$

Setting $Z_5(v) = -\theta_L$ gives

CHAPTER 2. A NEW MATHEMATICAL MODELING OF HEAT AND MASS TRANSFER IN FLUIDIZED BEDS

$$\begin{aligned}
& \nabla Z_5 \cdot \mathcal{F} |_{\theta_L=0} \\
&= (-1) \left\{ Q_{10} [\phi(\theta_{A2} - \theta_L) + f\phi(\theta_P - \theta_L)] - Q_{11}\phi(Y_{sat2} - Y_{A2}) (\Delta h_{V,0} + C_{pV2}\theta_{A2}) \right. \\
&\quad \left. + Q_{12}\dot{M}_{LV,eff} |_{\theta_L=0} \right\} \\
&= (-1) \left\{ Q_{10} [\phi\theta_{A2} + f\phi\theta_P] - Q_{11}\phi(Y_{sat2} - Y_{A2}) (\Delta h_{V,0} + C_{pV2}\theta_{A2}) + Q_{12}\dot{M}_{LV,eff} \right\}.
\end{aligned}$$

Due to the assumption of the lemma, the right hand side of the above equation is less than zero, i.e. $\nabla Z_5 \cdot \mathcal{F} |_{\theta_L=0} \leq 0$.

Now for $Z_6(v) = Y_{A2} - Y_{sat2}$ we obtain

$$\nabla Z_6 \cdot \mathcal{F} |_{Y_{A2}=Y_{sat2}} = Q_5\phi(Y_{sat2} - Y_{A2}) |_{Y_{A2}=Y_{sat2}} = 0.$$

If we set $Z_7(v) = \theta_{A2} - X$ then we have

$$\begin{aligned}
\nabla Z_7 \cdot \mathcal{F} |_{\theta_{A2}=X} &= \{-Q_6 \{\phi(\theta_{A2} - \theta_L) + (1 - \phi)(\theta_{A2} - \theta_P)\}\} |_{\theta_{A2}=X} \\
&= \{-Q_6 \{\phi(X - \theta_L) + (1 - \phi)(X - \theta_P)\}\} \leq 0.
\end{aligned}$$

Similarly $Z_8(v) = \theta_P - X$ leads to

$$\begin{aligned}
\nabla Z_8 \cdot \mathcal{F} |_{\theta_P=X} &= Q_7 [(1 - \phi)(\theta_{A2} - \theta_P) - f\phi(\theta_P - \theta_L)] |_{\theta_P=X} \\
&= Q_7 [(1 - \phi)(\theta_{A2} - X) - f\phi(X - \theta_L)].
\end{aligned}$$

From the assumption of the lemma we find that $\nabla Z_8 \cdot \mathcal{F} |_{\theta_P=X} \leq 0$.

Again for $Z_9(v) = \phi - 1$ we have

$$\begin{aligned}
\nabla Z_9 \cdot \mathcal{F} |_{\phi=1} &= \left\{ -Q_8\phi(Y_{sat2} - Y_{A2}) + Q_9\dot{M}_{LV,eff} \right\} |_{\phi=1} \\
&= \left\{ -Q_8(Y_{sat2} - Y_{A2}) + Q_9\dot{M}_{LV,eff} \right\}.
\end{aligned}$$

According to the condition in the statement of the lemma we see that $\nabla Z_9 \cdot \mathcal{F} |_{\phi=1} \leq 0$.

Finally for $Z_{10}(v) = \theta_L - X$ we get

$$\nabla Z_{10} \cdot \mathcal{F} |_{\theta_L=X}$$

$$\begin{aligned}
 &= \left\{ Q_{10} [\phi(\theta_{A2} - \theta_L) + f\phi(\theta_P - \theta_L)] - Q_{11}\phi(Y_{sat2} - Y_{A2}) (\Delta h_{V,0} + C_{pV2}\theta_{A2}) \right. \\
 &\quad \left. + Q_{12}\dot{M}_{LV,eff} |_{\theta_L=X} \right\} \\
 &= Q_{10} [\phi(\theta_{A2} - X) + f\phi(\theta_P - X)] - Q_{11}\phi(Y_{sat2} - Y_{A2}) (\Delta h_{V,0} + C_{pV2}\theta_{A2}) + Q_{12}\dot{M}_{LV,eff}.
 \end{aligned}$$

Due to the assumption of the lemma, the right hand side of the above equation is less than zero, i.e. $\nabla Z_{10} \cdot \mathcal{F} |_{\theta_L=X} \leq 0$.

□

In comparison with the previous model of Heinrich and Nagaiah we notice, e.g. that the outlet humidity in the new model is less than that one presented by Heinrich and Nagaiah for the same parameters. This comes from the fact that the droplets loose some of their mass in region (1) due to the evaporation.

The difference between the outlet humidity of air of the both cases can be calculated as follows

$$Y_{A,out,old} - Y_{A,out,new} = \frac{\dot{m}_{ev1}}{\dot{m}_A},$$

where $Y_{A,out,old}$, $Y_{A,out,new}$ are the outlet humidity of air of the old and the new model respectively, \dot{m}_{ev1} is the evaporation flow and \dot{m}_A is the mass flow rate of the air. Also the evaporation which takes place in region (1) causes decreasing in the degree of wetting which also effects at the same time the temperature of each of the air, the particles as well as the liquid film as we shall see later.

Chapter 3

Spray Drying Process

3.1 Introduction

In this chapter we study the so-called spray drying process. This process is similar to the process that takes place in region (1) as explained in Chapter 2. Here we study this process for longer time for droplets inside the chamber.

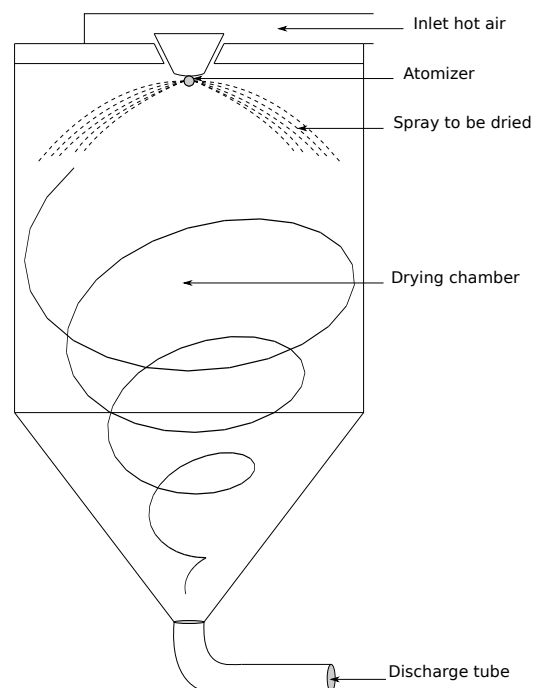


Figure 3.1: Spray dryer

Definition 3. *The spray drying process is a method used to convert slurry or nano-sized*

CHAPTER 3. SPRAY DRYING PROCESS

particles included in liquid into a dry powder.

In this process the liquid to be dried is atomized to small droplets, these droplets have contact with a hot gas as shown in Figure 3.1. Due to this contact a mass and heat transfer between the droplets and the hot air takes place. The hot gas causes the droplets to evaporate. Moisture is transferred to the bulk phase leaving solid particles.

The process of spray drying depends completely on the evaporation of liquid content and has wide applications such as:

Food production: vitamins, enzymes, milk powder.

Industrial purposes: ceramic materials, polyvinyl chloride.

Pharmaceutical industry: antibiotics.

Agricultural chemicals: herbicides, fungicides.

The spray drying process provides a flexible control over some properties of the product such as the size and the density. The drying rate is related to the liquid to be dried, temperature of the droplets, and the size of the droplets. While the size of the droplets is related to the design of the atomizer.

Several studies were made to depict the changes which take place during the process. These changes are related to temperature of the droplets, their concentration, their movement inside the spraying region, and aggregation of nano-sized solids inside the droplets. Contributions to this research can be found in [31, 73, 49, 27, 5, 86, 20, 16, 59].

Single droplet models were assumed in the all previous studies. These models focused on temperature, diameter, concentration of a single droplet, as well as aggregation of nano-particles inside the droplet.

3.2 Mechanism of the process

Liquid to be dried is atomized into small droplets by a convenient atomizer. The dryer is provided with an air disperser. Consequently the droplets and the hot gas will be in contact. Due to this contact a heat and mass transfer will take place in the drying chamber. Mass transfer can be represented as the evaporation of the solvent. This process lasts until there is no solvent on the surface of the droplet or inside it and the product is discharged through a discharge tube. The whole process can be summarized into three distinct periods.

Warm-up period

In this period the temperature of the droplets starts to increase from the initial temperature t_0 until it reaches the wet bulb temperature of the dry gas t_1 . Evaporation starts

3.3. MATHEMATICAL MODELS OF THE PROCESS

at the droplet surface.

First drying period

In this period the temperature of the droplet is close to the wet bulb temperature, and droplets start to shrink due to the evaporation at surface where the diameter decreases from the initial diameter value R_0 to R_1 . The temperature stays constant because the added heat is consumed by evaporation. This period lasts until the solvent is completely evaporated and a very thin solid shell starts to be formed at the surface of the droplet. At this point the second drying period starts.

Second drying period

This period starts when a solid crust begins to appear at the surface of the droplet. In this period the mass and the heat transfer are reduced due to the decrease of the drying rate. The droplet is now divided into two regions: the outer porous solid crust at the surface and the inner wet core. The outer diameter is constant during this period while the inner diameter decreases from $R_{i,0}$ to $R_{i,1}$ according to the evaporation which occurs through the inner boundary. This period ends when the moving boundary arrives at the center of the particle, i.e. when the particle is completely dry. It forms a compact particle, an extremely porous medium if the radius of the droplet at the end of the first drying period $R_{d,e}$

$$R_{d,e} > \left(\frac{3m_s}{4 * \pi(1 - \varepsilon)\rho_s} \right)^{1/3}. \quad (3.1)$$

Or it may be a hollow sphere if

$$R_{d,e} = \left(\frac{3m_s}{4 * \pi(1 - \varepsilon)\rho_s} \right)^{1/3}.$$

Figure 3.2 illustrates the three periods of the drying process.

3.3 Mathematical models of the process

In this section we study the change of water mass fraction, solid mass fraction, concentration, temperature of the droplets as well as the aggregation of the nano-sized particles inside the droplets. Here it is assumed that the droplets atomized by the nozzle are spheres with an initial radius R_0 .

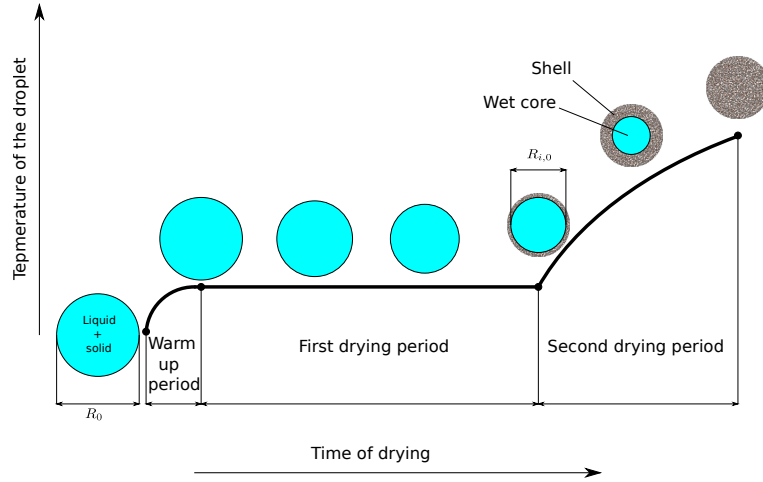


Figure 3.2: Droplet drying periods

3.3.1 Basic variables

Here we introduce some basic variables which are needed in the mathematical model. In a mixture of many substances with total mass m_{tot} , total volume v_{tot} , and total density ρ_{tot} we can define the following quantities.

Mass fraction: This quantity is defined as the ratio of the mass of the component i to the total mass, i.e.

$$X_i = \frac{m_i}{m_{tot}},$$

where

$$m_{tot} = \sum_i m_i.$$

Taking the summation of all components gives

$$\sum_i X_i = \sum_i \frac{m_i}{m_{tot}} = 1.$$

Mass concentration: The concentration of a substance in a mixture is known as the ratio of the mass of the component i to the total volume, i.e.

$$C_i = \frac{m_i}{v_{tot}}. \quad (3.2)$$

Again the summation of the concentrations of all components gives

$$\sum_i C_i = \sum_i \frac{m_i}{v_{tot}} = \frac{m_{tot}}{v_{tot}} = \rho.$$

For a mixture consisting of two components, like water and a binder, the mass fraction of the water is

$$X_l = \frac{m_l}{m_{tot}}, \quad (3.3)$$

3.3. MATHEMATICAL MODELS OF THE PROCESS

while the mass fraction of the binder is given as

$$X_b = \frac{m_b}{m_{tot}}. \quad (3.4)$$

From the above two equations we find that

$$X_l + X_b = \frac{m_l}{m_{tot}} + \frac{m_b}{m_{tot}} = 1, \quad (3.5)$$

where the total mass in this case is equal to the summation of the masses of the both components.

The concentration of the water in the mixture is given as

$$C_l = \frac{m_l}{v_{tot}}. \quad (3.6)$$

The concentration of the binder is

$$C_b = \frac{m_b}{v_{tot}}.$$

The relation between the mass fraction and the concentration can be found as follows.

From equation (3.3) we have

$$m_l = X_l m_{tot}.$$

Substituting into equation (3.6) leads to

$$C_l = \frac{X_l m_{tot}}{v_{tot}}. \quad (3.7)$$

Since the density of the mixture ρ is given as the ratio of the total mass to the total volume of the mixture equation (3.7) can be written in the form

$$C_l = X_l \rho.$$

Similarly we can find that

$$C_b = X_b \rho.$$

3.3.2 Change of the water mass fraction

Due to the evaporation of water from the surface of the droplets the water mass fraction must be changed. This change is given by Fick's law of diffusion in the following partial differential equation which is given in the spherical coordinates

$$\frac{\partial X_l}{\partial t} = \frac{1}{r^2} \frac{\partial}{\partial r} \left(r^2 \gamma_l \frac{\partial X_l}{\partial r} \right), \quad 0 \leq t < \infty, \quad 0 \leq r \leq R(t) \quad (3.8)$$

with the homogeneous Neumann inner boundary condition

$$\frac{\partial X_l}{\partial r} = 0, \text{ at the center of the droplet} \quad (3.9)$$

CHAPTER 3. SPRAY DRYING PROCESS

To find the outer boundary condition we note that the solid mass of the droplet is constant with respect to time, i.e.

$$\frac{dm_b}{dt} = 0.$$

But from equation (3.4) we find

$$m_b = X_b m_{tot}.$$

Substituting into the previous equation we get

$$\frac{d}{dt}(X_b m_{tot}) = 0$$

The total mass of the mixture equals to the multiplication of the density and the total volume, so the the above equation can be written as

$$\frac{d}{dt}(X_b \rho v_{tot}) = 0.$$

Taking into consideration that the density of the liquid and the solid are constant, the above equation gives

$$\frac{d}{dt}(X_b v_{tot}) = 0$$

which can be also written in the following integral form

$$\frac{d}{dt} \int_0^R (X_b 4\pi r^2) dr = 0$$

Dividing both sides by 4π and applying the Leibniz rule yields

$$\int_0^R r^2 \frac{dX_b}{dt} dr + R^2 X_b \frac{dR}{dt} = 0.$$

From equation (3.5) we have $X_b = 1 - X_l$, so the previous equation takes the form

$$- \int_0^R r^2 \frac{dX_l}{dt} dr + R^2 (1 - X_l)_R \frac{dR}{dt} = 0.$$

Using equation (3.8) leads us to the following form

$$\int_0^R \frac{\partial}{\partial r} \left(r^2 \gamma_l \frac{\partial X_l}{\partial r} \right) dr = R^2 (1 - X_l)_R \frac{dR}{dt}.$$

Integrating the left hand side and evaluating the outer boundary we get

$$R^2 \gamma_l \frac{\partial X_l}{\partial r} \Big|_{R=} = R^2 (1 - X_l)_R \frac{dR}{dt}.$$

3.3. MATHEMATICAL MODELS OF THE PROCESS

Dividing the both sides of this expression by $R^2\gamma_l$ gives the outer boundary condition of equation (3.8)

$$\frac{\partial X_l}{\partial r} = \frac{1}{\gamma_l}(1 - X_l)\frac{dR}{dt} \quad \text{at} \quad r = R.$$

The shrinkage of the droplet is represented by the decrease of the outer radius. The change of the outer radius is given by the following expression

$$\frac{dR}{dt} = -\beta\frac{\rho_a}{\rho_l}(Y_{sat} - Y_a). \quad (3.10)$$

See (2.13) for more detail about the derivation of this equation.

In the foregoing equations, r represents the radial coordinate of the droplet, γ_l is the diffusivity of the binder in the water. It is determined as an example by Sloth et al. [79] as

$$\gamma_l = 3.27 \times 10^{-11} \exp(5.97X_l) \quad \text{for trehalose,}$$

and

$$\gamma_l = 1.78 \times 10^{-13} \exp(13.12X_l) \quad \text{for maltodextrin,}$$

β is the mass transfer coefficient, ρ_a is the density of the hot gas, ρ_l is the density of water, Y_{sat} is the adiabatic saturation humidity and Y_a is the moisture content in the hot gas.

3.3.3 Temperature of the droplet

The mass and heat transfer between the droplet and the bulk phase is given by the following ODE, see [55],

$$\frac{d\theta_d}{dt} = \frac{1}{C_{p,l}m_l + C_{p,s}m_s} \left[\alpha(\theta_a - \theta_d)4\pi R^2 - \dot{M}_{ev}(-C_{p,l}\theta_d + \Delta h_{ev} + C_{p,v}\theta_a) \right]. \quad (3.11)$$

The change of the outer radius of the droplet is given again by equation (3.10). The previous equation assumes a uniform temperature of the droplet. For a non-uniform distribution of heat inside the droplet another equation for the energy balance of the droplet can be expressed as follows

$$\rho(C_{p,l}X_l + C_{p,s}X_s)\frac{\partial\theta_d}{\partial t} = \frac{1}{r^2}\frac{\partial}{\partial r} \left(\lambda_d r^2 \frac{\partial\theta_d}{\partial r} \right), \quad 0 \leq r \leq R, \quad (3.12)$$

with the inner boundary condition

$$\frac{\partial\theta_d}{\partial r} = 0, \text{ at the center of the droplet}$$

and the outer moving boundary condition

$$\frac{\partial\theta_d}{\partial r} = \frac{1}{\lambda_d} \left(\alpha(\theta_a - \theta_d) + \lambda_a \rho_l \frac{dR}{dt} \right),$$

where ρ and λ_d are the density and the thermal conductivity of the droplet. For more details about the previous equation the reader is referred to [48].

3.3.4 Study of a population balance model of nano-suspension droplets

One of the most important internal phenomena which take place inside droplets is the aggregation of nano-sized particles contained in these droplets. Due to the aggregation a thin shell appears. This shell turns into a porous medium forming a crust that reduces the evaporation rate. These pores allow the process of diffusion and flow of liquid. The evaporation of the wet core is assumed. The vapor diffuses through the pores into the bulk phase.

In the following mathematical model it is assumed that there is no deformation of the droplet shape, i.e. the droplet remains spherical during the process. The volume of suspended spherical particle ν is taken as an internal coordinate where $\nu \in [0, \infty[$.

The change of the number density n of the suspended nano-sized particles is given in the following population balance equation (PBE), see [63]

$$\frac{\partial n}{\partial t} + \frac{1}{r^2} \frac{\partial}{\partial r} (r^2 \omega n) = \frac{1}{r^2} \frac{\partial}{\partial r} (r^2 \gamma_l \frac{\partial n}{\partial r}) + B_{agg}(n, \nu, r, t) - D_{agg}(n, \nu, r, t), \quad (3.13)$$

where $r \in [0, R]$ and $\nu \in [0, \infty[$.

In the foregoing PBE ω is the local shrinkage rate of control volume. It has a nonzero value $\frac{dR}{dt}$ just at boundary i.e.

$$\omega = \begin{cases} \frac{dR}{dt}, & \text{if } r = R \\ 0, & \text{if } r \neq R \end{cases} \quad (3.14)$$

Also γ_l represents the diffusion coefficient of nano-sized particles in liquid. This coefficient is given as an example according to Nešić and Vodnik as follows

$$\gamma_l = \begin{cases} 10^{-7}, & \text{if } X_l > 0.6 \\ \exp\left(-\frac{28.1 + 282X_l}{1 + 15.47X_l}\right), & \text{if } X_l \leq 0.6. \end{cases} \quad (3.15)$$

The birth term $B_{agg}(n, \nu, r, t)$ and the death term $D_{agg}(n, \nu, r, t)$ are given respectively in the following formulas

$$B_{agg}(n, \nu, r, t) = \frac{1}{2} \int_0^\nu \beta'(u, \nu - u) n(t, r, u) n(t, r, \nu - u) du, \quad (3.16)$$

$$D_{agg}(n, \nu, r, t) = \int_0^\infty \beta'(u, \nu) n(t, r, u) n(t, r, \nu) du. \quad (3.17)$$

The above PBE is accompanied with the homogeneous Neumann boundary condition

$$\frac{\partial n}{\partial r} \Big|_{r=0} = 0 \quad (3.18)$$

and the outer boundary condition

$$-\gamma_l \frac{\partial n}{\partial r} \Big|_{r=R} = 0 \quad (3.19)$$

3.4 Numerical results

In order to solve the ordinary differential equations, the Dormand-Prince method is used. This method is explained in details in Chapter 4. Due to the mass transfer the liquid mass fraction decreases. This is because of the fact that some amount of water is converted into vapor causing a decrease of liquid mass. Consequently the solid mass fraction increases where there is an inverse proportion between the liquid and the solid mass fraction.

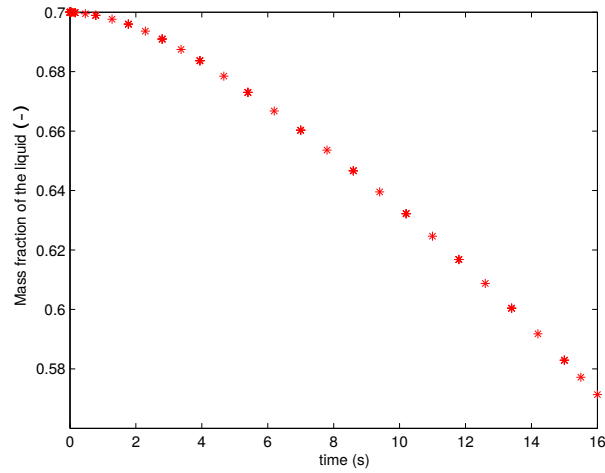


Figure 3.3: Liquid mass fraction of the droplet: $R_0 = 1mm$, $\theta_d = 19^\circ C$, $X_{s,0} = 0.3$, $\theta_a = 178^\circ C$.

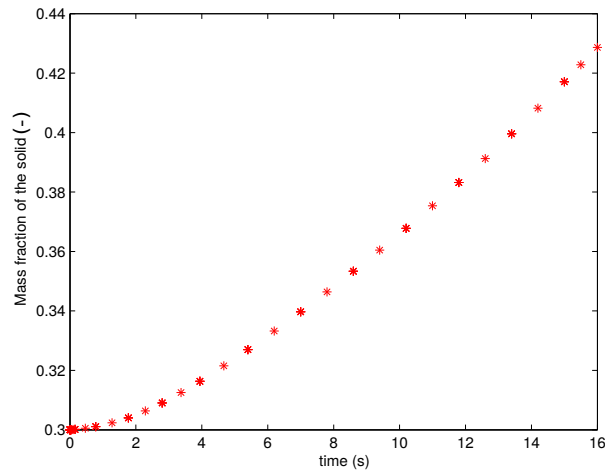


Figure 3.4: Solid mass fraction

Figures 3.3 and 3.4 illustrate the change of the solid and liquid mass fraction during the process. Figures 3.5, 3.6 predict the decrease of the droplet mass along with the decrease

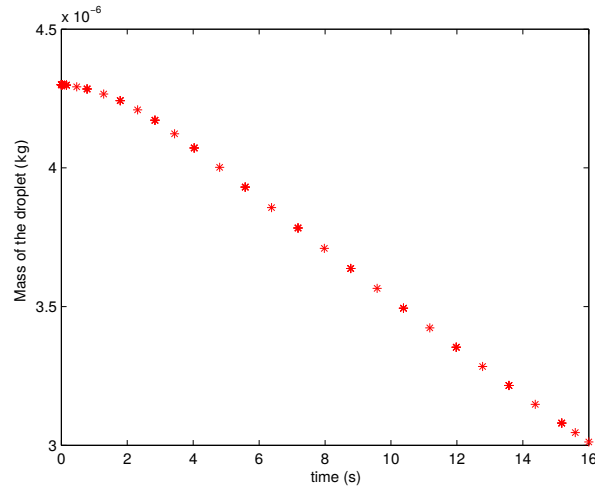


Figure 3.5: The change of the droplet mass

of the droplet radius while Figure 3.7 shows the increase of temperature of the droplet.

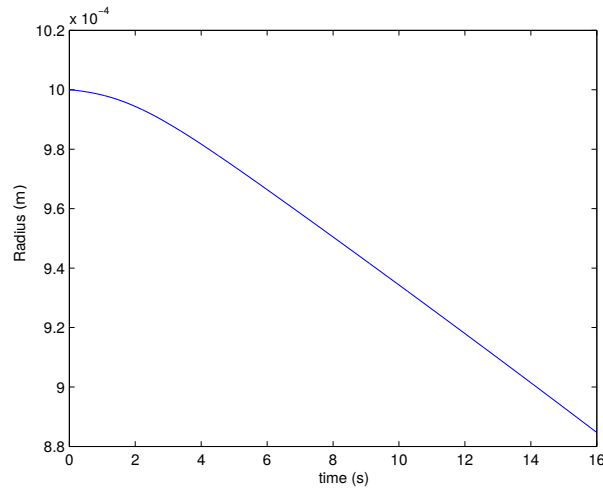


Figure 3.6: Droplet diameter evolution

These results are supported by experimental results. For more details about the experimental results the reader is referred to [6].

In the first drying period the diameter of the droplet decreases until a solid shell is formed at the surface of the droplet. At that point (locking point) the outer diameter remains constant. It is assumed that the locking point is obtained when the solid fraction at the surface of the droplet forms 40% of the mass at the outer diameter of the droplet. In order to determine the locking point equation (3.8) is solved using the local discontinuous Galerkin method of order $k = 1$.

Figure 3.8 shows the decrease of the liquid mass fraction from its initial value $X_l = 90\%$

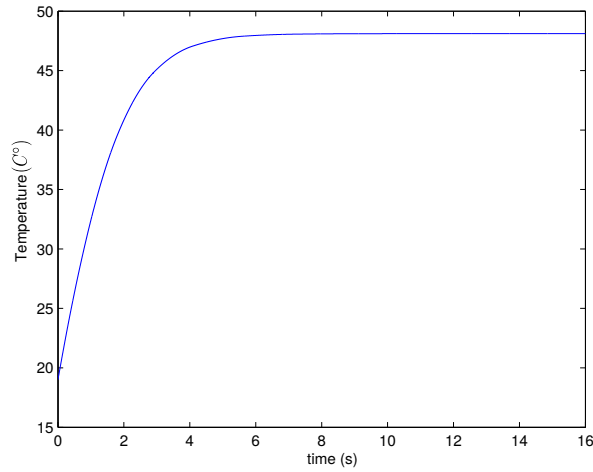
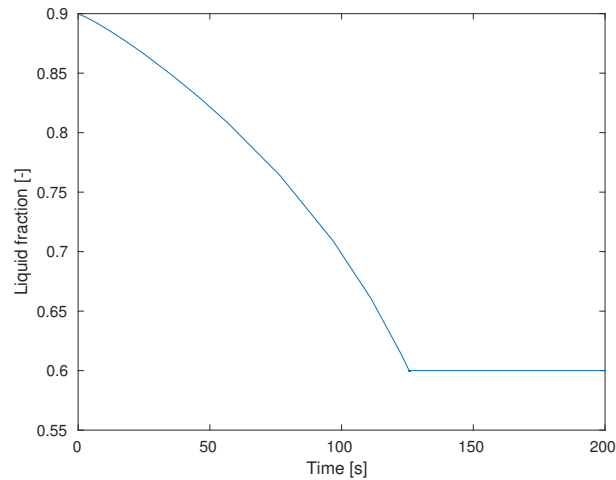


Figure 3.7: Temperature of the droplet


 Figure 3.8: Droplet mass fraction with solid mass fraction of 10%, $R_0 = 0.75mm$, $\theta_d = 19^\circ C$, $\theta_a = 60^\circ C$.

until it reaches the locking point with the value $X_l = 60\%$ at the surface of the droplet. Unlike the liquid mass fraction the solid mass fraction increases from $X_b = 10\%$ until it reaches the value $X_b = 40\%$ as seen in Figure 3.9. The outer radius of the droplet decreases from its initial size $R_0 = 0.75mm$ until it reaches the locking point at $t \simeq 126s$ where it stays constant, see Figure 3.10.

Figures 3.11 and 3.12 show the decrease and the increase of the liquid and the solid mass fractions for different initial values of the solid mass fraction with respect to time, while Figure 3.13 shows the decrease of the outer radius until it reaches the locking point. For a pure water droplet, i.e. $X_l = 100\%$ and $X_b = 0\%$ the liquid and the solid mass fractions stay constant until the droplet evaporates completely, i.e. the radius tends to

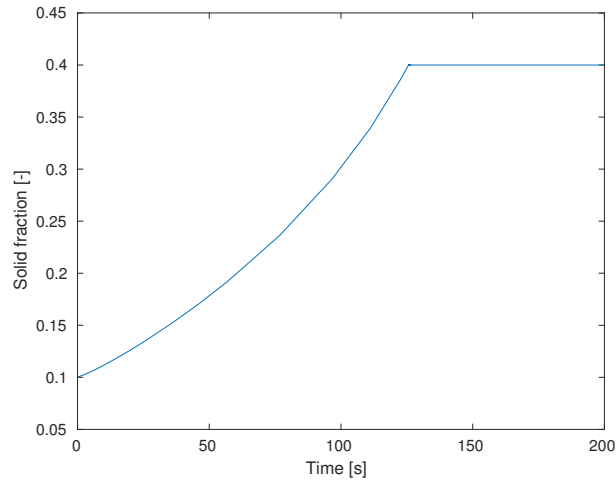


Figure 3.9: Droplet mass fraction with solid mass fraction of 10%, $R_0 = 0.75mm$, $\theta_d = 19^\circ C$, $\theta_a = 60^\circ C$.

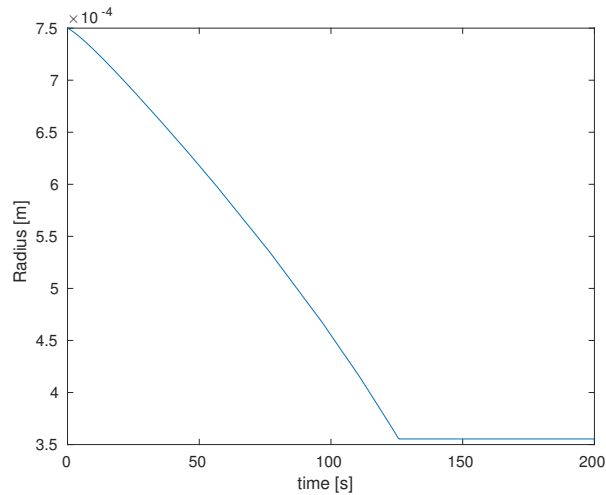


Figure 3.10: Radius of the droplet with solid mass fraction of 10%, $R_0 = 0.75mm$, $\theta_d = 19^\circ C$, $\theta_a = 60^\circ C$.

zero. These figures show that the droplets with higher initial solid mass fraction solidifies faster and at larger droplet size than the droplets with lower initial solid mass fraction.

The influence of the temperature of the bulk phase can be seen in Figures 3.14, 3.15 and 3.16. These figures show that the higher the temperature is, the faster solidification takes place.

3.5. VELOCITY DISTRIBUTION AND DROPLET MOVEMENT WITHIN THE NOZZLE SPRAY CONE

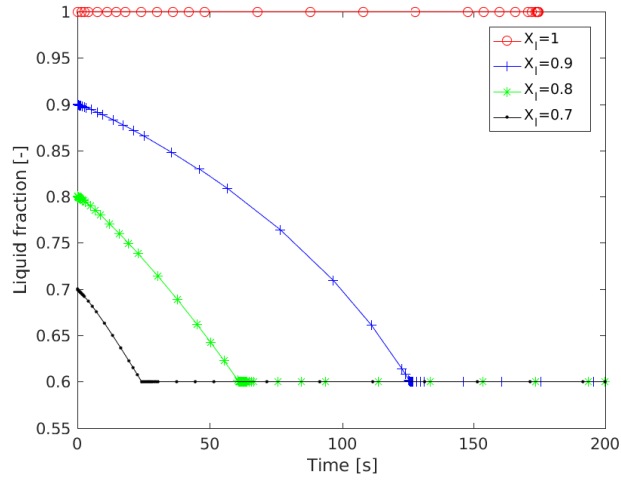


Figure 3.11: Liquid mass fraction with different initial values, $R_0 = 0.75mm$, $\theta_d = 19^\circ C$, $\theta_a = 60^\circ C$.

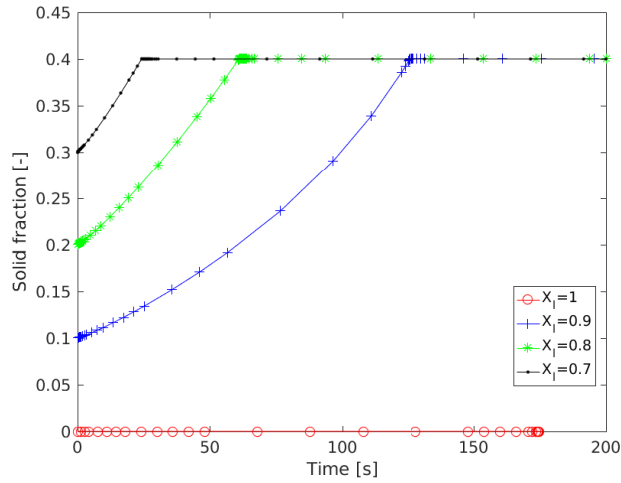


Figure 3.12: Solid mass fraction with different initial values, $R_0 = 0.75mm$, $\theta_d = 19^\circ C$, $\theta_a = 60^\circ C$.

3.5 Velocity distribution and droplet movement within the nozzle spray cone

The liquid to be dried is atomized into small droplets and sprayed conically within the chamber. These droplets are affected by some forces. These forces are the gravity force F_{gr} , the lifting force F_{li} and the drag force F_{dr} . The momentum of the droplet is given as [18]

$$\frac{d}{dt} (M_{drop} v_{drop}) = \sum \underline{F} = \underline{F}_{gr} + \underline{F}_{li} + c \underline{F}_{dr}.$$

CHAPTER 3. SPRAY DRYING PROCESS

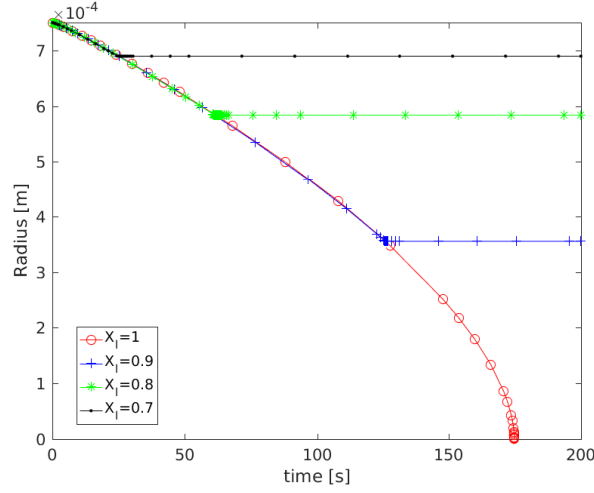


Figure 3.13: Radius of the droplet with different initial values of the liquid mass fraction with $R_0 = 0.75mm$, $\theta_d = 19^\circ C$, $\theta_a = 60^\circ C$.

Here M_{drop} , v_{drop} are the mass and the velocity of the droplet respectively. The constant c takes the values $\{-1, +1\}$. If the droplet is moving towards the top of the bed then c has the value (+1) otherwise it has the value (-1), see Fig(3.17) . Projecting these vectors onto the $z - axis$ leads to

$$\frac{d}{dt} (M_{drop} v_{drop,z}) = F_{gr} - F_{li} + c F_{dr}. \quad (3.20)$$

The mass of the droplet is given as the multiplication of the volume V_{drop} and the density ρ_{drop} of the droplet i.e. $M_{drop} = V_{drop} \rho_{drop}$. According to the evaporation, the mass of the droplet is changing during the process time. This change can be expressed as

$$\frac{dM_{drop}}{dt} = \frac{d}{dt} (\rho_{drop} V_{drop}) = \frac{d}{dt} \left(\rho_{drop} \frac{4}{3} \pi d_{drop}^3 \right) = 4\pi \rho_{drop} d_{drop}^2 \frac{dd_{drop}}{dt} \quad (3.21)$$

Equation (3.20) can be written as

$$M_{drop} \frac{dv_{drop,z}}{dt} + v_{drop,z} \frac{dM_{drop}}{dt} = F_{gr} - F_{li} + c F_{dr}.$$

Making use of (3.21) we can write

$$\frac{dv_{drop,z}}{dt} = \frac{F_{gr} - F_{li} + c F_{dr}}{M_{drop}} - \frac{3v_{drop,z}}{4\pi d_{drop}^3 \rho_{drop}} 4\pi \rho_{drop} d_{drop}^2 \frac{dd_{drop}}{dt},$$

or

$$\frac{dv_{drop,z}}{dt} = \frac{F_{gr} - F_{li} + c F_{dr}}{\rho_{drop} V_{drop}} - \frac{3v_{drop,z}}{d_{drop}} \frac{dd_{drop}}{dt}.$$

3.5. VELOCITY DISTRIBUTION AND DROPLET MOVEMENT WITHIN THE NOZZLE SPRAY CONE

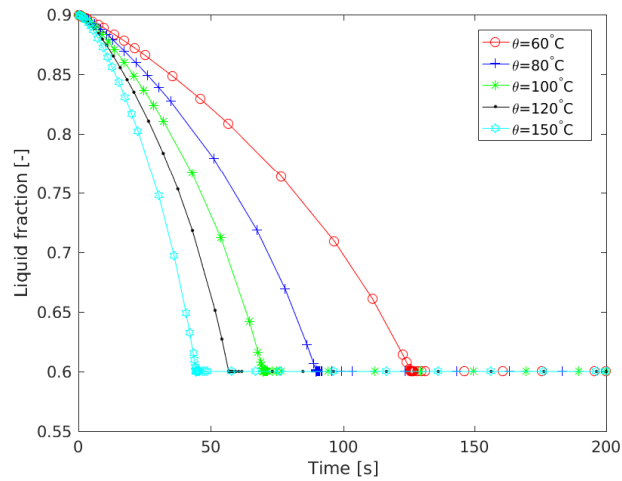


Figure 3.14: Liquid mass fraction with different air temperatures, $R_0 = 0.75mm$, $\theta_d = 19^\circ C$.

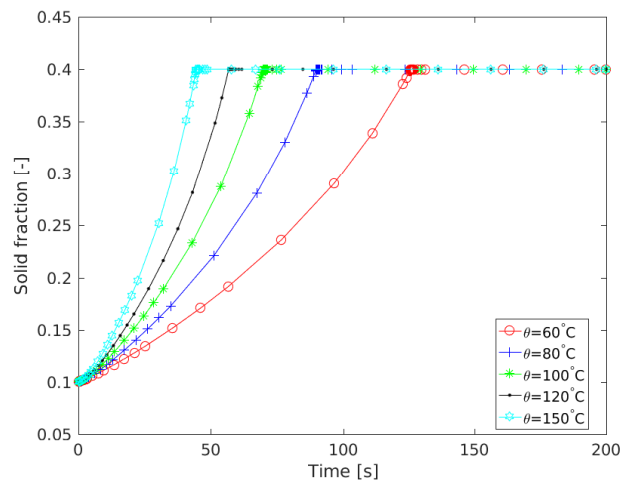


Figure 3.15: Solid mass fraction with different air temperatures, $R_0 = 0.75mm$, $\theta_d = 19^\circ C$.

CHAPTER 3. SPRAY DRYING PROCESS

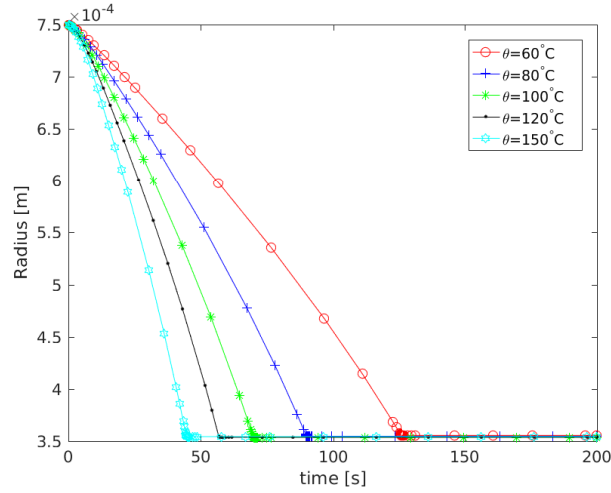


Figure 3.16: Radius of the droplet with different air temperature $R_0 = 0.75mm$, $\theta_d = 19^\circ C$.

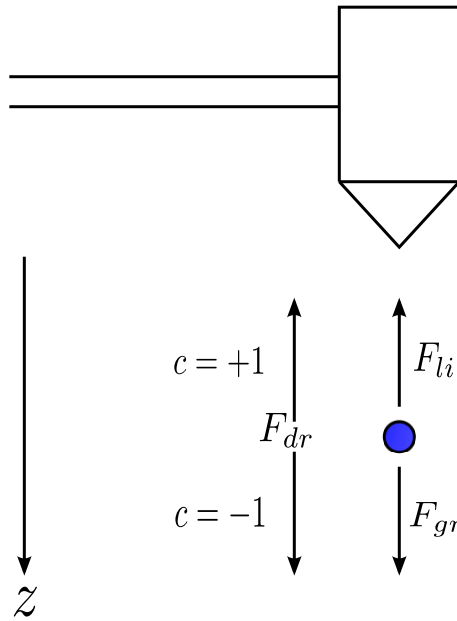


Figure 3.17: Forces affecting a single droplet

Reichardt [65] suggested that the velocity profile within the jet can be found using the Gauss error function

$$\omega_{g,nozz} = \exp(-\ln 2 \varrho^2) \omega_{g,nozz,center}. \quad (3.22)$$

Here $\omega_{g,center}$ is the centerline velocity and ϱ is the radial coordinate of the jet given by

$$\varrho = \frac{y}{r_a}, \quad (3.23)$$

3.5. VELOCITY DISTRIBUTION AND DROPLET MOVEMENT WITHIN THE NOZZLE SPRAY CONE

where y is the horizontal droplet position and r_a is the radius of the core spray where the gas velocity in the open jet equals 50% of the centerline velocity [18]. In Figure 3.18, the

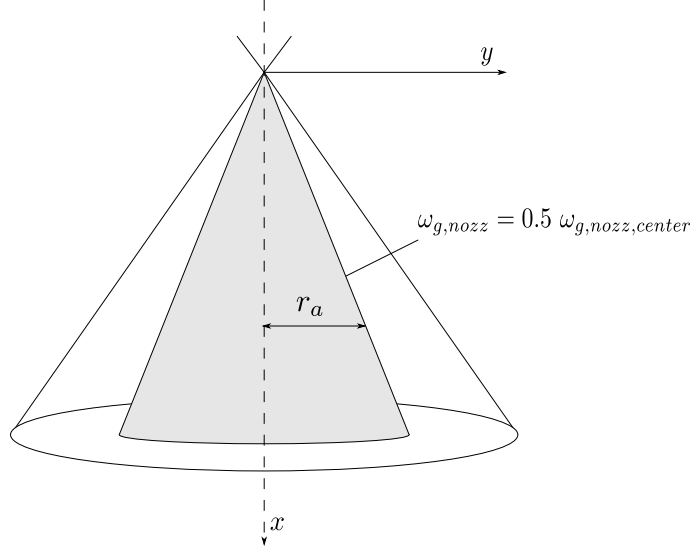


Figure 3.18: Scheme of the nozzle spray cone

shaded area represents the core of the nozzle gas cone according to Truckenbrodt [85]. To find the centerline velocity, the principle of momentum conservation along the jet is taken into consideration, see Malmström [47], [94].

Let A be the outlet area, d_{Nozz} the radius of the nozzle orifice, ω_0 the uniform outlet velocity. Then the initial momentum is given as

$$M_0 = \rho_a A \omega_0^2 = \rho_a \pi d_{Nozz}^2 \omega_0^2.$$

The momentum M_x at any distance x from the nozzle orifice is given by the following formula

$$M_x = 2\pi\rho_a \int_0^\infty \omega_{g,nozz}^2 y dy.$$

Due to the principle of momentum conservation we can write

$$M_0 = M_x,$$

or

$$\rho_a \pi d_{Nozz}^2 \omega_0^2 = 2\pi\rho_a \int_0^\infty \omega_{g,nozz}^2 y dy.$$

After some cancellations we get

$$d_{Nozz}^2 \omega_0^2 = 2 \int_0^\infty \omega_{g,nozz}^2 y dy.$$

CHAPTER 3. SPRAY DRYING PROCESS

Making use of equations (3.22), (3.23) and integrating the right hand side the centerline velocity $\omega_{g,center}$ can be written in the form

$$\omega_{g,center} = \frac{\sqrt{2 \ln 2}}{r_a} d_{Nozz} \omega_0.$$

Chapter 4

Numerical Scheme and Discretization of Hyperbolic and Parabolic Systems

4.1 Introduction

In this chapter we introduce a numerical method called discontinuous Galerkin method (DGM). This method has been used first by Reed and Hill [64] to solve the neutron transport equation which is a partial differential equation of the hyperbolic type. This method then was developed and modified to also solve parabolic and elliptic problems. It became very popular and is used very often to solve linear and nonlinear systems of PDE's. Several publications were made considering discontinuous Galerkin method, for instance see [37], [19], [68], [12], [90], [83], [23], [24], [25]. The discontinuous Galerkin method can be represented as a class of the finite element methods (FEM).

In this method, discontinuous piecewise polynomials for both the numerical solution and the test functions are used. The discontinuous Galerkin method has some very important properties such as good stability as well as accuracy, the possibility of handling complicated geometries, and the possibility of increasing the accuracy without taking finer meshes.

In the second section of this chapter we will consider the 1D hyperbolic equation and explain the discretization of space using the DGM. The local discontinuous Galerkin method for 1D problems of the second order diffusion equation is considered in the third section. Section 4 studies 2D hyperbolic problems, while a 2D parabolic equation is introduced in the fifth section. In Section 6, numerical methods are introduced to solve the resulting ordinary differential equations. Finally Section 7 introduces the methods which are used to approximate integrals. Simple examples for every case are presented in Section 8.

This chapter includes some materials drawn from Cockburn and Shu [15], Cockburn et al. [13].

4.2 Spatial discretization of a scalar conservation law in one space dimension

In this section we will consider the following simple 1D hyperbolic equation

$$\partial_t u + \partial_x f(u) = 0, \quad \text{in }]0, 1[\times]0, T[, \quad (4.1)$$

with the initial condition

$$u(x, 0) = u_0, \quad \text{for all } x \in]0, 1[, \quad (4.2)$$

and periodic boundary condition.

4.2.1 The weak formulation

For the spatial discretization we take a partition $\left\{ x_{i+\frac{1}{2}} \right\}_{i=0}^N$ of the domain $\Omega =]0, 1[$, where $x_{\frac{1}{2}} = 0$ and $x_{N+\frac{1}{2}} = 1$. This partition consists of N non-overlapping cells $I_i =]x_{i-\frac{1}{2}}, x_{i+\frac{1}{2}}[$. The length of the cell I_i is denoted by

$$\Delta x_i = x_{i+\frac{1}{2}} - x_{i-\frac{1}{2}}.$$

The maximum length Δx is given as

$$\Delta x = \max_{1 \leq i \leq N} \Delta x_i.$$

The midpoint of a cell I_i is

$$x_i = \frac{x_{i-1/2} + x_{i+1/2}}{2}.$$

The approximate solution u_h is taken from the finite element space

$$\Lambda_h = \left\{ s \in L^1(]0, 1[); s|_{I_i} \in P^k(I_i); i = 1, \dots, N \right\},$$

where

$$P^k = \{p; p \text{ is a polynomial of degree at most } k \text{ on } I\}.$$

One of the most important differences between the classical finite element method and the discontinuous Galerkin method is that in the latter the functions of the finite element space Λ_h have the possibility to have jumps at the interfaces $x_{i+\frac{1}{2}}$.

For a function $v_h \in \Lambda_h$ we introduce $v_h(x_{i-\frac{1}{2}}^+)$ to be the left hand limit obtained by considering values inside I_i , whereas $v_h(x_{i-\frac{1}{2}}^-)$ is the right hand limit on I_{i-1} .

The weak formulation can be constructed by multiplying the equations (4.1), (4.2) by an arbitrary test function $v_h \in \Lambda_h$ and replacing the exact solution u by the approximate solution u_h and finally by integrating over every cell I_i as follows

4.2. SPATIAL DISCRETIZATION OF A SCALAR CONSERVATION LAW IN ONE SPACE DIMENSION

$$\int_{I_i} \partial_t u_h(x, t) v_h(x) dx + \int_{I_i} \partial_x f(u_h(x, t)) v_h(x) dx = 0, \quad (4.3)$$

$$\int_{I_i} u(x, 0) v_h(x) dx = \int_{I_i} u_0 v_h(x) dx. \quad (4.4)$$

For the main equation we integrate the second term by parts. Consequently we get

$$\begin{aligned} & \int_{I_i} \partial_t u_h(x, t) v_h(x) dx - \int_{I_i} f(u_h(x, t)) \partial_x v_h(x) dx \\ & + f(u_h(x_{i+\frac{1}{2}}, t)) v_h(x_{i+\frac{1}{2}}^-) - f(u_h(x_{i-\frac{1}{2}}, t)) v_h(x_{i-\frac{1}{2}}^+) = 0. \end{aligned}$$

The function $f(u_h(x_{i+\frac{1}{2}}, t))$ is then replaced by a numerical flux $\hat{f}(u)_{i+\frac{1}{2}}(t)$ given by

$$\hat{f}(u)_{i+\frac{1}{2}}(t) = \hat{f}(u(x_{i+\frac{1}{2}}^-, t), u(x_{i+\frac{1}{2}}^+, t)).$$

The conservative formulation now has the following form

$$\begin{aligned} & \int_{I_i} \partial_t u_h(x, t) v_h(x) dx - \int_{I_i} f(u_h(x, t)) \partial_x v_h(x) dx \\ & + \hat{f}(u_h)_{i+\frac{1}{2}}(t) v_h(x_{i+\frac{1}{2}}^-) - \hat{f}(u_h)_{i-\frac{1}{2}}(t) v_h(x_{i-\frac{1}{2}}^+) = 0, \end{aligned} \quad (4.5)$$

$$\int_{I_i} u(x, 0) v_h(x) dx = \int_{I_i} u_0 v_h(x) dx. \quad (4.6)$$

4.2.2 Diagonalizing the mass matrix

The approximate solution u_h regarding the element I_i is taken as

$$u_h(x, t) = \sum_{r=0}^k u_i^r(t) \Psi_r(x) \quad \text{for } x \in I_i,$$

where

$$\Psi_r(x) = P_r \left(\frac{2(x - x_i)}{\Delta x_i} \right).$$

Here P_r is taken to be the Legendre polynomial given as

$$\begin{aligned} P_r(x) &= \frac{1}{2^r r!} \frac{d^r}{dx^r} [(x^2 - 1)^r] \\ &= \frac{1}{2^r} \sum_{k=0}^r \binom{r}{k}^2 (x - 1)^{r-k} (x + 1)^k \end{aligned} \quad (4.7)$$

CHAPTER 4. NUMERICAL SCHEME AND DISCRETIZATION OF HYPERBOLIC AND PARABOLIC SYSTEMS

The Legendre polynomials for $n = 0, 1, 2, 3$ are

$$P_0(x) = 1, \quad P_1(x) = x, \quad P_2(x) = \frac{1}{2}(3x^2 - 1), \quad P_3(x) = \frac{1}{2}(5x^3 - 3x)$$

respectively. Figure 4.4 shows the Legendre polynomials which are used as the basis

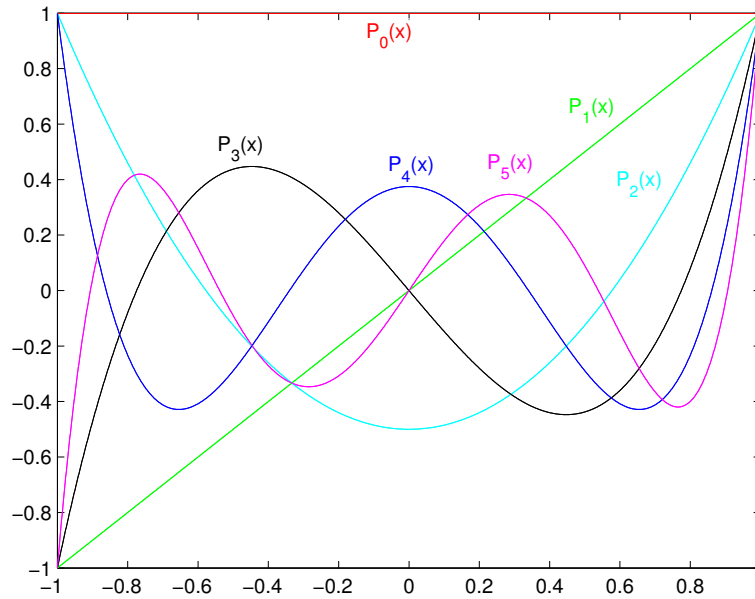


Figure 4.1: Legendre polynomials

functions. These polynomials have a very important property which is their orthogonality with respect to the L^2 inner product on $[-1, +1]$, i.e.

$$\int_{-1}^{+1} P_r(z)P_s(z)dz = \left(\frac{2}{2r+1}\right) \delta_{rs}, \quad (4.8)$$

where

$$\delta_{rs} = \begin{cases} 0, & \text{if } r \neq s \\ 1, & \text{if } r = s \end{cases}$$

is the Kronecker delta. From equation (4.7) we can find

$$P_n(1) = 1, \quad P_n(-1) = (-1)^n. \quad (4.9)$$

The test function $v_h(x)$ is taken as follows

$$v_h(x) = \Psi_s(x).$$

4.2. SPATIAL DISCRETIZATION OF A SCALAR CONSERVATION LAW IN ONE SPACE DIMENSION

Now we consider the first term of equation (4.5)

$$\begin{aligned} \int_{I_i} \partial_t u_h(x, t) v_h(x) dx &= \int_{x_{i-\frac{1}{2}}}^{x_{i+\frac{1}{2}}} \partial_t \left(\sum_{r=0}^k u_i^r(t) \Psi_r(x) \right) \Psi_s(x) dx \\ &= \partial_t \sum_{r=0}^k u_i^r(t) \int_{x_{i-\frac{1}{2}}}^{x_{i+\frac{1}{2}}} \Psi_r(x) \Psi_s(x) dx. \end{aligned}$$

In order to exploit the orthogonality property of the Legendre polynomials, we need to transform the domain of the integral from $[x_{i-\frac{1}{2}}, x_{i+\frac{1}{2}}]$ to $[-1, +1]$. Therefore we use the following transformation $z = Ax + B$ and solve the system

$$\begin{aligned} -1 &= Ax_{i-\frac{1}{2}} + B \\ +1 &= Ax_{i+\frac{1}{2}} + B. \end{aligned}$$

After solving this system we get the following transformation

$$z = \frac{2(x - x_i)}{\Delta x_i}.$$

The first term of equation (4.5) leads to the formula

$$\begin{aligned} \int_{I_i} \partial_t u_h(x, t) v_h(x) dx &= \partial_t \sum_{r=0}^k u_i^r(t) \int_{x_{i-\frac{1}{2}}}^{x_{i+\frac{1}{2}}} \Psi_r(x) \Psi_s(x) dx \\ &= \partial_t \sum_{r=0}^k u_i^r(t) \frac{\Delta x_i}{2} \int_{-1}^{+1} P_r(z) P_s(z) dz \\ &= \partial_t \sum_{r=0}^k u_i^r(t) \frac{\Delta x_i}{2} \frac{2}{2s+1} \delta_{rs} \\ &= \frac{\Delta x_i}{2s+1} \partial_t u_i^s(t). \end{aligned}$$

In a similar way, the left hand side of (4.6) can be written as

$$\int_{I_i} u(x, 0) v_h(x) dx = \frac{\Delta x_i}{2s+1} u_i^s(0).$$

The values of the test function $v_h(x)$ at the boundaries $x_{i-\frac{1}{2}}$ and $x_{i+\frac{1}{2}}$ of the cell I_i can be found as follows

$$v_h(x_{i-\frac{1}{2}}^+) = \Psi_s(x_{i-\frac{1}{2}}) = P_s \left(\frac{2(x_{i-\frac{1}{2}} - x_i)}{\Delta x_i} \right) = P_s(-1) = (-1)^s,$$

CHAPTER 4. NUMERICAL SCHEME AND DISCRETIZATION OF HYPERBOLIC AND PARABOLIC SYSTEMS

$$v_h(x_{i+\frac{1}{2}}^-) = \Psi_s(x_{i+\frac{1}{2}}) = P_s \left(\frac{2(x_{i+\frac{1}{2}} - x_i)}{\Delta x_i} \right) = P_s(+1) = +1.$$

Now the conservative formulation can be written as

For $i = 1, \dots, N$ and for $s = 0, \dots, k$

$$\begin{aligned} \frac{\partial u_i^s(t)}{\partial t} &= \frac{2s+1}{\Delta x_i} \int_{I_i} f(u_h(x, t)) \partial_x \Psi_s(x) dx \\ &\quad - \frac{2s+1}{\Delta x_i} \left\{ \hat{f}(u_h)_{i+\frac{1}{2}}(t) - (-1)^s \hat{f}(u_h)_{i-\frac{1}{2}}(t) \right\}. \end{aligned} \quad (4.10)$$

$$u_i^s(0) = \frac{2s+1}{\Delta x_i} \int_{I_i} u_0 \Psi_s(x) dx. \quad (4.11)$$

This shows that the spatial discretization leads to the following system of ordinary differential equation

$$\frac{d}{dt} u_h = M(u_h), \quad (4.12)$$

$$u_h(0) = u_h(x, 0). \quad (4.13)$$

In a special case, if $u_0 = C$ where C is a constant, then for (4.11) we can write

$$\begin{aligned} u_i^s(0) &= \frac{2s+1}{\Delta x_i} \int_{I_i} C \Psi_s(x) dx \\ &= \frac{2s+1}{\Delta x_i} C \int_{I_i} P_0 \left(\frac{2(x-x_i)}{\Delta x_i} \right) P_s \left(\frac{2(x-x_i)}{\Delta x_i} \right) dx \\ &= \frac{2s+1}{\Delta x_i} C \frac{\Delta x_i}{2} \int_{-1}^{+1} P_0(z) P_s(z) dz \\ &= \frac{2s+1}{2} C \frac{2}{2s+1} \delta_{0s} \\ &= C \delta_{0s} = \begin{cases} C, & \text{if } s = 0 \\ 0, & \text{otherwise} \end{cases} \end{aligned}$$

4.2.3 Numerical flux

The boundary flux $f(u_h(x_{i+\frac{1}{2}}, t))$ is approximated by the numerical flux $\hat{f}(u)_{i+\frac{1}{2}}(t)$ which can be chosen to be one of the following numerical schemes

4.2. SPATIAL DISCRETIZATION OF A SCALAR CONSERVATION LAW IN ONE SPACE DIMENSION

- The Lax-Friedrichs scheme:

$$\hat{f}(u_{i-\frac{1}{2}}, u_{i+\frac{1}{2}}) = \frac{1}{2} \left\{ f(u_{i-\frac{1}{2}}) + f(u_{i+\frac{1}{2}}) - \alpha(u_{i+\frac{1}{2}} - u_{i-\frac{1}{2}}) \right\},$$

$$\alpha = \max_u |f'(u)|.$$

- The local Lax-Friedrichs scheme:

$$\hat{f}(u_{i-\frac{1}{2}}, u_{i+\frac{1}{2}}) = \frac{1}{2} \left\{ f(u_{i-\frac{1}{2}}) + f(u_{i+\frac{1}{2}}) - \alpha(u_{i+\frac{1}{2}} - u_{i-\frac{1}{2}}) \right\},$$

$$\alpha = \max_{(u_{i-\frac{1}{2}}, u_{i+\frac{1}{2}})} |f'(u)|.$$

- The Engquist-Osher scheme:

$$\hat{f}(u_{i-\frac{1}{2}}, u_{i+\frac{1}{2}}) = f^+(u_{i-\frac{1}{2}}) + f^-(u_{i+\frac{1}{2}}) + f(0),$$

where

$$f^+(u) = \int_0^u \max(f'(u), 0) du,$$

$$f^-(u) = \int_0^u \min(f'(u), 0) du.$$

- The Roe scheme:

$$\hat{f}(u_{i-\frac{1}{2}}, u_{i+\frac{1}{2}}) = \begin{cases} f(u_{i-\frac{1}{2}}), & \text{if } \alpha_i \geq 0, \\ f(u_{i+\frac{1}{2}}), & \text{if } \alpha_i < 0, \end{cases}$$

where

$$\alpha_i = \frac{f(u_{i+\frac{1}{2}}) - f(u_{i-\frac{1}{2}})}{u_{i+\frac{1}{2}} - u_{i-\frac{1}{2}}}.$$

- The Godunov scheme:

$$\hat{f}(u_{i-\frac{1}{2}}, u_{i+\frac{1}{2}}) = \begin{cases} \min_{u_{i-\frac{1}{2}} \leq u \leq u_{i+\frac{1}{2}}} f(u), & \text{if } u_{i-\frac{1}{2}} \leq u_{i+\frac{1}{2}}, \\ \max_{u_{i-\frac{1}{2}} \geq u \geq u_{i+\frac{1}{2}}} f(u), & \text{if } u_{i-\frac{1}{2}} > u_{i+\frac{1}{2}}. \end{cases} \quad (4.14)$$

In the linear case where $f(u) = Cu$, all these numerical schemes are identical and have the flux

$$\hat{f}(u_{i-\frac{1}{2}}, u_{i+\frac{1}{2}}) = \begin{cases} Cu_{i-\frac{1}{2}}, & \text{if } C \geq 0, \\ Cu_{i+\frac{1}{2}}, & \text{if } C < 0. \end{cases}$$

CHAPTER 4. NUMERICAL SCHEME AND DISCRETIZATION OF HYPERBOLIC AND PARABOLIC SYSTEMS

In the discontinuous Galerkin method, the approximate solution u_h can be discontinuous at the boundaries of the cell. The fluxes at these boundaries depend on the following left and right limits [42] of u

$$u_{i+\frac{1}{2}}^- = \lim_{x \rightarrow x_{i+\frac{1}{2}}^-} u(x, t) \quad (\text{left}), \quad u_{i+\frac{1}{2}}^+ = \lim_{x \rightarrow x_{i+\frac{1}{2}}^+} u(x, t) \quad (\text{right}).$$

Figure 4.6 shows the jump across the boundary $x_{i-\frac{1}{2}}$ of the cell I_i . These fluxes are given in the following formulas [14]

$$u_{i+\frac{1}{2}}^- = \sum_{r=0}^k u_i^r(t) \Psi_r(x)|_{x_{i+\frac{1}{2}}}, \quad u_{i-\frac{1}{2}}^+ = \sum_{r=0}^k u_i^r(t) \Psi_r(x)|_{x_{i-\frac{1}{2}}}.$$

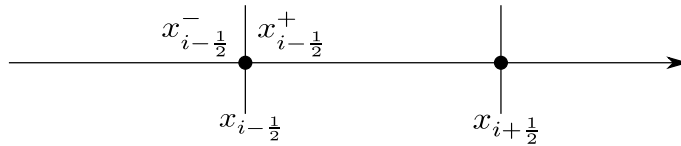


Figure 4.2: The jump across the boundary $x_{i-\frac{1}{2}}$

4.2.4 Error estimation

For the linear case, the following theorem holds [13].

Theorem 4.2.1. *Suppose that the initial condition u_0 belongs to $H^{k+1}([0, 1])$. Then we have*

$$\|u - u_h\|_{L^2(0,1)} \leq C' |u_0|_{H^{k+1}([0,1])} (\Delta x)^{k+\frac{1}{2}},$$

where C' depends on k , $|C|$, and T .

If the initial condition u_0 belongs to $H^{k+2}([0, 1])$. Then we have

$$\|u - u_h\|_{L^2(0,1)} \leq C' |u_0|_{H^{k+2}([0,1])} (\Delta x)^{k+1}.$$

Proof. See [13]. □

4.3 The local discontinuous Galerkin method for one dimensional second order diffusion problems

In this section we consider a one dimensional convection diffusion problem of the form

$$\partial_t u + \partial_x f(u) - (A(u)u_x)_x = 0, \quad \text{in }]0, 1[\times]0, T[, \quad (4.15)$$

4.3. THE LOCAL DISCONTINUOUS GALERKIN METHOD FOR ONE DIMENSIONAL SECOND ORDER DIFFUSION PROBLEMS

with the initial condition

$$u(x, 0) = u_0, \quad \text{for all } x \in]0, 1[. \quad (4.16)$$

This section includes material drawn from [13], [15], [77]. Before we proceed with our problem we introduce the following notations

$$[Q] = Q^+ - Q^-, \quad Q_{i+\frac{1}{2}}^+ = Q(x_{i+\frac{1}{2}}^+), \quad Q_{i+\frac{1}{2}}^- = Q(x_{i+\frac{1}{2}}^-).$$

For the system (4.15) and (4.16) we insert the variables

$$q = \sqrt{A(u)} \partial_x u, \quad S(u) = \int^u \sqrt{A(z)} dz.$$

Making use of these new variables our system (4.15) and (4.16) can be rewritten in the form

$$\partial_t u + \partial_x \left(f(u) - \sqrt{A(u)} q \right) = 0, \quad \text{in }]0, 1[\times]0, T[\quad (4.17)$$

$$q - \partial_x S(u) = 0, \quad \text{in }]0, 1[\times]0, T[\quad (4.18)$$

$$u(x, 0) = u_0, \quad \text{for all } x \in]0, 1[. \quad (4.19)$$

Note that the system (4.18) is not a hyperbolic system. The second equation also does not include the time derivative.

4.3.1 The weak formulation

As we did in the previous section we take a partition $\left\{ x_{i+\frac{1}{2}} \right\}_{i=0}^N$ for the interval $]0, 1[$ consisting of non-overlapping elements $I_i =]x_{i-\frac{1}{2}}, x_{i+\frac{1}{2}}[$. Now we set

$$\Delta x_i = x_{i+\frac{1}{2}} - x_{i-\frac{1}{2}}.$$

The center of a cell I_i is

$$x_i = \frac{x_{i-1/2} + x_{i+1/2}}{2}.$$

To discretize in space we multiply (4.17), (4.18) and (4.19) respectively by arbitrary test functions $v_{h,u}$, $v_{h,q}$ and $v_{h,c}$ from the finite element space

$$\Lambda_h = \left\{ s \in L^1(]0, 1[); s|_{I_i} \in P^k(I_i); i = 1, \dots, N \right\},$$

where

$$P^k = \{p; p \text{ is a polynomial of degree at most } k \text{ in } I\}.$$

Then we replace the exact solution (u, q) by the approximate solution (u_h, q_h) and integrate over every element I_i for $i = 1, \dots, N$ as follows

$$\int_{I_i} \partial_t u_h(x, t) v_{h,u}(x) dx + \int_{I_i} \partial_x \left(f(u_h) - \sqrt{A(u_h)} q_h(x, t) \right) v_{h,u}(x) dx = 0, \quad (4.20)$$

CHAPTER 4. NUMERICAL SCHEME AND DISCRETIZATION OF HYPERBOLIC AND PARABOLIC SYSTEMS

$$\int_{I_i} q_h(x, t) v_{h,q}(x) dx - \int_{I_i} \partial_x S(u_h) v_{h,q}(x) dx = 0, \quad (4.21)$$

$$\int_{I_i} u_h(x, 0) v_{h,c}(x) dx = \int_{I_i} u_0 v_{h,c}(x) dx. \quad (4.22)$$

Now we set $f(u_h) - \sqrt{A(u_h)} q_h(x, t) = H_h$ and integrate the second term of (4.20) and (4.21) by parts. This leads to the following system

$$\begin{aligned} & \int_{I_i} \partial_t u_h(x, t) v_{h,u}(x) dx - \int_{I_i} H_h(u_h(x, t), q_h(x, t)) \partial_x v_{h,u}(x) dx \\ & + H_h(u_h(x_{i+\frac{1}{2}}, t), q_h(x_{i+\frac{1}{2}}, t)) v_{h,u}(x_{i+\frac{1}{2}}^-) - H_h(u_h(x_{i-\frac{1}{2}}, t), q_h(x_{i-\frac{1}{2}}, t)) v_{h,u}(x_{i-\frac{1}{2}}^+) = 0, \end{aligned} \quad (4.23)$$

$$\begin{aligned} & \int_{I_i} q_h(x, t) v_{h,q}(x) dx + \int_{I_i} S(u(x, t)) \partial_x v_{h,q}(x) dx \\ & - S(u_h(x_{i+\frac{1}{2}}, t)) v_{h,q}(x_{i+\frac{1}{2}}^-) + S(u_h(x_{i-\frac{1}{2}}, t)) v_{h,q}(x_{i-\frac{1}{2}}^+) = 0 \end{aligned} \quad (4.24)$$

$$\int_{I_i} u_h(x, 0) v_{h,c}(x) dx = \int_{I_i} u_0 v_{h,c}(x) dx. \quad (4.25)$$

Since the functions u_h and q_h are discontinuous at the boundaries of every cell, the functions $H_h(u_h(x_{i+\frac{1}{2}}, t), q_h(x_{i+\frac{1}{2}}, t))$ and $S(u_h(x_{i+\frac{1}{2}}, t))$ must be replaced by the numerical fluxes $\hat{H}_h(u_h(x_{i+\frac{1}{2}}, t), q_h(x_{i+\frac{1}{2}}, t))$ and $\hat{S}(u_h(x_{i+\frac{1}{2}}, t))$ respectively.

Our system now is given as

$$\begin{aligned} & \int_{I_i} \partial_t u_h(x, t) v_{h,u}(x) dx - \int_{I_i} H_h(u_h(x, t), q_h(x, t)) \partial_x v_{h,u}(x) dx \\ & + \hat{H}_h(u_h(x_{i+\frac{1}{2}}, t), q_h(x_{i+\frac{1}{2}}, t)) v_{h,u}(x_{i+\frac{1}{2}}^-) - \hat{H}_h(u_h(x_{i-\frac{1}{2}}, t), q_h(x_{i-\frac{1}{2}}, t)) v_{h,u}(x_{i-\frac{1}{2}}^+) = 0, \end{aligned} \quad (4.26)$$

$$\begin{aligned} & \int_{I_i} q_h(x, t) v_{h,q}(x) dx + \int_{I_i} S(u(x, t)) \partial_x v_{h,q}(x) dx \\ & - \hat{S}(u_h(x_{i+\frac{1}{2}}, t)) v_{h,q}(x_{i+\frac{1}{2}}^-) + \hat{S}(u_h(x_{i-\frac{1}{2}}, t)) v_{h,q}(x_{i-\frac{1}{2}}^+) = 0, \end{aligned} \quad (4.27)$$

$$\int_{I_i} u_h(x, 0) v_{h,c}(x) dx = \int_{I_i} u_0 v_{h,c}(x) dx. \quad (4.28)$$

The numerical fluxes $\hat{H}_h(u_h(x_{i+\frac{1}{2}}, t), q_h(x_{i+\frac{1}{2}}, t))$ and $\hat{S}(u_h(x_{i+\frac{1}{2}}, t))$ are determined either as

$$\hat{H} = \hat{f} - \frac{[S(u_h)]}{[u]} q_h^+, \quad \hat{S} = S(u_h^-),$$

or as

$$\hat{H} = \hat{f} - \frac{[S(u_h)]}{[u]} q_h^-, \quad \hat{S} = S(u_h^+),$$

4.3. THE LOCAL DISCONTINUOUS GALERKIN METHOD FOR ONE DIMENSIONAL SECOND ORDER DIFFUSION PROBLEMS

see [77]. The convection flux \hat{f} can be taken to be any locally Lipschitz E-flux, see Osher [57].

As we did in Section 4.2 we take the approximate solution (u_h, q_h) as follows

$$u_h(x, t) = \sum_{r=0}^k u_i^r(t) \Psi_r(x), \quad q_h(x, t) = \sum_{r=0}^k q_i^r(t) \Psi_r(x) \quad \text{for } x \in I_i.$$

Here

$$\Psi_r(x) = P_r \left(\frac{2(x - x_i)}{\Delta x_i} \right), \quad (4.29)$$

where P_r is considered to be the Legendre polynomial of degree r . The test functions $v_{h,u}(x)$, $v_{h,q}(x)$ and $v_{h,c}(x)$ can be taken also as

$$v_{h,u}(x) = v_{h,q}(x) = v_{h,c}(x) = \Psi_s(x). \quad (4.30)$$

Taking this into consideration and taking the transformation

$$Z = \frac{2(x - x_i)}{\Delta x_i},$$

the first term of (4.26) can be written as follows

$$\int_{I_i} \partial_t u_h(x, t) v_{h,u}(x) dx = \frac{\Delta x_i}{2s + 1} \partial_t u_i^s(t).$$

The first term of (4.27) can be similarly written as

$$\int_{I_i} q_h(x, t) v_{h,q}(x) dx = \frac{\Delta x_i}{2s + 1} q_i^s.$$

Finally the left hand side of (4.28) is written as

$$\int_{I_i} u_h(x, 0) v_{h,c}(x) dx = \frac{\Delta x_i}{2s + 1} u_i^s(0).$$

The values of the test functions at the cell boundaries $x_{i+\frac{1}{2}}$ and $x_{i-\frac{1}{2}}$ are calculated as follows

$$v_{h,u}(x_{i+\frac{1}{2}}) = v_{h,q}(x_{i+\frac{1}{2}}) = v_{h,c}(x_{i+\frac{1}{2}}) = \Psi_s(x_{i+\frac{1}{2}}) = P_s(1) = 1.$$

$$v_{h,u}(x_{i-\frac{1}{2}}) = v_{h,q}(x_{i-\frac{1}{2}}) = v_{h,c}(x_{i-\frac{1}{2}}) = \Psi_s(x_{i-\frac{1}{2}}) = P_s(-1) = (-1)^s.$$

Our system now can be written as follows:

For $i = 1, \dots, N$ and for $s = 0, \dots, k$

$$\frac{\partial u_i^s(t)}{\partial t} = \frac{2s + 1}{\Delta x_i} \int_{I_i} H_h(u_h(x, t), q_h(x, t)) \partial_x P_s \left(\frac{2(x - x_i)}{\Delta x_i} \right) dx$$

CHAPTER 4. NUMERICAL SCHEME AND DISCRETIZATION OF HYPERBOLIC AND PARABOLIC SYSTEMS

$$- \frac{2s+1}{\Delta x_i} \left\{ \hat{H}_h(u_h(x_{i+\frac{1}{2}}, t), q_h(x_{i+\frac{1}{2}}, t)) - (-1)^s \hat{H}_h(u_h(x_{i-\frac{1}{2}}, t), q_h(x_{i-\frac{1}{2}}, t)) \right\}, \quad (4.31)$$

$$q_i^s = - \frac{2s+1}{\Delta x_i} \int_{I_i} S(u(x, t)) \partial_x P_s \left(\frac{2(x-x_i)}{\Delta x_i} \right) dx + \frac{2s+1}{\Delta x_i} \left\{ \hat{S}(u_h(x_{i+\frac{1}{2}}, t)) - (-1)^s \hat{S}(u_h(x_{i-\frac{1}{2}}, t)) \right\}, \quad (4.32)$$

$$u_i^s(0) = \frac{2s+1}{\Delta x_i} \int_{I_i} u_0 P_s \left(\frac{2(x-x_i)}{\Delta x_i} \right) dx. \quad (4.33)$$

As we did before, if the initial condition is constant, i.e. $u_0 = C$ then (4.33) takes the form

$$u_i^s(0) = \begin{cases} C, & \text{if } s = 0 \\ 0, & \text{otherwise.} \end{cases} \quad (4.34)$$

Now we see that after the spatial discretization the system was converted into an ODE system.

4.3.2 Error estimation

Theorem 4.3.1. *Let u be the exact solution of (4.15), u_h the numerical solution. For a small h we have the error estimates*

$$\|u - u_h\| \leq Ch^{k+\frac{1}{2}},$$

where C is a constant depends on the time t and k is the degree of the polynomials in the finite element space Λ_h .

Proof. See [92]. □

As a special case we take $A(u) = 1$ and $f(u) = 0$. This leads us to the heat equation

$$u_t - u_{xx} = 0, \quad \text{in }]0, 2\pi[\times]0, T[. \quad (4.35)$$

This equation can be decomposed into two equations

$$u_t - q_x = 0, \quad (4.36)$$

$$q - u_x = 0. \quad (4.37)$$

This system is written in the semi-discretized form as

$$\frac{\partial}{\partial t} u_i^s(t) = \frac{2s+1}{\Delta x_i} \left\{ \hat{q}(x_{i+\frac{1}{2}}) - (-1)^s \hat{q}(x_{i-\frac{1}{2}}) \right\} - \frac{2s+1}{\Delta x_i} \int_{I_i} q_h(x, t) \partial_x P_s \left(\frac{2(x-x_i)}{\Delta x_i} \right) dx,$$

$$q_i^s = \frac{2s+1}{\Delta x_i} \left\{ \hat{u}(x_{i+\frac{1}{2}}) - (-1)^s \hat{u}(x_{i-\frac{1}{2}}) \right\} - \frac{2s+1}{\Delta x_i} \int_{I_i} u_h(x, t) \partial_x P_s \left(\frac{2(x-x_i)}{\Delta x_i} \right) dx.$$

4.4. DISCONTINUOUS GALERKIN METHOD FOR TWO DIMENSIONAL HYPERBOLIC PROBLEMS

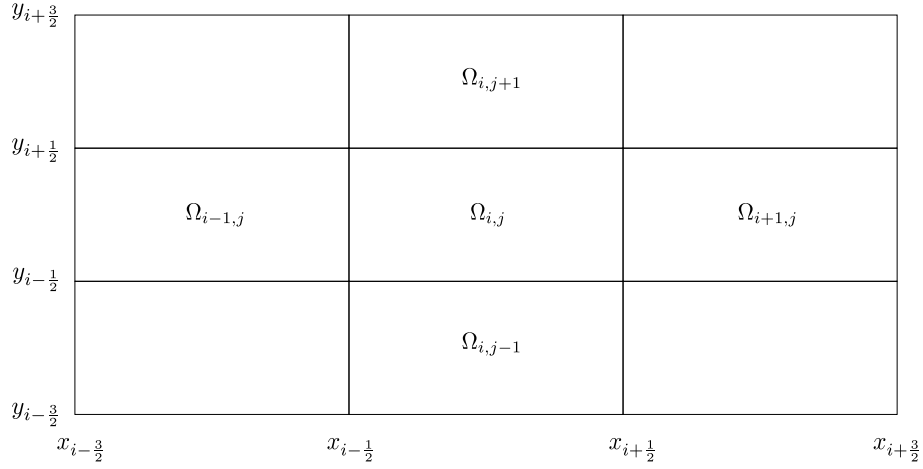


Figure 4.3: Partition of a rectangular domain into rectangular elements

The numerical fluxes for the heat equation are given either as

$$\hat{u}_{i+\frac{1}{2}} = u_{i+\frac{1}{2}}^-, \quad \hat{q}_{i+\frac{1}{2}} = q_{i+\frac{1}{2}}^+$$

or as

$$\hat{u}_{i+\frac{1}{2}} = u_{i+\frac{1}{2}}^+, \quad \hat{q}_{i+\frac{1}{2}} = q_{i+\frac{1}{2}}^-.$$

4.4 Discontinuous Galerkin method for two dimensional hyperbolic problems

This section includes materials taken from [92], [41], [3], [76]. Here we consider a simple 2D hyperbolic equation

$$\partial_t u + \partial_x f(u) + \partial_y g(u) = 0, \quad (x, y) \in \Omega, \quad t \in [0, T], \quad (4.38)$$

with the initial condition

$$u(x, y, 0) = u_0, \quad \text{for all } (x, y) \in \Omega \quad (4.39)$$

Here we assume that Ω is a rectangular domain.

4.4.1 Spatial discretization and weak formulation

For simplicity we assume a partition of the domain Ω into rectangular elements as seen in Figure 4.3.

In the x -direction we take the partition $\left\{ x_{i+\frac{1}{2}} \right\}_{i=0}^{N_x}$ where

$$x_{\frac{1}{2}} < x_{\frac{3}{2}} < \cdots < x_{N_x+\frac{1}{2}},$$

CHAPTER 4. NUMERICAL SCHEME AND DISCRETIZATION OF HYPERBOLIC AND PARABOLIC SYSTEMS

while in the y -direction the partition $\left\{y_{j+\frac{1}{2}}\right\}_{j=0}^{N_y}$ is taken, where

$$y_{\frac{1}{2}} < y_{\frac{3}{2}} < \cdots < y_{N_y+\frac{1}{2}}.$$

In this way the domain Ω is partitioned into rectangular elements Ω_{ij} as follows

for $i = 1, \dots, N_x$ and $j = 1, \dots, N_y$

$$\Omega_{ij} = \left\{ (x, y) \mid x_{i-\frac{1}{2}} \leq x \leq x_{i+\frac{1}{2}}, y_{j-\frac{1}{2}} \leq y \leq y_{j+\frac{1}{2}} \right\}.$$

The length of the cell in the x -direction is given as

$$\Delta x_i = x_{i+\frac{1}{2}} - x_{i-\frac{1}{2}}.$$

The maximum length in the x -direction is

$$\Delta x = \max_{1 \leq i \leq N_x} \Delta x_i,$$

while the center of the cell is

$$x_i = \frac{x_{i-1/2} + x_{i+1/2}}{2}.$$

Similarly, the length of the cell Ω_{ij} in the y -direction is

$$\Delta y_j = y_{j+\frac{1}{2}} - y_{j-\frac{1}{2}}.$$

The maximum length is denoted by

$$\Delta y = \max_{1 \leq j \leq N_y} \Delta y_j.$$

The center of the cell in the y -direction is taken as

$$y_j = \frac{y_{j-1/2} + y_{j+1/2}}{2}.$$

The approximate solution u_h is taken from the finite element space

$$\Lambda_h = \left\{ s \in L^1(\Omega); s|_{\Omega_{ij}} \in P^k; i = 1 : \dots : N_x, j = 1 : \dots : N_y \right\},$$

where

$$P^k = \{P; P \text{ is a polynomial of degree up to } k \text{ in } \Omega\}.$$

To construct the weak formulation we multiply (4.38) and (4.39) by the test function $v_h(x, y)$ from the finite element space Λ_h and then by replacing the exact solution $u(x, y, t)$ by the approximate solution $u_h(x, y, t)$ taken from the finite element space Λ_h and finally by integrating every term over the rectangular element Ω_{ij} as follows

$$\int_{\Omega_{ij}} \partial_t u_h(x, y, t) v_h(x, y) d\Omega_{ij} + \int_{\Omega_{ij}} \partial_x f(u_h(x, y, t)) v_h(x, y) d\Omega_{ij}$$

4.4. DISCONTINUOUS GALERKIN METHOD FOR TWO DIMENSIONAL HYPERBOLIC PROBLEMS

$$+ \int_{\Omega_{ij}} \partial_y g(u_h(x, y, t)) v_h(x, y) d\Omega_{ij} = 0, \quad (4.40)$$

$$\int_{\Omega_{ij}} u_h(x, y, 0) v_h(x, y) d\Omega_{ij} = \int_{\Omega_{ij}} u_0(x, y) v_h(x, y) d\Omega_{ij}. \quad (4.41)$$

The approximate solution $u_h(x, y, t)$ on the rectangular element Ω_{ij} is given as

$$u_h(x, y, t) = \sum_{r=0}^k \sum_{s=0}^k u_{ij}^{rs}(t) \Psi_r(x) \Psi_s(y), \quad (x, y) \in \Omega_{ij}, \quad (4.42)$$

where Ψ_r, Ψ_s are Legendre polynomials given as

$$\Psi_r(x) = P_r \left(\frac{2(x - x_i)}{\Delta x_i} \right), \quad \Psi_s(y) = P_s \left(\frac{2(y - y_j)}{\Delta y_j} \right). \quad (4.43)$$

The test function $v_h(x, y)$ can be taken as

$$v_h(x, y) = \Psi_l(x) \Psi_m(y). \quad (4.44)$$

Now let's consider the first term of (4.40)

$$\begin{aligned} I_1 &= \int_{\Omega_{ij}} \partial_t u_h(x, y, t) v_h(x, y) d\Omega_{ij} \\ &= \partial_t \int_{x_{i-\frac{1}{2}}}^{x_{i+\frac{1}{2}}} \int_{y_{j-\frac{1}{2}}}^{y_{j+\frac{1}{2}}} \sum_{r=0}^k \sum_{s=0}^k u_{ij}^{rs}(t) \Psi_r(x) \Psi_s(y) \Psi_l(x) \Psi_m(y) dx dy \\ &= \partial_t \sum_{r=0}^k \sum_{s=0}^k u_{ij}^{rs}(t) \int_{x_{i-\frac{1}{2}}}^{x_{i+\frac{1}{2}}} \Psi_r(x) \Psi_l(x) dx \int_{y_{j-\frac{1}{2}}}^{y_{j+\frac{1}{2}}} \Psi_s(y) \Psi_m(y) dy. \end{aligned}$$

Here

$$\int_{x_{i-\frac{1}{2}}}^{x_{i+\frac{1}{2}}} \Psi_r(x) \Psi_l(x) dx = \int_{x_{i-\frac{1}{2}}}^{x_{i+\frac{1}{2}}} P_r \left(\frac{2(x - x_i)}{\Delta x_i} \right) P_l \left(\frac{2(x - x_i)}{\Delta x_i} \right) dx.$$

Now we take the transformation

$$\frac{2(x - x_i)}{\Delta x_i} = z \Rightarrow dx = \frac{\Delta x_i}{2} dz$$

and then we substitute into the above equality. This leads to

CHAPTER 4. NUMERICAL SCHEME AND DISCRETIZATION OF
HYPERBOLIC AND PARABOLIC SYSTEMS

$$\begin{aligned} \int_{x_{i-\frac{1}{2}}}^{x_{i+\frac{1}{2}}} \Psi_r(x) \Psi_l(x) dx &= \frac{\Delta x_i}{2} \int_{-1}^{+1} P_r(z) P_l(z) dz \\ &= \frac{\Delta x_i}{2} \frac{2}{2l+1} \delta_{lr} \\ &= \frac{\Delta x_i}{2l+1} \delta_{lr} \end{aligned}$$

Similarly, we find that

$$\int_{y_{j-\frac{1}{2}}}^{y_{j+\frac{1}{2}}} \Psi_s(y) \Psi_m(y) dy = \frac{\Delta y_j}{2m+1} \delta_{sm}.$$

Consequently the first term of (4.40) takes the formulation

$$\begin{aligned} I_1 &= \int_{\Omega_{ij}} \partial_t u_h(x, y, t) v_h(x, y) d\Omega_{ij} = \partial_t \sum_{r=0}^k \sum_{s=0}^k u_{ij}^{rs}(t) \frac{\Delta x_i}{2l+1} \delta_{lr} \frac{\Delta y_j}{2m+1} \delta_{sm} \\ &= \frac{\Delta x_i}{2l+1} \frac{\Delta y_j}{2m+1} \partial_t u_{ij}^{lm}(t). \end{aligned} \quad (4.45)$$

Now we consider the second term of (4.40)

$$\begin{aligned} I_2 &= \int_{\Omega_{ij}} \partial_x f(u_h(x, y, t)) v_h(x, y) d\Omega_{ij} \\ &= \int_{y_{j-\frac{1}{2}}}^{y_{j+\frac{1}{2}}} \int_{x_{i-\frac{1}{2}}}^{x_{i+\frac{1}{2}}} \partial_x f(u_h(x, y, t)) v_h(x, y) dx dy. \end{aligned}$$

Integrating by parts leads to

$$\begin{aligned} I_2 &= \int_{y_{j-\frac{1}{2}}}^{y_{j+\frac{1}{2}}} \left\{ f(u_h(x, y, t)) v_h(x, y) \Big|_{x_{i-\frac{1}{2}}}^{x_{i+\frac{1}{2}}} - \int_{x_{i-\frac{1}{2}}}^{x_{i+\frac{1}{2}}} f(u_h(x, y, t)) \partial_x v_h(x, y) dx \right\} dy \\ &= \int_{y_{j-\frac{1}{2}}}^{y_{j+\frac{1}{2}}} \left\{ f(u_h(x_{i+\frac{1}{2}}, y, t)) v_h(x_{i+\frac{1}{2}}^-, y) - f(u_h(x_{i-\frac{1}{2}}, y, t)) v_h(x_{i-\frac{1}{2}}^+, y) \right\} dy \\ &\quad - \int_{y_{j-\frac{1}{2}}}^{y_{j+\frac{1}{2}}} \int_{x_{i-\frac{1}{2}}}^{x_{i+\frac{1}{2}}} f(u_h(x, y, t)) \partial_x v_h(x, y) dx dy. \end{aligned}$$

4.4. DISCONTINUOUS GALERKIN METHOD FOR TWO DIMENSIONAL HYPERBOLIC PROBLEMS

Since the flux f is discontinuous at the edges $x_{i-\frac{1}{2}}$, $x_{i+\frac{1}{2}}$ it is replaced by the numerical flux \hat{f} which can be taken to be the Lax-Friedrich flux. We have also

$$\begin{aligned} v_h(x_{i+\frac{1}{2}}, y) &= P_l \left(\frac{2(x - x_i)}{\Delta x_i} \right) P_m \left(\frac{2(y - y_j)}{\Delta y_j} \right) \Big|_{x=x_{i+\frac{1}{2}}} \\ &= P_l(1) P_m \left(\frac{2(y - y_j)}{\Delta y_j} \right) = P_m \left(\frac{2(y - y_j)}{\Delta y_j} \right), \end{aligned}$$

$$\begin{aligned} v_h(x_{i-\frac{1}{2}}, y) &= P_l \left(\frac{2(x - x_i)}{\Delta x_i} \right) P_m \left(\frac{2(y - y_j)}{\Delta y_j} \right) \Big|_{x=x_{i-\frac{1}{2}}} \\ &= P_l(-1) P_m \left(\frac{2(y - y_j)}{\Delta y_j} \right) = (-1)^l P_m \left(\frac{2(y - y_j)}{\Delta y_j} \right). \end{aligned}$$

Now we can write

$$\begin{aligned} I_2 &= \int_{y_{j-\frac{1}{2}}}^{y_{j+\frac{1}{2}}} \left\{ \hat{f}(u_h(x_{i+\frac{1}{2}}, y, t)) - (-1)^l \hat{f}(u_h(x_{i-\frac{1}{2}}, y, t)) \right\} P_m \left(\frac{2(y - y_j)}{\Delta y_j} \right) dy \\ &\quad - \int_{y_{j-\frac{1}{2}}}^{y_{j+\frac{1}{2}}} \int_{x_{i-\frac{1}{2}}}^{x_{i+\frac{1}{2}}} f(u_h(x, y, t)) P_m \left(\frac{2(y - y_j)}{\Delta y_j} \right) \partial_x P_l \left(\frac{2(x - x_i)}{\Delta x_i} \right) dx dy. \end{aligned}$$

In a very similar way the third term of (4.40)

$$I_3 = \int_{\Omega_{ij}} \partial_y g(u_h(x, y, t)) v_h(x, y) dx dy$$

can be written as

$$\begin{aligned} I_3 &= \int_{x_{i-\frac{1}{2}}}^{x_{i+\frac{1}{2}}} \left\{ \hat{g}(u_h(x, y_{j+\frac{1}{2}}, t)) - (-1)^m \hat{g}(u_h(x, y_{j-\frac{1}{2}}, t)) \right\} P_l \left(\frac{2(x - x_i)}{\Delta x_i} \right) dx \\ &\quad - \int_{x_{i-\frac{1}{2}}}^{x_{i+\frac{1}{2}}} \int_{y_{j-\frac{1}{2}}}^{y_{j+\frac{1}{2}}} g(u_h(x, y, t)) P_l \left(\frac{2(x - x_i)}{\Delta x_i} \right) \partial_y P_m \left(\frac{2(y - y_j)}{\Delta y_j} \right) dy dx \end{aligned}$$

CHAPTER 4. NUMERICAL SCHEME AND DISCRETIZATION OF HYPERBOLIC AND PARABOLIC SYSTEMS

In the following we consider the left hand side of (4.41)

$$\begin{aligned}
I_{left} &= \int_{\Omega_{ij}} u_h(x, y, 0) v_h(x, y) dx dy \\
&= \int_{x_{i-\frac{1}{2}}}^{x_{i+\frac{1}{2}}} \int_{y_{j-\frac{1}{2}}}^{y_{j+\frac{1}{2}}} u_h(x, y, 0) v_h(x, y) dy dx \\
&= \int_{x_{i-\frac{1}{2}}}^{x_{i+\frac{1}{2}}} \int_{y_{j-\frac{1}{2}}}^{y_{j+\frac{1}{2}}} \sum_{r=0}^k \sum_{s=0}^k u_{ij}^{rs}(0) \Psi_r(x) \Psi_s(y) \Psi_l(x) \Psi_m(y) dy dx \\
&= \sum_{r=0}^k \sum_{s=0}^k u_{ij}^{rs}(0) \left[\int_{x_{i-\frac{1}{2}}}^{x_{i+\frac{1}{2}}} \Psi_r(x) \Psi_l(x) dx \right] \left[\int_{y_{j-\frac{1}{2}}}^{y_{j+\frac{1}{2}}} \Psi_s(y) \Psi_m(y) dy \right] \\
&= \sum_{r=0}^k \sum_{s=0}^k u_{ij}^{rs}(0) \frac{\Delta x_i}{2l+1} \delta_{lr} \frac{\Delta y_j}{2m+1} \delta_{sm} \\
&= \frac{\Delta x_i}{2l+1} \frac{\Delta y_j}{2m+1} u_{ij}^{lm}(0).
\end{aligned}$$

Now the equations (4.40), (4.41) are written as

$$\begin{aligned}
\frac{\partial}{\partial t} u_{ij}^{lm} &= -\frac{2l+1}{\Delta x_i} \frac{2m+1}{\Delta y_j} \left[\int_{y_{j-\frac{1}{2}}}^{y_{j+\frac{1}{2}}} \left\{ \hat{f}(u_h(x_{i+\frac{1}{2}}, y, t)) - (-1)^l \hat{f}(u_h(x_{i-\frac{1}{2}}, y, t)) \right\} P_m \left(\frac{2(y-y_j)}{\Delta y_j} \right) dy \right. \\
&\quad \left. - \int_{y_{j-\frac{1}{2}}}^{y_{j+\frac{1}{2}}} \int_{x_{i-\frac{1}{2}}}^{x_{i+\frac{1}{2}}} f(u_h(x, y, t)) P_m \left(\frac{2(y-y_j)}{\Delta y_j} \right) \partial_x P_l \left(\frac{2(x-x_i)}{\Delta x_i} \right) dx dy \right] \\
&\quad - \frac{2l+1}{\Delta x_i} \frac{2m+1}{\Delta y_j} \left[\int_{x_{i-\frac{1}{2}}}^{x_{i+\frac{1}{2}}} \left\{ \hat{g}(u_h(x, y_{j+\frac{1}{2}}, t)) - (-1)^m \hat{g}(u_h(x, y_{j-\frac{1}{2}}, t)) \right\} P_l \left(\frac{2(x-x_i)}{\Delta x_i} \right) dx \right. \\
&\quad \left. - \int_{x_{i-\frac{1}{2}}}^{x_{i+\frac{1}{2}}} \int_{y_{j-\frac{1}{2}}}^{y_{j+\frac{1}{2}}} g(u_h(x, y, t)) P_l \left(\frac{2(x-x_i)}{\Delta x_i} \right) \partial_y P_m \left(\frac{2(y-y_j)}{\Delta y_j} \right) dy dx \right], \quad (4.46)
\end{aligned}$$

with the initial condition

$$u_{ij}^{lm}(0) = \frac{2l+1}{\Delta x_i} \frac{2m+1}{\Delta y_j} \int_{x_{i-\frac{1}{2}}}^{x_{i+\frac{1}{2}}} \int_{y_{j-\frac{1}{2}}}^{y_{j+\frac{1}{2}}} u_0(x, y, 0) P_l \left(\frac{2(x-x_i)}{\Delta x_i} \right) P_m \left(\frac{2(y-y_j)}{\Delta y_j} \right) dy dx. \quad (4.47)$$

The fluxes at the boundaries of a cell are given as

$$u^-(x_{i+\frac{1}{2}}, y) = \sum_{r=0}^k \sum_{s=0}^k u_{ij}^{rs} \Psi_r(x) \Psi_s(y) \Big|_{x_{i+\frac{1}{2}}},$$

4.5. THE LOCAL DISCONTINUOUS GALERKIN METHOD FOR TWO DIMENSIONAL SECOND ORDER DIFFUSION PROBLEMS

$$\begin{aligned}
 u^+(x_{i-\frac{1}{2}}, y) &= \sum_{r=0}^k \sum_{s=0}^k u_{ij}^{rs} \Psi_r(x) \Psi_s(y) \Big|_{x_{i-\frac{1}{2}}}, \\
 u^-(x, y_{j+\frac{1}{2}}) &= \sum_{r=0}^k \sum_{s=0}^k u_{ij}^{rs} \Psi_r(x) \Psi_s(y) \Big|_{y_{j+\frac{1}{2}}}, \\
 u^+(x, y_{j-\frac{1}{2}}) &= \sum_{r=0}^k \sum_{s=0}^k u_{ij}^{rs} \Psi_r(x) \Psi_s(y) \Big|_{y_{j-\frac{1}{2}}}.
 \end{aligned}$$

In a special case, if the initial condition is constant, i.e. $u_0(x, y, 0) = C$, then (4.47) can be written as

$$\begin{aligned}
 u_{ij}^{lm} &= \frac{2l+1}{\Delta x_i} \frac{2m+1}{\Delta y_j} C \int_{x_{i-\frac{1}{2}}}^{x_{i+\frac{1}{2}}} \int_{y_{j-\frac{1}{2}}}^{y_{j+\frac{1}{2}}} P_l \left(\frac{2(x-x_i)}{\Delta x_i} \right) P_m \left(\frac{2(y-y_j)}{\Delta y_j} \right) dy dx \\
 &= \frac{2l+1}{\Delta x_i} \frac{2m+1}{\Delta y_j} C \left[\int_{x_{i-\frac{1}{2}}}^{x_{i+\frac{1}{2}}} P_0 \left(\frac{2(x-x_i)}{\Delta x_i} \right) P_l \left(\frac{2(x-x_i)}{\Delta x_i} \right) dx \right] \\
 &\quad \left[\int_{y_{j-\frac{1}{2}}}^{y_{j+\frac{1}{2}}} P_0 \left(\frac{2(y-y_j)}{\Delta y_j} \right) P_m \left(\frac{2(y-y_j)}{\Delta y_j} \right) dy \right] \\
 &= \frac{2l+1}{\Delta x_i} \frac{2m+1}{\Delta y_j} C \frac{\Delta x_i}{2} \frac{\Delta y_j}{2} \frac{2}{2l+1} \delta_{0l} \frac{2}{2m+1} \delta_{0m} \\
 &= C \delta_{0l} \delta_{0m} = \begin{cases} C, & \text{if } l = m = 0 \\ 0, & \text{otherwise.} \end{cases}
 \end{aligned}$$

4.5 The local discontinuous Galerkin method for two dimensional second order diffusion problems

Now we consider the convection diffusion problem of the form

$$\partial_t u + \sum_{i=1}^d \partial_{x_i} \left(f_i(u) - \sum_{j=1}^d A_{ij}(u) \partial_{x_j} u \right) = 0, \quad x \in \Omega, \quad t \in [0, T] \quad (4.48)$$

with the initial condition

$$u(x_1, x_2, \dots, 0) = u_0, \quad \text{for all } x \in \Omega. \quad (4.49)$$

Here we assume that the matrix $A_{ij}(u)$ is a symmetric, positive semi-definite matrix. In two dimensions we take the form

CHAPTER 4. NUMERICAL SCHEME AND DISCRETIZATION OF HYPERBOLIC AND PARABOLIC SYSTEMS

$$\begin{aligned}
 u_t + \partial_x f(u) - \partial_x [A_{11}(u)\partial_x u + A_{12}(u)\partial_y u] \\
 + \partial_y g(u) - \partial_y [A_{21}(u)\partial_x u + A_{22}(u)\partial_y u] = 0,
 \end{aligned} \tag{4.50}$$

with the initial condition

$$u(x, y, 0) = u_0. \tag{4.51}$$

It is known that a real symmetric matrix A_{ij} is semi-definite if and only if there exists a non-singular symmetric matrix M_{ij} such that

$$A_{ij} = M_{ij}M_{ij}^t,$$

where M_{ij}^t is the transposed matrix of M_{ij} . The matrix A_{ij} can be written also as

$$A_{ij}(u) = \sum_{\nu=1}^2 M_{i\nu}(u)M_{\nu j}(u).$$

The entries of the matrix A_{ij} are

$$\begin{aligned}
 A_{11} &= M_{11}M_{11} + M_{12}M_{21} \\
 A_{12} &= M_{11}M_{12} + M_{12}M_{22} \\
 A_{21} &= M_{21}M_{11} + M_{22}M_{21} \\
 A_{22} &= M_{21}M_{12} + M_{22}M_{22}
 \end{aligned}$$

After substituting in (4.50) and doing some manipulations we get

$$\begin{aligned}
 u_t + \partial_x f(u) + \partial_y g(u) - \partial_x [M_{11}(M_{11}\partial_x u + M_{12}\partial_y u) + M_{12}(M_{21}\partial_x u + M_{22}\partial_y u)] \\
 - \partial_y [M_{21}(M_{11}\partial_x u + M_{12}\partial_y u) + M_{22}(M_{21}\partial_x u + M_{22}\partial_y u)] = 0.
 \end{aligned} \tag{4.52}$$

Taking

$$q_1 = M_{11}\partial_x u + M_{12}\partial_y u, \tag{4.53}$$

$$q_2 = M_{21}\partial_x u + M_{22}\partial_y u \tag{4.54}$$

equation (4.52) takes the form

$$u_t + \partial_x f(u) + \partial_y g(u) - \partial_x(M_{11}q_1 + M_{12}q_2) - \partial_y(M_{21}q_1 + M_{22}q_2) = 0.$$

Now we introduce a new variable

$$S_{\nu i}(u) = \int^u M_{\nu i}(z) dz. \tag{4.55}$$

Our system can now be written as

$$u_t + \partial_x f(u) + \partial_y g(u) - \partial_x(M_{11}q_1 + M_{12}q_2) - \partial_y(M_{21}q_1 + M_{22}q_2) = 0, \tag{4.56}$$

$$q_1 - \partial_x S_{11}(u) - \partial_y S_{12}(u) = 0, \tag{4.57}$$

$$q_2 - \partial_x S_{21}(u) - \partial_y S_{22}(u) = 0, \tag{4.58}$$

$$u(x, y, 0) = u_0. \tag{4.59}$$

4.5. THE LOCAL DISCONTINUOUS GALERKIN METHOD FOR TWO DIMENSIONAL SECOND ORDER DIFFUSION PROBLEMS

4.5.1 The weak formulation

Again for simplicity we assume that the domain Ω is partitioned into rectangular elements Ω_{ij} as seen in Figure 4.3.

$$\Omega_{ij} = \left\{ (x, y) \mid x_{i-\frac{1}{2}} \leq x \leq x_{i+\frac{1}{2}}, y_{j-\frac{1}{2}} \leq y \leq y_{j+\frac{1}{2}} \right\}.$$

The length of the cell on the x -direction and on the y -direction are given respectively as

$$\begin{aligned} \Delta x_i &= x_{i+\frac{1}{2}} - x_{i-\frac{1}{2}}, \\ \Delta y_j &= y_{j+\frac{1}{2}} - y_{j-\frac{1}{2}}. \end{aligned}$$

The maximum length in both the x -direction and the y -direction are

$$\begin{aligned} \Delta x &= \max_{1 \leq i \leq N_x} \Delta x_i, \\ \Delta y &= \max_{1 \leq j \leq N_y} \Delta y_j. \end{aligned}$$

The center of the any cell Ω_{ij} is

$$(x_i, y_j) = \left(\frac{x_{i-1/2} + x_{i+1/2}}{2}, \frac{y_{j-1/2} + y_{j+1/2}}{2} \right).$$

The approximate solution (u_h, q_{1h}, q_{2h}) is taken from the finite element space

$$\Lambda_h = \{s; s|_{\Omega_{ij}} \in P^k; i = 1 : \dots : N_x, j = 1 : \dots : N_y\},$$

where

$$P^k = \{P; P \text{ is a polynomial of degree up to } k \text{ in } \Omega\}.$$

To construct the weak formulation we multiply (4.56), (4.57), (4.58) and (4.59) respectively by the test functions $v_{h,u}$, v_{h,q_1} , v_{h,q_2} and $v_{h,c}$ taken from the finite element space Λ_h . Then we integrate over every cell Ω_{ij} and replace the exact solution (u, q_1, q_2) by the approximate solution $(u_h, q_{1,h}, q_{2,h})$ as follows

$$\begin{aligned} & \int_{\Omega_{ij}} \partial_t u_h(x, y, t) v_{h,u}(x, y) dx dy + \int_{\Omega_{ij}} \partial_x f(u(x, y, t)) v_{h,u}(x, y) dx dy \\ & + \int_{\Omega_{ij}} \partial_y g(u(x, y, t)) v_{h,u}(x, y) dx dy - \int_{\Omega_{ij}} \partial_x (M_{11} q_{1,h} + M_{12} q_{2,h}) v_{h,u}(x, y) dx dy \\ & \quad - \int_{\Omega_{ij}} \partial_y (M_{21} q_{1,h} + M_{22} q_{2,h}) v_{h,u}(x, y) dx dy = 0, \end{aligned} \tag{4.60}$$

$$\int_{\Omega_{ij}} q_{1,h} v_{h,q_1}(x, y) dx dy - \int_{\Omega_{ij}} \partial_x S_{11}(u) v_{h,q_1}(x, y) dx dy - \int_{\Omega_{ij}} \partial_y S_{12}(u) v_{h,q_1}(x, y) dx dy = 0, \tag{4.61}$$

CHAPTER 4. NUMERICAL SCHEME AND DISCRETIZATION OF HYPERBOLIC AND PARABOLIC SYSTEMS

$$\int_{\Omega_{ij}} q_{2,h} v_{h,q_2}(x, y) dx dy - \int_{\Omega_{ij}} \partial_x S_{21}(u) v_{h,q_2}(x, y) dx dy - \int_{\Omega_{ij}} \partial_y S_{22}(u) v_{h,q_2}(x, y) dx dy = 0, \quad (4.62)$$

$$\int_{\Omega_{ij}} u(x, y, 0) v_{h,c}(x, y) dx dy = \int_{\Omega_{ij}} u_0 v_{h,c}(x, y) dx dy. \quad (4.63)$$

We assume that the solution $(u_h, q_{1,h}, q_{2,h})$ is expressed as

$$u_h = \sum_{r=0}^k \sum_{s=0}^k u_{ij}^{rs}(t) \Psi_r(x) \Psi_s(y), \quad q_{1,h} = \sum_{r=0}^k \sum_{s=0}^k q_{1ij}^{rs}(t) \Psi_r(x) \Psi_s(y),$$

$$q_{2,h} = \sum_{r=0}^k \sum_{s=0}^k q_{2ij}^{rs}(t) \Psi_r(x) \Psi_s(y). \quad (4.64)$$

Here

$$\Psi_r(x) = \left(\frac{2(x - x_i)}{\Delta x_i} \right), \quad \Psi_s(y) = \left(\frac{2(y - y_j)}{\Delta y_j} \right), \quad (4.65)$$

where $\Psi_r(x)$ and $\Psi_s(y)$ are the Legendre polynomials of degree r and s respectively. The test functions $v_{h,u}$, v_{h,q_1} , v_{h,q_2} and $v_{h,c}$ are given as

$$v_{h,u} = v_{h,q_1} = v_{h,q_2} = v_{h,c} = \Psi_l(x) \Psi_m(y). \quad (4.66)$$

Now we consider the first term of (4.60)

$$I_1 = \int_{\Omega_{ij}} \partial_t u_h(x, y, t) v_{h,u}(x, y) dx dy$$

$$= \frac{\Delta x_i}{2l+1} \frac{\Delta y_j}{2m+1} \partial_t u_{ij}^{lm}(t).$$

Applying the integration by parts for the second term of (4.60) we get

$$I_2 = \int_{y_{j-\frac{1}{2}}}^{y_{j+\frac{1}{2}}} \left\{ f(u_h(x, y, t)) v_{h,u}(x, y) \Big|_{x_{i-\frac{1}{2}}}^{x_{i+\frac{1}{2}}} - \int_{x_{i-\frac{1}{2}}}^{x_{i+\frac{1}{2}}} f(u_h(x, y, t)) \partial_x v_{h,u}(x, y) dx \right\} dy$$

$$= \int_{y_{j-\frac{1}{2}}}^{y_{j+\frac{1}{2}}} \left\{ f(u_h(x_{i+\frac{1}{2}}, y, t)) v_{h,u}(x_{i+\frac{1}{2}}^-, y) - f(u_h(x_{i-\frac{1}{2}}, y, t)) v_{h,u}(x_{i-\frac{1}{2}}^+, y) \right\} dy$$

$$- \int_{y_{j-\frac{1}{2}}}^{y_{j+\frac{1}{2}}} \int_{x_{i-\frac{1}{2}}}^{x_{i+\frac{1}{2}}} f(u_h(x, y, t)) \partial_x v_{h,u}(x, y) dx dy.$$

4.5. THE LOCAL DISCONTINUOUS GALERKIN METHOD FOR TWO DIMENSIONAL SECOND ORDER DIFFUSION PROBLEMS

The flux f is discontinuous at the edges $x_{i-\frac{1}{2}}$, $x_{i+\frac{1}{2}}$, therefore it is replaced by the numerical flux \hat{f} . Also we have

$$\begin{aligned} v_{h,u}(x_{i+\frac{1}{2}}, y) &= P_l \left(\frac{2(x - x_i)}{\Delta x_i} \right) P_m \left(\frac{2(y - y_j)}{\Delta y_j} \right) \Big|_{x=x_{i+\frac{1}{2}}} \\ &= P_l(1) P_m \left(\frac{2(y - y_j)}{\Delta y_j} \right) = P_m \left(\frac{2(y - y_j)}{\Delta y_j} \right) \end{aligned}$$

and

$$\begin{aligned} v_{h,u}(x_{i-\frac{1}{2}}, y) &= P_l \left(\frac{2(x - x_i)}{\Delta x_i} \right) P_m \left(\frac{2(y - y_j)}{\Delta y_j} \right) \Big|_{x=x_{i-\frac{1}{2}}} \\ &= P_l(-1) P_m \left(\frac{2(y - y_j)}{\Delta y_j} \right) = (-1)^l P_m \left(\frac{2(y - y_j)}{\Delta y_j} \right). \end{aligned}$$

Now we can insert these to give

$$\begin{aligned} I_2 &= \int_{y_{j-\frac{1}{2}}}^{y_{j+\frac{1}{2}}} \left\{ \hat{f}(u_h(x_{i+\frac{1}{2}}, y, t)) - (-1)^l \hat{f}(u_h(x_{i-\frac{1}{2}}, y, t)) \right\} P_m \left(\frac{2(y - y_j)}{\Delta y_j} \right) dy \\ &\quad - \int_{y_{j-\frac{1}{2}}}^{y_{j+\frac{1}{2}}} \int_{x_{i-\frac{1}{2}}}^{x_{i+\frac{1}{2}}} f(u_h(x, y, t)) P_m \left(\frac{2(y - y_j)}{\Delta y_j} \right) \partial_x P_l \left(\frac{2(x - x_i)}{\Delta x_i} \right) dx dy. \end{aligned}$$

The third term of (4.60) is handled in a very similar way as the second term

$$\begin{aligned} I_3 &= \int_{x_{i-\frac{1}{2}}}^{x_{i+\frac{1}{2}}} \left\{ \hat{g}(u_h(x, y_{j+\frac{1}{2}}, t)) - (-1)^m \hat{g}(u_h(x, y_{j-\frac{1}{2}}, t)) \right\} P_l \left(\frac{2(x - x_i)}{\Delta x_i} \right) dx \\ &\quad - \int_{x_{i-\frac{1}{2}}}^{x_{i+\frac{1}{2}}} \int_{y_{j-\frac{1}{2}}}^{y_{j+\frac{1}{2}}} g(u_h(x, y, t)) P_l \left(\frac{2(x - x_i)}{\Delta x_i} \right) \partial_y P_m \left(\frac{2(y - y_j)}{\Delta y_j} \right) dy dx. \end{aligned}$$

Now we consider the fourth term of (4.60)

$$I_4 = \int_{\Omega_{ij}} \partial_x (M_{11}q_{1,h} + M_{12}q_{2,h}) v_{h,u}(x, y) dx dy.$$

Integrating by parts leads us to

$$I_4 = \int_{y_{j-\frac{1}{2}}}^{y_{j+\frac{1}{2}}} \left[(M_{11}q_{1,h} + M_{12}q_{2,h}) v_{h,u} \Big|_{x_{i-\frac{1}{2}}}^{x_{i+\frac{1}{2}}} - \int_{x_{i-\frac{1}{2}}}^{x_{i+\frac{1}{2}}} (M_{11}q_{1,h} + M_{12}q_{2,h}) \partial_x v_{h,u} dx \right] dy.$$

CHAPTER 4. NUMERICAL SCHEME AND DISCRETIZATION OF HYPERBOLIC AND PARABOLIC SYSTEMS

The functions M_{11} , M_{12} , $q_{1,h}$ and $q_{2,h}$ are replaced by \hat{M}_{11} , \hat{M}_{12} , $\hat{q}_{1,h}$ and $\hat{q}_{2,h}$ respectively. The last equation takes now the following form

$$I_4 = \int_{y_{j-\frac{1}{2}}}^{y_{j+\frac{1}{2}}} \left[\left(\hat{M}_{11}(x_{i+\frac{1}{2}}, y) \hat{q}_{1,h}(x_{i+\frac{1}{2}}, y) + \hat{M}_{12}(x_{i+\frac{1}{2}}, y) \hat{q}_{2,h}(x_{i+\frac{1}{2}}, y) \right) - \right. \\ \left. (-1)^l \left(\hat{M}_{11}(x_{i-\frac{1}{2}}, y) \hat{q}_{1,h}(x_{i-\frac{1}{2}}, y) + \hat{M}_{12}(x_{i-\frac{1}{2}}, y) \hat{q}_{2,h}(x_{i-\frac{1}{2}}, y) \right) \right] P_m \left(\frac{2(y-y_j)}{\Delta y_j} \right) dy - \\ \int_{y_{j-\frac{1}{2}}}^{y_{j+\frac{1}{2}}} \int_{x_{i-\frac{1}{2}}}^{x_{i+\frac{1}{2}}} (M_{11}q_{1,h} + M_{12}q_{2,h}) P_m \left(\frac{2(y-y_j)}{\Delta y_j} \right) \partial_x P_l \left(\frac{2(x-x_i)}{\Delta x_i} \right) dx dy.$$

Similarly the fifth term can be written as

$$I_5 = \int_{x_{i-\frac{1}{2}}}^{x_{i+\frac{1}{2}}} \left[\left(\hat{M}_{21}(x, y_{j+\frac{1}{2}}) \hat{q}_{1,h}(x, y_{j+\frac{1}{2}}) + \hat{M}_{22}(x, y_{j+\frac{1}{2}}) \hat{q}_{2,h}(x, y_{j+\frac{1}{2}}) \right) - \right. \\ \left. (-1)^m \left(\hat{M}_{21}(x, y_{j-\frac{1}{2}}) \hat{q}_{1,h}(x, y_{j-\frac{1}{2}}) + \hat{M}_{22}(x, y_{j-\frac{1}{2}}) \hat{q}_{2,h}(x, y_{j-\frac{1}{2}}) \right) \right] P_l \left(\frac{2(x-x_i)}{\Delta x_i} \right) dx - \\ \int_{y_{j-\frac{1}{2}}}^{y_{j+\frac{1}{2}}} \int_{x_{i-\frac{1}{2}}}^{x_{i+\frac{1}{2}}} (M_{21}q_{1,h} + M_{22}q_{2,h}) P_l \left(\frac{2(x-x_i)}{\Delta x_i} \right) \partial_y P_m \left(\frac{2(y-y_j)}{\Delta y_j} \right) dx dy.$$

Now we consider equation (4.61) and start with the first term

$$I_1 = \int_{\Omega_{ij}} q_{1,h} v_{h,q_1}(x, y) dx dy \\ = \int_{x_{i-\frac{1}{2}}}^{x_{i+\frac{1}{2}}} \int_{y_{j-\frac{1}{2}}}^{y_{j+\frac{1}{2}}} \sum_{r=0}^k \sum_{s=0}^k q_{1ij}^{rs} \Psi_r(x) \Psi_s(y) \Psi_l(x) \Psi_m(y) dy dx \\ = \sum_{r=0}^k \sum_{s=0}^k q_{1ij}^{rs} \int_{x_{i-\frac{1}{2}}}^{x_{i+\frac{1}{2}}} \Psi_r(x) \Psi_l(x) dx \int_{y_{j-\frac{1}{2}}}^{y_{j+\frac{1}{2}}} \Psi_s(y) \Psi_m(y) dy \\ = \frac{\Delta x_i}{2} \frac{\Delta y_j}{2} \sum_{r=0}^k \sum_{s=0}^k q_{1ij}^{rs} \int_{-1}^{+1} P_r(x) P_l(x) dx \int_{-1}^{+1} P_s(y) P_m(y) dy \\ = \frac{\Delta x_i}{2} \frac{\Delta y_j}{2} \sum_{r=0}^k \sum_{s=0}^k q_{1ij}^{rs} \frac{2}{2l+1} \frac{2}{2m+1} \delta_{rl} \delta_{sm} \\ = \frac{\Delta x_i}{2l+1} \frac{\Delta y_j}{2m+1} q_{1ij}^{lm}.$$

The second term of (4.61) is handled as follows

4.5. THE LOCAL DISCONTINUOUS GALERKIN METHOD FOR TWO DIMENSIONAL SECOND ORDER DIFFUSION PROBLEMS

$$\begin{aligned}
I_2 &= \int_{\Omega_{ij}} \partial_x S_{11}(u) v_{h,q_1}(x, y) dx dy \\
&= \int_{y_{j-\frac{1}{2}}}^{y_{j+\frac{1}{2}}} \left\{ S_{11}(u) v(x, y) \Big|_{x_{i-\frac{1}{2}}}^{x_{i+\frac{1}{2}}} - \int_{x_{i-\frac{1}{2}}}^{x_{i+\frac{1}{2}}} S_{11}(u) \partial_x v(x, y) dx \right\} dy \\
&= \int_{y_{j-\frac{1}{2}}}^{y_{j+\frac{1}{2}}} \left\{ \hat{S}_{11}(u(x_{i+\frac{1}{2}}, y)) - (-1)^l \hat{S}_{11}(u(x_{i-\frac{1}{2}}, y)) \right\} P_m \left(\frac{2(y - y_j)}{\Delta y_j} \right) dy \\
&\quad - \int_{y_{j-\frac{1}{2}}}^{y_{j+\frac{1}{2}}} \int_{x_{i-\frac{1}{2}}}^{x_{i+\frac{1}{2}}} S_{11}(u(x, y)) P_m \left(\frac{2(y - y_j)}{\Delta y_j} \right) \partial_x P_l \left(\frac{2(x - x_i)}{\Delta x_i} \right) dx dy.
\end{aligned}$$

The third term of (4.61)

$$I_3 = \int_{\Omega_{ij}} \partial_x S_{12}(u) v_{h,q_1}(x, y) dx dy$$

can be written in a similar way as

$$\begin{aligned}
I_3 &= \int_{x_{i-\frac{1}{2}}}^{x_{i+\frac{1}{2}}} \left\{ \hat{S}_{12}(u(x, y_{j+\frac{1}{2}})) - (-1)^m \hat{S}_{12}(u(x, y_{j-\frac{1}{2}})) \right\} P_l \left(\frac{2(x - x_i)}{\Delta x_i} \right) dx \\
&\quad - \int_{x_{i-\frac{1}{2}}}^{x_{i+\frac{1}{2}}} \int_{y_{j-\frac{1}{2}}}^{y_{j+\frac{1}{2}}} S_{12}(u(x, y)) P_l \left(\frac{2(x - x_i)}{\Delta x_i} \right) \partial_y P_m \left(\frac{2(y - y_j)}{\Delta y_j} \right) dx dy.
\end{aligned}$$

Equation (4.62) is handled exactly as equation (4.61). For the last equation (4.63) we can write

$$u_{ij}^{lm}(0) = \frac{2l+1}{\Delta x_i} \frac{2m+1}{\Delta y_j} \int_{x_{i-\frac{1}{2}}}^{x_{i+\frac{1}{2}}} \int_{y_{j-\frac{1}{2}}}^{y_{j+\frac{1}{2}}} u_0(x, y, 0) P_l \left(\frac{2(x - x_i)}{\Delta x_i} \right) P_m \left(\frac{2(y - y_j)}{\Delta y_j} \right) dx dy.$$

For $i, j = 1, \dots, N$ and for $l, m = 1, 2$ our System can now be written in the semi-discrete form as

$$\begin{aligned}
\frac{\partial u_{ij}^{lm}}{\partial t} &= \frac{2l+1}{\Delta x_i} \frac{2m+1}{\Delta y_j} \int_{y_{j-\frac{1}{2}}}^{y_{j+\frac{1}{2}}} \int_{x_{i-\frac{1}{2}}}^{x_{i+\frac{1}{2}}} f(u_h(x, y, t)) P_m \left(\frac{2(y - y_j)}{\Delta y_j} \right) \partial_x P_l \left(\frac{2(x - x_i)}{\Delta x_i} \right) dx dy \\
&\quad + \frac{2l+1}{\Delta x_i} \frac{2m+1}{\Delta y_j} \int_{x_{i-\frac{1}{2}}}^{x_{i+\frac{1}{2}}} \int_{y_{j-\frac{1}{2}}}^{y_{j+\frac{1}{2}}} g(u_h(x, y, t)) P_l \left(\frac{2(x - x_i)}{\Delta x_i} \right) \partial_y P_m \left(\frac{2(y - y_j)}{\Delta y_j} \right) dy dx
\end{aligned}$$

CHAPTER 4. NUMERICAL SCHEME AND DISCRETIZATION OF
HYPERBOLIC AND PARABOLIC SYSTEMS

$$\begin{aligned}
& - \frac{2l+1}{\Delta x_i} \frac{2m+1}{\Delta y_j} \int_{y_{j-\frac{1}{2}}}^{y_{j+\frac{1}{2}}} \left\{ \hat{f}(u_h(x_{i+\frac{1}{2}}, y, t)) - (-1)^l \hat{f}(u_h(x_{i-\frac{1}{2}}, y, t)) \right\} P_m \left(\frac{2(y-y_j)}{\Delta y_j} \right) dy \\
& - \frac{2l+1}{\Delta x_i} \frac{2m+1}{\Delta y_j} \int_{x_{i-\frac{1}{2}}}^{x_{i+\frac{1}{2}}} \left\{ \hat{g}(u_h(x, y_{j+\frac{1}{2}}, t)) - (-1)^m \hat{g}(u_h(x, y_{j-\frac{1}{2}}, t)) \right\} P_l \left(\frac{2(x-x_i)}{\Delta x_i} \right) dx \\
& + \frac{2l+1}{\Delta x_i} \frac{2m+1}{\Delta y_j} \int_{y_{j-\frac{1}{2}}}^{y_{j+\frac{1}{2}}} \left[\left(\hat{M}_{11}(x_{i+\frac{1}{2}}, y) \hat{q}_{1,h}(x_{i+\frac{1}{2}}, y) + \hat{M}_{12}(x_{i+\frac{1}{2}}, y) \hat{q}_{2,h}(x_{i+\frac{1}{2}}, y) \right) \right. \\
& - (-1)^l \left(\hat{M}_{11}(x_{i-\frac{1}{2}}, y) \hat{q}_{1,h}(x_{i-\frac{1}{2}}, y) + \hat{M}_{12}(x_{i-\frac{1}{2}}, y) \hat{q}_{2,h}(x_{i-\frac{1}{2}}, y) \right) \left. \right] P_m \left(\frac{2(y-y_j)}{\Delta y_j} \right) dy \\
& + \frac{2l+1}{\Delta x_i} \frac{2m+1}{\Delta y_j} \int_{x_{i-\frac{1}{2}}}^{x_{i+\frac{1}{2}}} \left[\left(\hat{M}_{21}(x, y_{j+\frac{1}{2}}) \hat{q}_{1,h}(x, y_{j+\frac{1}{2}}) + \hat{M}_{22}(x, y_{j+\frac{1}{2}}) \hat{q}_{2,h}(x, y_{j+\frac{1}{2}}) \right) \right. \\
& - (-1)^m \left(\hat{M}_{21}(x, y_{j-\frac{1}{2}}) \hat{q}_{1,h}(x, y_{j-\frac{1}{2}}) + \hat{M}_{22}(x, y_{j-\frac{1}{2}}) \hat{q}_{2,h}(x, y_{j-\frac{1}{2}}) \right) \left. \right] P_l \left(\frac{2(x-x_i)}{\Delta x_i} \right) dx \\
& - \frac{2l+1}{\Delta x_i} \frac{2m+1}{\Delta y_j} \int_{y_{j-\frac{1}{2}}}^{y_{j+\frac{1}{2}}} \int_{x_{i-\frac{1}{2}}}^{x_{i+\frac{1}{2}}} (M_{11}q_{1,h} + M_{12}q_{2,h}) P_m \left(\frac{2(y-y_j)}{\Delta y_j} \right) \partial_x P_l \left(\frac{2(x-x_i)}{\Delta x_i} \right) dx dy \\
& - \frac{2l+1}{\Delta x_i} \frac{2m+1}{\Delta y_j} \int_{y_{j-\frac{1}{2}}}^{y_{j+\frac{1}{2}}} \int_{x_{i-\frac{1}{2}}}^{x_{i+\frac{1}{2}}} (M_{21}q_{1,h} + M_{22}q_{2,h}) P_l \left(\frac{2(x-x_i)}{\Delta x_i} \right) \partial_y P_m \left(\frac{2(y-y_j)}{\Delta y_j} \right) dx dy.
\end{aligned} \tag{4.67}$$

$$\begin{aligned}
q_{1ij}^{lm} &= \frac{2l+1}{\Delta x_i} \frac{2m+1}{\Delta y_j} \int_{y_{j-\frac{1}{2}}}^{y_{j+\frac{1}{2}}} \int_{x_{i-\frac{1}{2}}}^{x_{i+\frac{1}{2}}} S_{11}(u(x, y)) P_m \left(\frac{2(y-y_j)}{\Delta y_j} \right) \partial_x P_l \left(\frac{2(x-x_i)}{\Delta x_i} \right) dx dy \\
& + \frac{2l+1}{\Delta x_i} \frac{2m+1}{\Delta y_j} \int_{x_{i-\frac{1}{2}}}^{x_{i+\frac{1}{2}}} \int_{y_{j-\frac{1}{2}}}^{y_{j+\frac{1}{2}}} S_{12}(u(x, y)) P_l \left(\frac{2(x-x_i)}{\Delta x_i} \right) \partial_y P_m \left(\frac{2(y-y_j)}{\Delta y_j} \right) dx dy \\
& - \frac{2l+1}{\Delta x_i} \frac{2m+1}{\Delta y_j} \int_{y_{j-\frac{1}{2}}}^{y_{j+\frac{1}{2}}} \left\{ \hat{S}_{11}(u(x_{i+\frac{1}{2}}, y)) - (-1)^l \hat{S}_{11}(u(x_{i-\frac{1}{2}}, y)) \right\} P_m \left(\frac{2(y-y_j)}{\Delta y_j} \right) dy \\
& - \frac{2l+1}{\Delta x_i} \frac{2m+1}{\Delta y_j} \int_{x_{i-\frac{1}{2}}}^{x_{i+\frac{1}{2}}} \left\{ \hat{S}_{12}(u(x, y_{j+\frac{1}{2}})) - (-1)^m \hat{S}_{12}(u(x, y_{j-\frac{1}{2}})) \right\} P_l \left(\frac{2(x-x_i)}{\Delta x_i} \right) dx.
\end{aligned} \tag{4.68}$$

$$\begin{aligned}
q_{2ij}^{lm} &= \frac{2l+1}{\Delta x_i} \frac{2m+1}{\Delta y_j} \int_{y_{j-\frac{1}{2}}}^{y_{j+\frac{1}{2}}} \int_{x_{i-\frac{1}{2}}}^{x_{i+\frac{1}{2}}} S_{21}(u(x, y)) P_m \left(\frac{2(y-y_j)}{\Delta y_j} \right) \partial_x P_l \left(\frac{2(x-x_i)}{\Delta x_i} \right) dx dy \\
& + \frac{2l+1}{\Delta x_i} \frac{2m+1}{\Delta y_j} \int_{x_{i-\frac{1}{2}}}^{x_{i+\frac{1}{2}}} \int_{y_{j-\frac{1}{2}}}^{y_{j+\frac{1}{2}}} S_{22}(u(x, y)) P_l \left(\frac{2(x-x_i)}{\Delta x_i} \right) \partial_y P_m \left(\frac{2(y-y_j)}{\Delta y_j} \right) dx dy
\end{aligned}$$

4.5. THE LOCAL DISCONTINUOUS GALERKIN METHOD FOR TWO DIMENSIONAL SECOND ORDER DIFFUSION PROBLEMS

$$\begin{aligned}
& - \frac{2l+1}{\Delta x_i} \frac{2m+1}{\Delta y_j} \int_{y_{j-\frac{1}{2}}}^{y_{j+\frac{1}{2}}} \left\{ \hat{S}_{21}(u(x_{i+\frac{1}{2}}, y)) - (-1)^l \hat{S}_{21}(u(x_{i-\frac{1}{2}}, y)) \right\} P_m \left(\frac{2(y-y_j)}{\Delta y_j} \right) dy \\
& - \frac{2l+1}{\Delta x_i} \frac{2m+1}{\Delta y_j} \int_{x_{i-\frac{1}{2}}}^{x_{i+\frac{1}{2}}} \left\{ \hat{S}_{22}(u(x, y_{j+\frac{1}{2}})) - (-1)^m \hat{S}_{22}(u(x, y_{j-\frac{1}{2}})) \right\} P_l \left(\frac{2(x-x_i)}{\Delta x_i} \right) dx,
\end{aligned} \tag{4.69}$$

with the initial condition

$$u_{ij}^{lm}(0) = \frac{2l+1}{\Delta x_i} \frac{2m+1}{\Delta y_j} \int_{x_{i-\frac{1}{2}}}^{x_{i+\frac{1}{2}}} \int_{y_{j-\frac{1}{2}}}^{y_{j+\frac{1}{2}}} u_0(x, y, 0) P_l \left(\frac{2(x-x_i)}{\Delta x_i} \right) P_m \left(\frac{2(y-y_j)}{\Delta y_j} \right) dx dy. \tag{4.70}$$

In a special case, if the initial condition is constant, i.e. $u_0(x, y, 0) = C$ then the last equation can be written as

$$u_{ij}^{lm}(0) = \begin{cases} C, & \text{if } l = m = 0 \\ 0, & \text{otherwise.} \end{cases}$$

Before we continue we introduce the following notations

$$[Q] = Q^+ - Q^-, \quad Q_{i+\frac{1}{2}}^+ = Q(x_{i+\frac{1}{2}}^+), \quad Q_{i+\frac{1}{2}}^- = Q(x_{i+\frac{1}{2}}^-).$$

The numerical convection fluxes \hat{f} and \hat{g} are chosen as any monotone fluxe, while the other numerical fluxes are given as

$$\hat{M}_{ij} = \frac{[S_{ij}]}{[u]}, \quad \hat{S}_{ij} = S_{ij}^-, \quad \hat{q}_i = q_i^+, \quad \text{for } i, j = 1, 2.$$

In a special case if

$$\begin{aligned}
f(u) &= g(u) = A_{12}(u) = A_{21}(u) = 0, \\
A_{11} &= A_{22} = \alpha \text{ (constant)},
\end{aligned}$$

then (4.50) takes the form

$$\frac{\partial u}{\partial t} - \frac{\partial^2 u}{\partial x^2} - \frac{\partial^2 u}{\partial y^2} = 0.$$

By introducing the variables q_1 and q_2 we get

$$q_1 = \frac{\partial u}{\partial x}, \quad q_2 = \frac{\partial u}{\partial y}, \quad \frac{\partial u}{\partial t} - \frac{\partial q_1}{\partial x} - \frac{\partial q_2}{\partial y} = 0,$$

and the semi-discretization is

$$\begin{aligned}
\frac{\partial u_{ij}^{lm}}{\partial t} &= \frac{2l+1}{\Delta x_i} \frac{2m+1}{\Delta y_j} \int_{y_{j-\frac{1}{2}}}^{y_{j+\frac{1}{2}}} \left\{ \hat{q}_1(x_{i+\frac{1}{2}}, y) - (-1)^l \hat{q}_1(x_{i-\frac{1}{2}}, y) \right\} P_m \left(\frac{2(y-y_j)}{\Delta y_j} \right) dy \\
& - \frac{2l+1}{\Delta x_i} \frac{2m+1}{\Delta y_j} \int_{y_{j-\frac{1}{2}}}^{y_{j+\frac{1}{2}}} \int_{x_{i-\frac{1}{2}}}^{x_{i+\frac{1}{2}}} q_1(x, y) P_m \left(\frac{2(y-y_j)}{\Delta y_j} \right) \partial_x P_l \left(\frac{2(x-x_i)}{\Delta x_i} \right) dx dy
\end{aligned}$$

CHAPTER 4. NUMERICAL SCHEME AND DISCRETIZATION OF HYPERBOLIC AND PARABOLIC SYSTEMS

$$\begin{aligned}
& + \frac{2l+1}{\Delta x_i} \frac{2m+1}{\Delta y_j} \int_{x_{i-\frac{1}{2}}}^{x_{i+\frac{1}{2}}} \left\{ \hat{q}_2(x, y_{j+\frac{1}{2}}) - (-1)^m \hat{q}_2(x, y_{j-\frac{1}{2}}) \right\} P_l \left(\frac{2(x-x_i)}{\Delta x_i} \right) dx \\
& - \frac{2l+1}{\Delta x_i} \frac{2m+1}{\Delta y_j} \int_{y_{j-\frac{1}{2}}}^{y_{j+\frac{1}{2}}} \int_{x_{i-\frac{1}{2}}}^{x_{i+\frac{1}{2}}} q_2(x, y) P_l \left(\frac{2(x-x_i)}{\Delta x_i} \right) \partial_y P_m \left(\frac{2(y-y_j)}{\Delta y_j} \right) dx dy, \\
q_{1ij}^{lm} & = \frac{2l+1}{\Delta x_i} \frac{2m+1}{\Delta y_j} \int_{y_{j-\frac{1}{2}}}^{y_{j+\frac{1}{2}}} \left\{ \hat{u}(x_{i+\frac{1}{2}}, y) - (-1)^l \hat{u}(x_{i-\frac{1}{2}}, y) \right\} P_m \left(\frac{2(y-y_j)}{\Delta y_j} \right) dy \\
& - \frac{2l+1}{\Delta x_i} \frac{2m+1}{\Delta y_j} \int_{y_{j-\frac{1}{2}}}^{y_{j+\frac{1}{2}}} \int_{x_{i-\frac{1}{2}}}^{x_{i+\frac{1}{2}}} u(x, y) P_m \left(\frac{2(y-y_j)}{\Delta y_j} \right) \partial_x P_l \left(\frac{2(x-x_i)}{\Delta x_i} \right) dx dy, \\
q_{2ij}^{lm} & = \frac{2l+1}{\Delta x_i} \frac{2m+1}{\Delta y_j} \int_{x_{i-\frac{1}{2}}}^{x_{i+\frac{1}{2}}} \left\{ \hat{u}(x, y_{j+\frac{1}{2}}) - (-1)^m \hat{u}(x, y_{j-\frac{1}{2}}) \right\} P_l \left(\frac{2(x-x_i)}{\Delta x_i} \right) dx \\
& - \frac{2l+1}{\Delta x_i} \frac{2m+1}{\Delta y_j} \int_{y_{j-\frac{1}{2}}}^{y_{j+\frac{1}{2}}} \int_{x_{i-\frac{1}{2}}}^{x_{i+\frac{1}{2}}} u(x, y) P_l \left(\frac{2(x-x_i)}{\Delta x_i} \right) \partial_y P_m \left(\frac{2(y-y_j)}{\Delta y_j} \right) dx dy.
\end{aligned}$$

The numerical fluxes for this case are

$$\begin{aligned}
\hat{u}(x_{i+\frac{1}{2}}, y) & = u^-(x_{i+\frac{1}{2}}, y), & \hat{u}(x, y_{j+\frac{1}{2}}) & = u^-(x, y_{j+\frac{1}{2}}), \\
\hat{q}_1(x_{i+\frac{1}{2}}, y) & = q_1^+(x_{i+\frac{1}{2}}, y), & \hat{q}_1(x, y_{j+\frac{1}{2}}) & = q_1^+(x, y_{j+\frac{1}{2}}), \\
\hat{q}_2(x_{i+\frac{1}{2}}, y) & = q_2^+(x_{i+\frac{1}{2}}, y), & \hat{q}_2(x, y_{j+\frac{1}{2}}) & = q_2^+(x, y_{j+\frac{1}{2}}),
\end{aligned}$$

where

$$\begin{aligned}
u^-(x_{i+\frac{1}{2}}, y) & = \sum_{r=0}^k \sum_{s=0}^k u_{ij}^{rs}(t) P_r \left(\frac{2(x-x_i)}{\Delta x_i} \right) P_s \left(\frac{2(y-y_j)}{\Delta y_j} \right) \Big|_{x=x_{i+\frac{1}{2}}}, \\
u^-(x, y_{j+\frac{1}{2}}) & = \sum_{r=0}^k \sum_{s=0}^k u_{ij}^{rs}(t) P_r \left(\frac{2(x-x_i)}{\Delta x_i} \right) P_s \left(\frac{2(y-y_j)}{\Delta y_j} \right) \Big|_{y=y_{j+\frac{1}{2}}}, \\
q_1^+(x_{i+\frac{1}{2}}, y) & = \sum_{r=0}^k \sum_{s=0}^k q_{1i+1,j}^{rs}(t) P_r \left(\frac{2(x-x_i)}{\Delta x_i} \right) P_s \left(\frac{2(y-y_j)}{\Delta y_j} \right) \Big|_{x=x_{i+\frac{1}{2}}}, \\
q_1^+(x, y_{j+\frac{1}{2}}) & = \sum_{r=0}^k \sum_{s=0}^k q_{1i,j+1}^{rs}(t) P_r \left(\frac{2(x-x_i)}{\Delta x_i} \right) P_s \left(\frac{2(y-y_j)}{\Delta y_j} \right) \Big|_{y=y_{j+\frac{1}{2}}}, \\
q_2^+(x_{i+\frac{1}{2}}, y) & = \sum_{r=0}^k \sum_{s=0}^k q_{2i+1,j}^{rs}(t) P_r \left(\frac{2(x-x_i)}{\Delta x_i} \right) P_s \left(\frac{2(y-y_j)}{\Delta y_j} \right) \Big|_{x=x_{i+\frac{1}{2}}}, \\
q_2^+(x, y_{j+\frac{1}{2}}) & = \sum_{r=0}^k \sum_{s=0}^k q_{2i,j+1}^{rs}(t) P_r \left(\frac{2(x-x_i)}{\Delta x_i} \right) P_s \left(\frac{2(y-y_j)}{\Delta y_j} \right) \Big|_{y=y_{j+\frac{1}{2}}}.
\end{aligned}$$

4.6 Numerical solution of ordinary differential equations

4.6.1 Runge-Kutta method

To integrate the ordinary differential equations (ODEs) an explicit Runge-Kutta method is used. This method gives very precise results and is very easy to implement. To illustrate this method we take a simple first order ordinary differential equation $u' = f(t, u)$ with the initial condition $u(t_0) = u_0$. Denoting the number of stages by r , the general form of the family of Runge-Kutta method is given as

$$u_{n+1} = u_n + \Delta t \sum_{i=1}^r \beta_i H_i,$$

where

$$\begin{aligned} H_1 &= f(t_n, u_n), \\ H_2 &= f(t_n + \gamma_2 \Delta t, u_n + \Delta t \alpha_{21} H_1), \\ H_3 &= f(t_n + \gamma_3 \Delta t, u_n + \Delta t (\alpha_{31} H_1 + \alpha_{32} H_2)), \\ &\vdots \\ H_r &= f(t_n + \gamma_r \Delta t, u_n + \Delta t (\alpha_{r1} H_1 + \alpha_{r2} H_2 + \cdots + \alpha_{r,r-1} H_{r-1})). \end{aligned}$$

Here the matrix $[\alpha_{ij}]$ for $1 \leq j < i \leq r$ denotes the Runge-Kutta matrix, while the coefficients β_i for $i = 1, \dots, r$ and γ_i for $i = 2, \dots, r$ are the weights and the nodes respectively. The Runge-Kutta formula can be expressed using the so-called *Butcher array*. For explicit methods it has the form

$$\begin{array}{c|cccccc} 0 & & & & & & \\ \gamma_2 & \alpha_{21} & & & & & \\ \gamma_3 & \alpha_{31} & \alpha_{32} & & & & \\ \vdots & \vdots & & \ddots & & & \\ \gamma_r & \alpha_{r1} & \alpha_{r2} & \cdots & \alpha_{r,r-1} & & \\ \hline & \beta_1 & \beta_2 & \cdots & \beta_{r-1} & \beta_r & \end{array}$$

with the property

$$\gamma_i = \sum_{j=1}^r \alpha_{ij}.$$

For $r = 1$ we get the simplest Runge-Kutta method. In comparison with Taylor expansion we find that $\beta_1 = 1$. In this case we get

$$u_{n+1} = u_n + \Delta t f(t_n, u_n),$$

which is exactly the explicit Euler's method.

For $r = 2$ we get a two stage Runge-Kutta method with the Butcher array

CHAPTER 4. NUMERICAL SCHEME AND DISCRETIZATION OF HYPERBOLIC AND PARABOLIC SYSTEMS

$$\begin{array}{c|c} 0 & \\ \hline 1/2 & 1/2 \\ \hline & 0 \quad 1 \end{array}$$

In this case the second order Runge-Kutta method is given as

$$u_{n+1} = u_n + \Delta t f\left(t_n + \frac{\Delta t}{2}, u_n + \frac{\Delta t}{2} f(t_n, u_n)\right).$$

For $r = 4$ a corresponding Butcher array is

$$\begin{array}{c|ccc} 0 & & & \\ \hline 1/2 & 1/2 & & \\ 1/2 & 0 & 1/2 & \\ 1 & 0 & 0 & 1 \\ \hline & 1/6 & 1/3 & 1/3 & 1/6 \end{array}$$

giving the classical fourth order Runge-Kutta method that has the form

$$u_{n+1} = u_n + \frac{\Delta t}{2}(H_1 + 2H_2 + 2H_3 + H_4),$$

with

$$\begin{aligned} H_1 &= f(t_n, u_n), \\ H_2 &= f\left(t_n + \frac{\Delta t}{2}, u_n + \frac{\Delta t}{2} H_1\right), \\ H_3 &= f\left(t_n + \frac{\Delta t}{2}, u_n + \frac{\Delta t}{2} H_2\right), \\ H_4 &= f(t_n + \Delta t, u_n + \Delta t H_2). \end{aligned}$$

For more details about Runge-Kutta methods the reader is referred to [75], [9], [93], [8], [58].

4.6.2 Adaptive Runge-Kutta methods

Dormand-Prince method

The embedded Runge-Kutta methods include two Runge-Kutta formulas usually of orders p and $p - 1$, see [62]. One member of the Runge-Kutta family is the *Dormand-Prince method*. In this method p is taken to be 5. The corresponding Butcher array is given as

4.6. NUMERICAL SOLUTION OF ORDINARY DIFFERENTIAL EQUATIONS

0							
$\frac{1}{5}$	$\frac{1}{5}$						
$\frac{3}{10}$	$\frac{3}{40}$	$\frac{9}{40}$					
$\frac{4}{5}$	$\frac{44}{45}$	$-\frac{56}{15}$	$\frac{32}{9}$				
$\frac{8}{9}$	$\frac{19372}{6561}$	$-\frac{25360}{2187}$	$\frac{64448}{6561}$	$-\frac{212}{729}$			
1	$\frac{9017}{3168}$	$-\frac{355}{33}$	$\frac{46732}{5247}$	$\frac{49}{176}$	$-\frac{5103}{18656}$		
1	$\frac{35}{384}$	0	$\frac{500}{1113}$	$\frac{125}{192}$	$-\frac{2187}{6784}$	$\frac{11}{84}$	
	$\frac{5179}{57600}$	0	$\frac{7571}{16695}$	$\frac{393}{640}$	$-\frac{92097}{339200}$	$\frac{187}{2100}$	$\frac{1}{40}$
	$\frac{35}{384}$	0	$\frac{500}{1113}$	$\frac{125}{192}$	$-\frac{2187}{6784}$	$\frac{11}{84}$	0

The scheme of the lower order step is given as

$$\hat{u}_{n+1} = u_n + \Delta t \sum_{i=1}^{p-1} \hat{\beta}_i H_i,$$

where the H_i 's are given as above. Now we can write

$$\hat{u}_{n+1} = u_n + \frac{35}{384} H_1 + \frac{500}{1113} H_3 + \frac{125}{192} H_4 - \frac{2187}{6784} H_5 + \frac{11}{84} H_6,$$

and

$$u_{n+1} = u_n + \frac{5179}{57600} H_1 + \frac{7571}{16695} H_3 + \frac{393}{640} H_4 - \frac{92097}{339200} H_5 + \frac{187}{2100} H_6 + \frac{1}{40} H_7.$$

The error is given as

$$|\hat{u}_{n+1} - u_{n+1}| = \left| \frac{71}{57600} H_1 - \frac{71}{16695} H_3 + \frac{71}{1920} H_4 - \frac{17253}{339200} H_5 + \frac{22}{525} H_6 - \frac{1}{40} H_7 \right|.$$

More details about this method can be found in [46], [78], [82], [21].

CHAPTER 4. NUMERICAL SCHEME AND DISCRETIZATION OF HYPERBOLIC AND PARABOLIC SYSTEMS

4.6.3 Backward and Numerical Differentiation Formulas

Backward Differentiation Formulas (BDF)

The $k - step$ BDF method has the form

$$\sum_{i=0}^k \alpha_i u_{n+i-k+1} = \Delta t \beta_k f(t_{n+1}, u_{n+1}). \tag{4.71}$$

Here Δt is the step size and α_i and β_k are parameters given in Table 4.1

k	α_5	α_4	α_3	α_2	α_1	α_0	β_k	p
1					1	-1	1	1
2				1	$-\frac{4}{3}$	$\frac{1}{3}$	$\frac{2}{3}$	2
3			1	$-\frac{18}{11}$	$\frac{9}{11}$	$-\frac{2}{11}$	$\frac{6}{11}$	3
4		1	$-\frac{48}{25}$	$\frac{36}{25}$	$-\frac{16}{25}$	$\frac{3}{25}$	$\frac{12}{25}$	4
5	1	$-\frac{300}{137}$	$\frac{300}{137}$	$-\frac{200}{137}$	$\frac{175}{137}$	$-\frac{12}{137}$	$\frac{60}{137}$	5

Table 4.1: Coefficients of the BDF methods

In this table p denotes the order of the method. As an example, the backward differentiation formula (BDF2) is given as

$$u_{n+1} = \frac{2}{3} \Delta t f(t_{n+1}, u_{n+1}) - \frac{1}{3} u_{n-1} + \frac{4}{3} u_n.$$

Equation (4.71) can be also written as

$$\sum_{m=1}^k \frac{1}{m} \nabla^m u_{n+1} = \Delta t f(t_{n+1}, u_{n+1}), \tag{4.72}$$

where the operator ∇ is given as

$$\nabla y_k = y_k - y_{k-1}.$$

Higher order differences can be obtained by repeating the operations of the backward difference operator, e.g.

4.6. NUMERICAL SOLUTION OF ORDINARY DIFFERENTIAL EQUATIONS

$$\begin{aligned}
 \nabla^2 y_k &= \nabla(\nabla y_k) = \nabla(y_k - y_{k-1}) \\
 &= \nabla y_k - \nabla y_{k-1} \\
 &= y_k - y_{k-1} - y_{k-1} + y_{k-2} \\
 &= y_k - 2y_{k-1} + y_{k-2}.
 \end{aligned}$$

In general we can write

$$\nabla^r y_k = \sum_{s=0}^r (-1)^s \binom{r}{s} y_{k-s},$$

where $\binom{r}{s}$ is the binomial coefficient.

Numerical Differentiation Formulas (NDF)

Numerical differentiation methods are a modification of the backward differentiation methods where a new term is added. For a k -step method these methods have the formula

$$\sum_{m=1}^k \frac{1}{m} \nabla^m u_{n+1} = \Delta t f(t_{n+1}, u_{n+1}) + \kappa \gamma_k (u_{n+1} - u_{n+1}^{[0]}), \quad (4.73)$$

where

$$u_{n+1}^{[0]} = \sum_{m=0}^k \nabla^m u_n.$$

In this formula κ is a scalar parameter and γ_k is given by $\gamma_k = \sum_{i=1}^k 1/i$. The coefficients of the NDF methods of order 1 to 5 are given in Table 4.2.

It is simple by induction to prove the following formula

$$u_{n+1} - u_{n+1}^{[0]} = \nabla^{k+1} u_{n+1}. \quad (4.74)$$

Using this formula it is possible also with induction to prove the following identity

$$\sum_{m=1}^k \frac{1}{m} \nabla^m u_{n+1} = \gamma_k (u_{n+1} - u_{n+1}^{[0]}) + \sum_{m=1}^k \gamma_m \nabla^m u_n.$$

Due to this formula, equation (4.73) is equivalent to the following equation

$$(1 - \kappa) \gamma_k (u_{n+1} - u_{n+1}^{[0]}) + \sum_{m=1}^k \gamma_m \nabla^m u_n - \Delta t f(t_{n+1}, u_{n+1}) = 0.$$

To solve this algebraic equation the simplified Newton's method is used. This method will be clarified in the following subsection. More details about the BDF and the NDF can be found in [30], [74] [69].

CHAPTER 4. NUMERICAL SCHEME AND DISCRETIZATION OF HYPERBOLIC AND PARABOLIC SYSTEMS

k	κ	α_5	α_4	α_3	α_2	α_1	α_0	β_k	p
1	-37/200					1	-1	1	1
2	-1/9				1	$-\frac{4}{3}$	$\frac{1}{3}$	$\frac{2}{3}$	2
3	-0.0823			1	$-\frac{18}{11}$	$\frac{9}{11}$	$-\frac{2}{11}$	$\frac{6}{11}$	3
4	-0.0415		1	$-\frac{48}{25}$	$\frac{36}{25}$	$-\frac{16}{25}$	$\frac{3}{25}$	$\frac{12}{25}$	4
5	0	1	$-\frac{300}{137}$	$\frac{300}{137}$	$-\frac{200}{137}$	$\frac{175}{137}$	$-\frac{12}{137}$	$\frac{60}{137}$	5

Table 4.2: Coefficients of the NDF methods

4.6.4 Newton and Simplified Newton's Iteration

Let $\varphi : \mathcal{D} \subseteq \mathbb{R}^n \rightarrow \mathbb{R}^n$ be a differential function. Newton iteration is a method used to solve non-linear algebraic equations as

$$\varphi_i(x_1, \dots, x_N) = 0, \quad i = 1 : \dots, N.$$

In the Newton iteration the function $\varphi(X)$ where $X = (x_1, \dots, x_N)$ is approximated in the vicinity of $X^k = (x_1^k, \dots, x_N^k)$ by a function $\varphi_k(X)$ and the solution is used as the next iterate $X^{k+1} = (x_1^{k+1}, \dots, x_N^{k+1})$. Making use of Taylor expansion we get

$$0 = \varphi_k(X) = \varphi(X^k) + J_\varphi(X^k)(X - X^k).$$

Here $J_\varphi(X)$ is the Jacobi matrix given by

$$[J_\varphi(X)]_{ij} = \frac{\partial \varphi_i(X)}{\partial x_j}.$$

Next we solve the equation $\varphi_k(X^{k+1}) = 0$ for the iterate X^{k+1}

$$0 = \varphi_k(X^{k+1}) = \varphi(X^k) + J_\varphi(X^k)(X^{k+1} - X^k)$$

or

$$X^{k+1} = X^k - [J_\varphi(X^k)]^{-1} \varphi(X^k).$$

This is called the Newton iteration. If the same Jacobi matrix is used successively then we get the so-called the simplified Newton's method where the iteration is given by

$$X^{k+1} = X^k - [J_\varphi(X^0)]^{-1} \varphi(X^k).$$

The iteration is terminated if the convergence is not achieved. In this case the step size is reduced. For more details the reader is referred to [10], [75], [40].

4.7 Numerical integration

For some integrands it is very complicated to find the integrals because of the complicated nature of these integrands. In order to solve this problem some numerical integrations are used, e.g. *trapezoidal rule*, *rectangle rule*, *Simpson's rule*, *Newton-Cotes formulas*, *Gauß-Legendre quadrature*. In our work *Gauß-Legendre quadrature* is used for 1D and 2D domains.

Gauß-Legendre quadrature for 1D

The integral

$$I_f = \int_{-1}^{+1} f(x) dx$$

is approximated by the sum

$$I_f \approx \sum_{i=1}^n w_i f(x_i).$$

Here w_i and x_i represent the weights and the nodes respectively. The Gauß node x_i is the i^{th} root of the Legendre polynomial P_n given by

$$P_n = \frac{1}{2^n n!} \frac{d^n}{dx^n} [(x^2 - 1)^n].$$

The weights are given by

$$w_i = \frac{2}{(1 - x_i^2)[P_n'(x_i)]^2},$$

see [17].

Example 4.7.1. For two points, i.e. $n = 2$ we have two nodes located at $x_1 = -1/\sqrt{3}$ and $x_2 = 1/\sqrt{3}$. The corresponding weights are $w_1 = w_2 = 1$

$$\int_{-1}^{+1} f(\zeta) d\zeta = f\left(\frac{1}{\sqrt{3}}\right) + f\left(-\frac{1}{\sqrt{3}}\right).$$

The nodes and the weights up to 5 points are listed in Table 4.3. The nodes and the weights up to $n = 16$ can be found in [2].

In general, in order to integrate

$$I_f = \int_a^b f(x) dx \tag{4.75}$$

we take a transformation $T = \alpha x + \beta$ and solve the system

$$\begin{aligned} -1 &= \alpha a + \beta, \\ +1 &= \alpha b + \beta. \end{aligned}$$

CHAPTER 4. NUMERICAL SCHEME AND DISCRETIZATION OF HYPERBOLIC AND PARABOLIC SYSTEMS

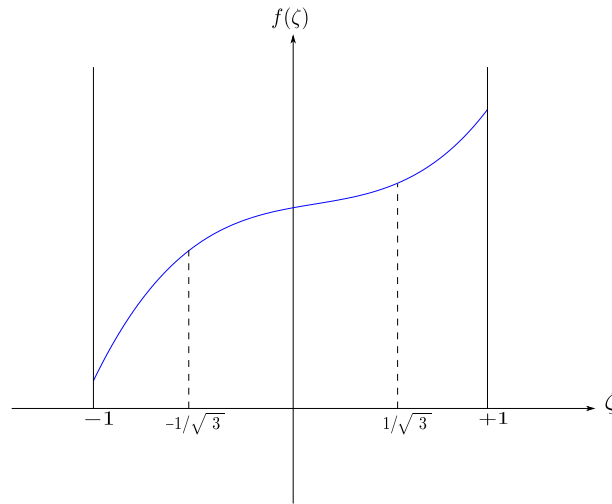


Figure 4.4: A 2-point Gauß-Legendre quadrature rule

Number of points, n	Nodes, x_i	Weights, w_i
1	0	2
2	$\pm 1/\sqrt{3}$	1
3	0	8/9
	$\pm \sqrt{3/5}$	5/9
4	$\pm \sqrt{\frac{3}{7} - \frac{2}{7}\sqrt{\frac{6}{5}}}$	$\frac{18+\sqrt{30}}{36}$
	$\pm \sqrt{\frac{3}{7} + \frac{2}{7}\sqrt{\frac{6}{5}}}$	$\frac{18-\sqrt{30}}{36}$
5	0	128/225
	$\pm \frac{1}{3}\sqrt{5 - 2\sqrt{\frac{10}{7}}}$	$\frac{322+13\sqrt{70}}{900}$
	$\pm \frac{1}{3}\sqrt{5 + 2\sqrt{\frac{10}{7}}}$	$\frac{322-13\sqrt{70}}{900}$

Table 4.3: Table of nodes and weights up to $n = 5$

The solution of this system gives

$$\alpha = \frac{2}{b-a}, \quad \beta = \frac{a+b}{a-b}.$$

The transformation we seek now is

$$T = \frac{1}{b-a} \left(2x - (a+b) \right).$$

The integral I_f can be written now as

$$\int_a^b f(x) dx = \frac{b-a}{2} \int_{-1}^{+1} f \left(\frac{b-a}{2} T + \frac{a+b}{2} \right) dT.$$

The approximation of this integral is given due to Gauß-Legendre by

$$\int_a^b f(x)dx \approx \frac{b-a}{2} \sum_{i=1}^n w_i f\left(\frac{b-a}{2}T_i + \frac{a+b}{2}\right). \quad (4.76)$$

Gauß-Legendre quadrature for 2D

The integral

$$I_f = \int_{-1}^{+1} \int_{-1}^{+1} f(x, y) dx dy$$

is approximated by the sum

$$I_f \approx \sum_{i=1}^n \sum_{j=1}^n w_i w_j f(x_i, y_j).$$

Again w_i, w_j represent the weights and x_i, x_i represent the nodes. For one point i.e. $n = 1$ we have

$$I_f = \int_{-1}^{+1} \int_{-1}^{+1} f(x, y) dx dy = 4f(0, 0).$$

For two points i.e. $n = 2$ we get the formula

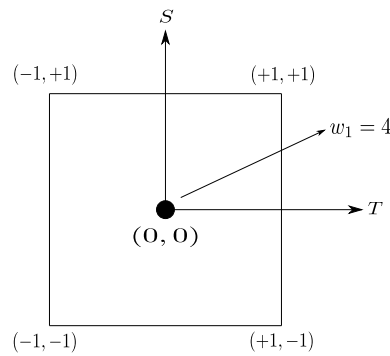


Figure 4.5: One point Gauß-Legendre rule

$$\begin{aligned} I_f &= \int_{-1}^{+1} \int_{-1}^{+1} f(x, y) dx dy \\ &= f\left(\frac{1}{\sqrt{3}}, \frac{1}{\sqrt{3}}\right) + f\left(-\frac{1}{\sqrt{3}}, \frac{1}{\sqrt{3}}\right) + f\left(\frac{1}{\sqrt{3}}, -\frac{1}{\sqrt{3}}\right) + f\left(-\frac{1}{\sqrt{3}}, -\frac{1}{\sqrt{3}}\right). \end{aligned}$$

In general, the integral

$$I_f = \int_a^b \int_c^d f(x, y) dy dx$$

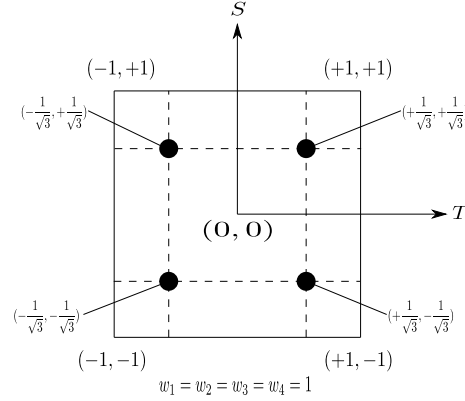


Figure 4.6: Two points Gauß-Legendre rule

can be written after taking the following two transformations with respect to x and y

$$T = \frac{1}{b-a} \left(2x - (a+b) \right), \quad S = \frac{1}{d-c} \left(2y - (c+d) \right),$$

as

$$I_f = \frac{b-a}{2} \frac{d-c}{2} \int_{-1}^{+1} \int_{-1}^{+1} f \left(\frac{b-a}{2} T + \frac{a+b}{2}, \frac{d-c}{2} S + \frac{c+d}{2} \right) dS dT.$$

The approximation of this integral is given due to Gauß-Legendre quadrature by

$$I_f = \frac{b-a}{2} \frac{d-c}{2} \sum_{i=1}^n \sum_{j=1}^n w_i w_j f \left(\frac{b-a}{2} T_i + \frac{a+b}{2}, \frac{d-c}{2} S_j + \frac{c+d}{2} \right). \quad (4.77)$$

For more details about Gauß-Legendre quadrature and some other methods, the reader is referred to [22] and [67].

4.8 The L^2 error and the experimental order of convergence EOC

The L^2 error in the region Ω is given in the following formula

$$\|u - u_h\|_{L^2(\Omega)} = \left(\int_{\Omega} |u - u_h|^2 d\Omega \right)^{1/2},$$

where u and u_h are the exact and the approximate solutions respectively.

The experimental order of convergence (EOC) of the mesh sizes h and h' can be calculated with respect to the L^p - norm as follows

$$EOC(h, h') := \frac{\log(\|u - u_{h'}\|_{L^p}) - \log(\|u - u_h\|_{L^p})}{\log h - \log h'}.$$

4.9 Numerical examples

In the following the discontinuous Galerkin method with piecewise linear elements has been used for the spatial discretization, while the resulting ODEs were solved using the Dormand-Prince method. Both methods have been already explained in Sections 4.2, 4.3, 4.4 and 4.5 as well as in Subsection 4.6.2.

4.9.1 1D hyperbolic partial differential equation example

In the following we consider the advection equation given by

$$u_t + u_x = 0, \quad \text{in }]0, 2\pi[\times]0, 10[, \quad (4.78)$$

with the initial condition

$$u(x, 0) = \sin(x), \quad \text{for all } x \in]0, 2\pi[, \quad (4.79)$$

and the periodic boundary condition. The exact solution for this equation is given as $u(x, t) = \sin(x - t)$. Figure 4.7 shows both the exact and the approximate solution taken

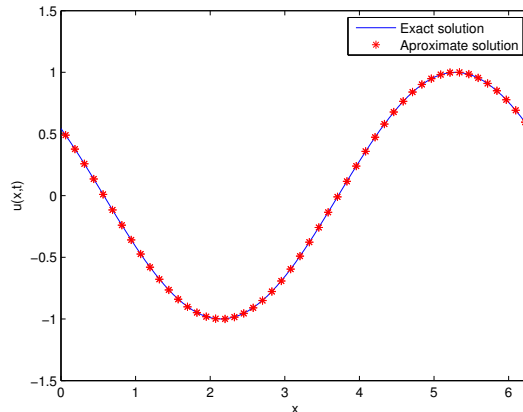


Figure 4.7: Comparison of the exact solution and the approximate solution.

with $N = 50$ points and piecewise linear elements.

In the table below we see the L^2 errors and the orders of convergence for the discontinuous Galerkin method applied to the equation (4.78) with the initial condition $u(x, 0) = \sin(x)$ at $t=10$.

Δx	L^2 error	order
$2\pi/50$	1.77e-03	—
$2\pi/100$	4.31e-04	2.04
$2\pi/200$	1.07e-04	2.00
$2\pi/400$	2.66e-05	2.00

4.9.2 1D parabolic partial differential equation example

Here we take the following heat equation

$$u_t - u_{xx} = 0, \quad \text{in }]0, 2\pi[\times]0, 1[, \quad (4.80)$$

with the initial condition

$$u(x, 0) = \sin(x), \quad \text{for all } x \in]0, 2\pi[, \quad (4.81)$$

and the periodic boundary condition. The exact solution for this equation is given as $u(x, t) = \exp(-t) \sin(x)$

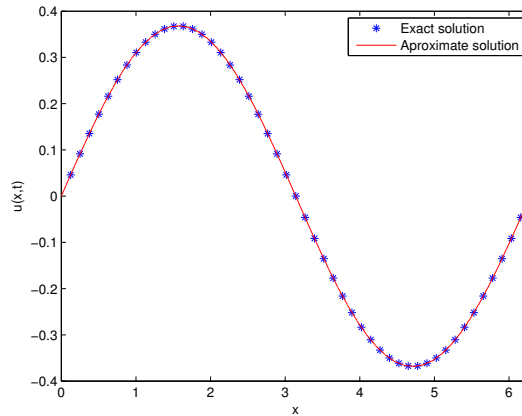


Figure 4.8: Comparison of the exact solution and the approximate solution.

Figure 4.8 shows both the exact and the approximate solution taken with $N = 50$ points and again with piecewise linear elements.

In the table below we see the L^2 errors and the orders of convergence for the discontinuous Galerkin method applied to the equation (4.80) with the initial condition $u(x, 0) = \sin(x)$ at $t=1$.

Δx	L^2 error	order
$2\pi/50$	6.26e-04	—
$2\pi/100$	1.56e-04	2.00
$2\pi/200$	3.89e-05	2.00
$2\pi/400$	9.64e-06	2.00

4.9.3 2D hyperbolic partial differential equation example

Here we find the numerical solution for the following 2D partial differential equation

$$u_t + u_x + u_y = 0, \quad (x, y) \in \Omega = [0, 4\pi] \times [0, 4\pi], \quad t \in [0, 2], \quad (4.82)$$

with the initial condition

$$u(x, y, 0) = \sin(x + y), \text{ for all } (x, y) \in \Omega \quad (4.83)$$

and the periodic boundary condition. The exact solution for this equation is $u(x, y) = \sin(x + y - 2t)$. Figure 4.9 shows the numerical solution of equation (4.82) at the left hand side next to the exact solution at the right hand side. The L^2 errors as well as the orders of convergence are presented in the following table.

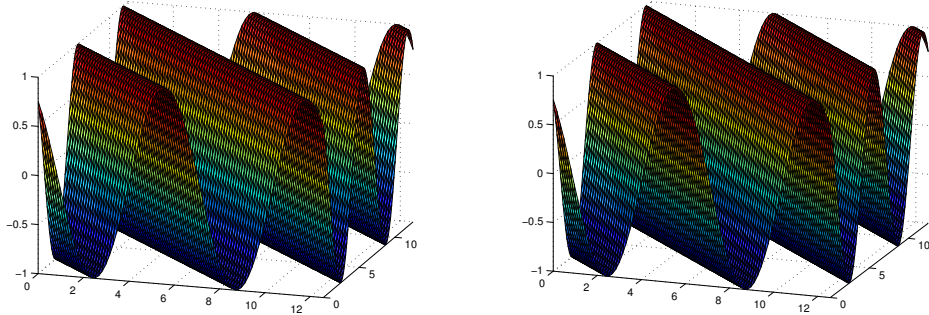


Figure 4.9: Numerical solution (left) and the exact solution (right).

mesh size	L^2 error	order
40×40	6.21e-02	—
80×80	1.51e-02	2.03
160×160	3.75e-03	2.01
320×320	9.35e-04	2.00

4.9.4 2D parabolic partial differential equation example

Now we consider the following 2D heat equation

$$u_t - \Delta u = 0, \quad (x, y) \in \Omega = [0, 2\pi] \times [0, 2\pi], \quad t \in [0, 0.4], \quad (4.84)$$

with the initial condition

$$u(x, y, 0) = \sin(x + y), \text{ for all } (x, y) \in \Omega \quad (4.85)$$

and the periodic boundary condition. Here Δ is the Laplacian operator given as

$$\Delta u = \nabla^2 u = \frac{\partial^2 u}{\partial x^2} + \frac{\partial^2 u}{\partial y^2}.$$

This PDE has an exact solution given as $u(x, y, t) = \exp(-2t) \sin(x + y)$.

Figure 4.10 presents the numerical solution for the equation (4.84) beside the exact solution with $N = 80$ and $T = 0.4$. The L^2 errors and the orders of convergence are shown in the bottom table.

CHAPTER 4. NUMERICAL SCHEME AND DISCRETIZATION OF HYPERBOLIC AND PARABOLIC SYSTEMS

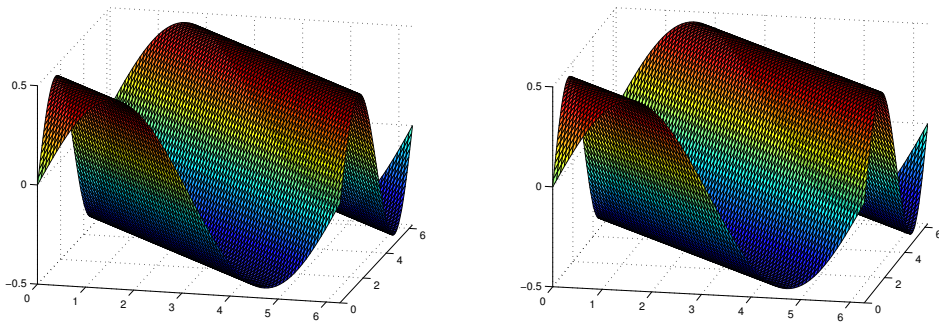


Figure 4.10: Numerical solution (left) and the exact solution (right).

mesh size	L^2 error	order
10×10	5.94e-02	—
20×20	1.41e-02	2.07
40×40	3.43e-03	2.03
80×80	8.48e-04	2.01

Chapter 5

Numerical Results

In this chapter we present the numerical results for the two systems given in Chapter 2. In the first section we show the numerical results in 1D for the uniform distribution of liquid droplets where we present the influence of the mass flow rate of the air \dot{m}_A , the temperature of air θ_{A2} , the heat transfer ratio f , the thickness of the film F as well as the mass flow rate of the liquid \dot{M}_{LV} . In the second section a 2D simulation for the case of a non-uniform distribution is presented. The results are computed at the top of the fluidized bed with respect to time and at the last moment $t = 250s$ with respect to the height.

5.1 Numerical results in 1D

The liquid is atomized and sprayed from the nozzle covering an area in the fluidized bed chamber. These droplets adhere on the surface of the particles forming a film on each particle. The water evaporates increasing the humidity of the air. As we see in Figure 5.1, the humidity is increasing almost linearly in the axial direction in both regions. The air temperature is decreasing also in axial direction, see Figure 5.2. The maximum value the temperature of air takes place directly at the bottom of the chamber where the distributor plate is. This is because of the inflow of the air.

The left hand side of Figure 5.3 shows that in region (2) the humidity of air is increasing with respect to time until it arrives the steady state. At this point the outlet humidity verifies the balance equation (2.23). The right hand side of Figure 5.3 shows that the degree of wetting is increasing at first very fast from its initial value 10^{-8} at $t = 0$ and then very slowly toward the outlet value. The temperature of air along with the temperature of particles are decreasing from the initial time $t = 0$ to the final time as seen in Figure 5.4. The temperature of the liquid film increases very sharply from the inlet liquid temperature to a certain value before it starts to decrease till it arrives to the steady state, see Figure 5.5. The interpretation of this phenomenon is that after a while the process reaches the equilibrium point between the heat supplied by the hot gas and the heat loss due to evaporation of the film.

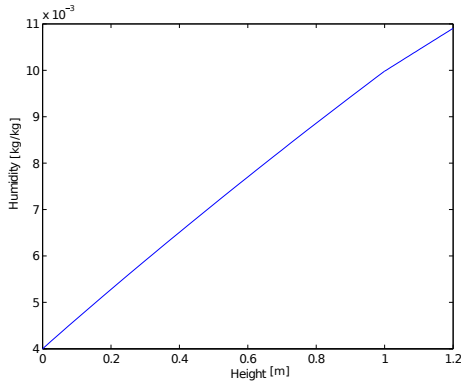


Figure 5.1: Humidity with respect to the height

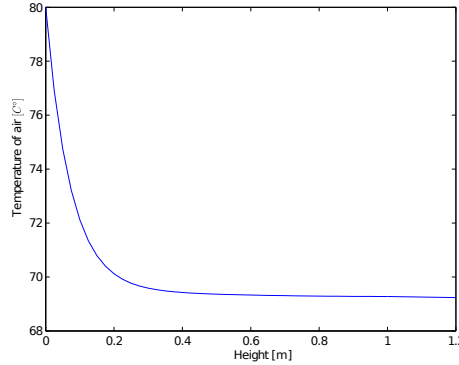


Figure 5.2: Temperature of air with respect to the height

Influence of the air mass flow rate \dot{m}_A

Figures 5.6 and 5.8 show that the air mass flow rate is inversely proportional to the humidity of air and the degree of wetting, while it is directly proportional to the air temperature and the particle temperature as seen in Figures 5.7 and 5.9. The outlet values of the liquid temperature at the steady state are changing slightly due to the change of the air mass flow rate, see Figure 5.10.

Influence of air temperature θ_{A2}

Figure 5.11 shows that the humidity is increasing towards the top of region (2). We can see in this figure that the outflow humidity at the top of region (2) for the lower temperature of air is larger than the outflow of the humidity for the higher temperature of air. In region (2) all of them have the same outflow value at the steady state to verify the balance equation (2.23). This can be interpreted as follows: At a higher temperature of air more evaporation takes place in region (1), consequently less water arrives in region (2). This leads to a lower humidity in the outflow in region (2). This can be also seen at the left hand side of Figure 5.13 which shows the humidity at the top of region (2). Different values of the air temperature lead to different outflow values at the steady state. Higher inlet air temperatures lead to higher outflow temperatures for each of the temperature of air, the particles and the liquid, see Figures 5.12, 5.14, and 5.15. In contrast to this, higher inlet air temperatures give lower values of the degree of wetting at the outlet, see the right hand side of Figure 5.13

Influence of the thickness of the liquid film F

From the Figures 5.16, 5.17 and 5.18 it is possible to see that every balance quantity has almost the same outlet value for different thicknesses of the liquid film. The only difference can be seen is the behavior of the balance equations in few seconds after the injection of the liquid. The thickness of the film has no influence on the heat transfer

5.1. NUMERICAL RESULTS IN 1D

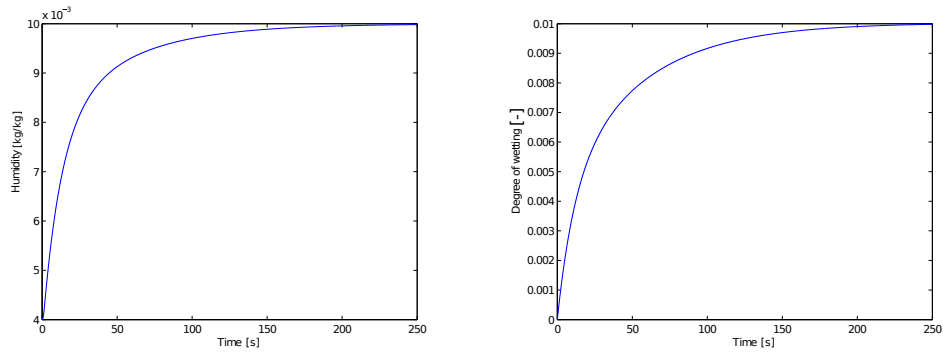


Figure 5.3: Simulation of air humidity and the degree of wetting with respect to the time.

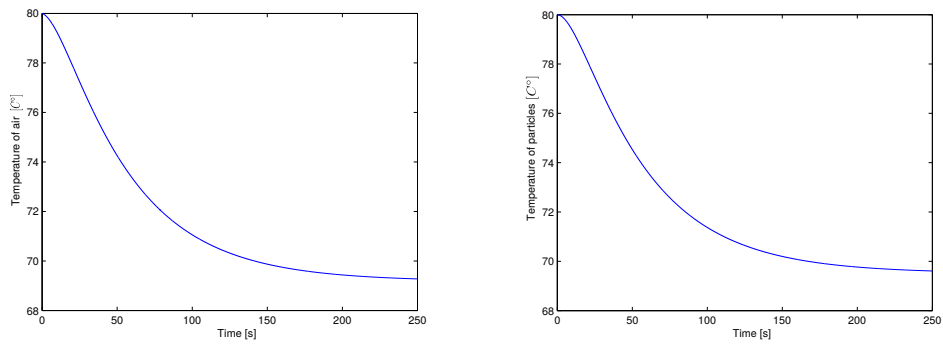


Figure 5.4: Simulation of the temperature of air and the temperature of particle with respect to the time.

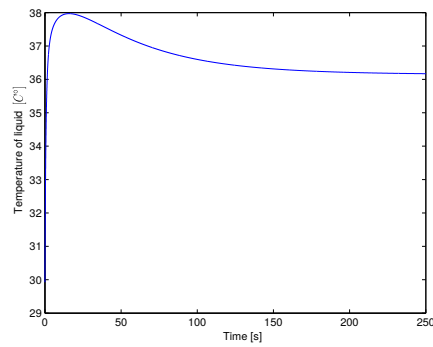


Figure 5.5: Simulation of the temperature of liquid with respect to the time.

between the liquid film and the air. It has an influence on just the particle. The stronger the thickness is, the more time is needed to arrive at the steady state.

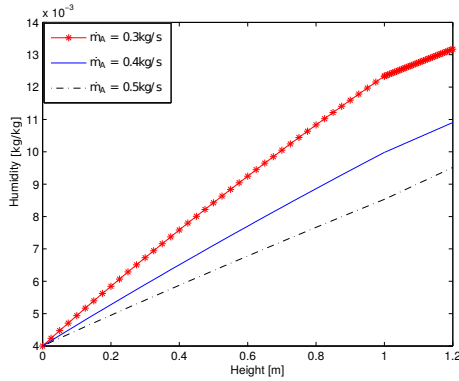


Figure 5.6: Simulation of air humidity with respect to the height for different values of \dot{m}_A

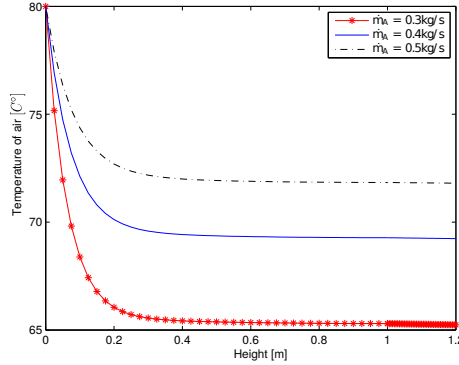


Figure 5.7: Simulation of air temperature with respect to the height for different values of \dot{m}_A

Influence of the mass flow rate of the liquid \dot{M}_{LV}

Increasing the mass flow rate of the liquid results in a higher humidity of the air. This matches with the balance equation (2.23). Also this increase leads to a larger degree of wetting where the wetted surface becomes larger which means that the interface between the liquid film and the air, as well as the liquid film and the particle becomes larger. This leads to a decrease in the temperatures of air, particles and the liquid film, see Figures 5.19, 5.20, 5.21, 5.22 and 5.23.

Influence of the heat transfer coefficient f

To see the effect of the ratio of the heat transfer coefficient f we present the simulations for two different thicknesses $F = 1 \mu m$ and $F = 100 \mu m$ each with a different ratio of heat transfer coefficient. As seen in Figure 5.27 for $F = 1 \mu m$ the humidity curves for different values of f are almost identical. This comes from the fact that for very small thicknesses, f has no effect on the evaporation flow. This also can be seen in Figure 5.28 for the temperature of air and the temperature of particle. The heat transfer coefficient has a strong effect on both the degree of wetting and the temperature of liquid, where a smaller value of f results in a higher outflow of the degree of wetting at the final value in contrast to the temperature of liquid outflow. This means that for a better heat transfer between the hot particles and the cold liquid film we get a higher temperature of liquid film, see Figures 5.24, 5.27, 5.26 and 5.29.

5.2 Numerical results in 2D

In this section we take into consideration the non-uniform distribution of the spray in the fluidized bed which was described in Chapter 2. The spraying is assumed to be down from the top. The nozzle is located at the top of the fluidized bed and in the middle of the

5.2. NUMERICAL RESULTS IN 2D

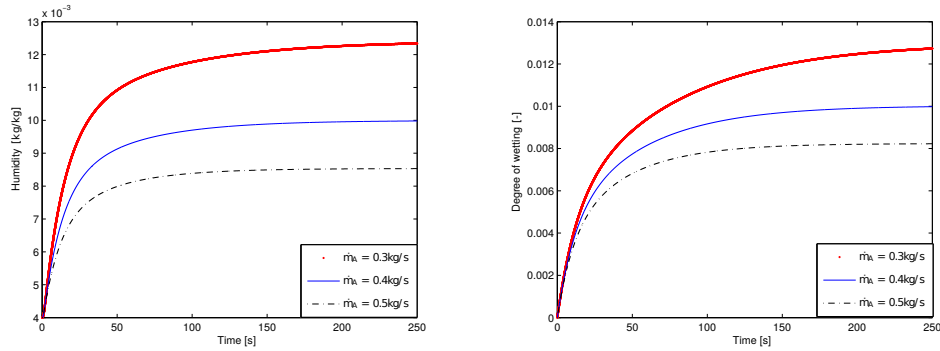


Figure 5.8: Simulation of air humidity and the degree of wetting for different values of \dot{m}_A .

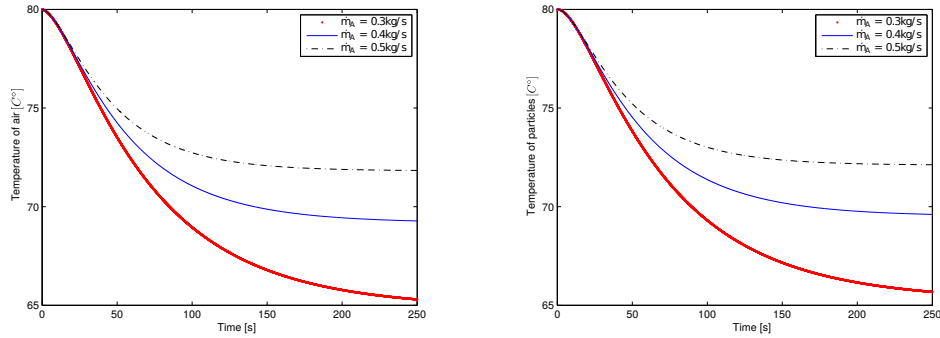


Figure 5.9: Simulation of the temperature of air and the temperature of particle for different values of \dot{m}_A .

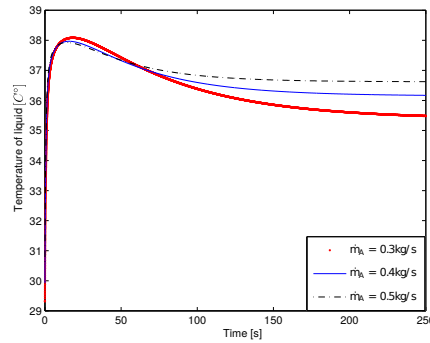


Figure 5.10: Simulation of the temperature of liquid for different values of \dot{m}_A .

diameter of the apparatus, i.e. at the point $(\frac{d_{app}}{2}, H_{tot})$ as seen in Figure 2.3. The spraying angle θ_{Nozz} is taken to be $\frac{\pi}{6}$ while the deposition efficiency is taken as $\phi_{dep} = 30\%$. Here we present the numerical results of the humidity of air, the temperature of the air, the degree of wetting, the temperature of the particles as well as the temperature of the liquid film. The humidity of the air is increasing almost linearly from its initial value until it

CHAPTER 5. NUMERICAL RESULTS

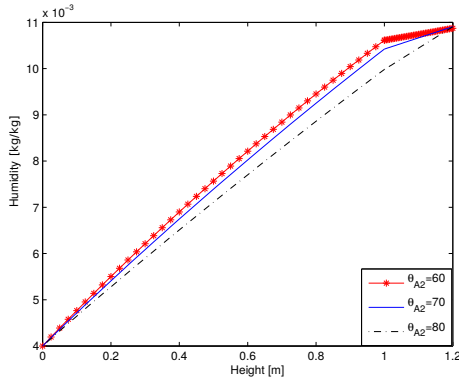


Figure 5.11: Simulation of air humidity with respect to the height for different values of θ_{A2}

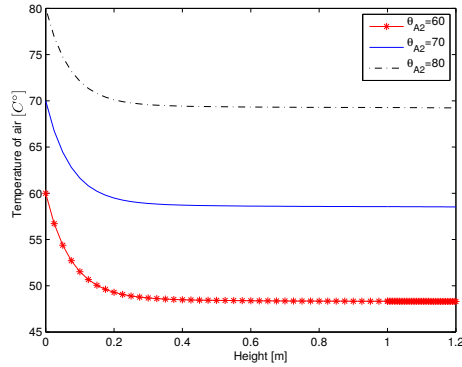


Figure 5.12: Simulation of the temperature of air with respect to the height for different values of θ_{A2}

arrives at the steady state where it reaches its maximum value at the top of the fluidized bed, see the left hand side of Figure 5.30. The temperature of air is decreasing from the initial value at $t = 0$ at the distribution plate until it arrives at the stationary state as seen in the right hand side of Figure 5.30. On the right hand side of Figure 5.31 we see that the temperature of particles has a very slight difference with respect to the height. This is because of the very high heat transfer between the air and the particles as well as between the air and the liquid film, also because of the high axial intermixing of the particles. Due to this we see a very small difference between the lowest and the highest value, where the difference does not exceed a few percent. The degree of wetting reaches its maximum value near the nozzle region and decreases after that. This is because of the fact that we have an almost complete deposition of the liquid droplets onto the particles after few centimeters from the nozzle, see the left hand side of Figure 5.31. Unlike the degree of wetting the temperature of the liquid film reaches the lowest value near the nozzle region. This is because of the fact that temperature of the injected liquid is 20°C , so the temperature decreases when the energy of the particles is absorbed and increases when the energy is emitted as seen in Figure 5.32. The patterns of the parameters in the 2D computations behave exactly as the 1D patterns. Because of this they will not be presented here. Instead of this we shall show the behavior of the parameters in different time levels. This can be seen in the figures from Fig 5.33 to Fig 5.62.

5.2. NUMERICAL RESULTS IN 2D

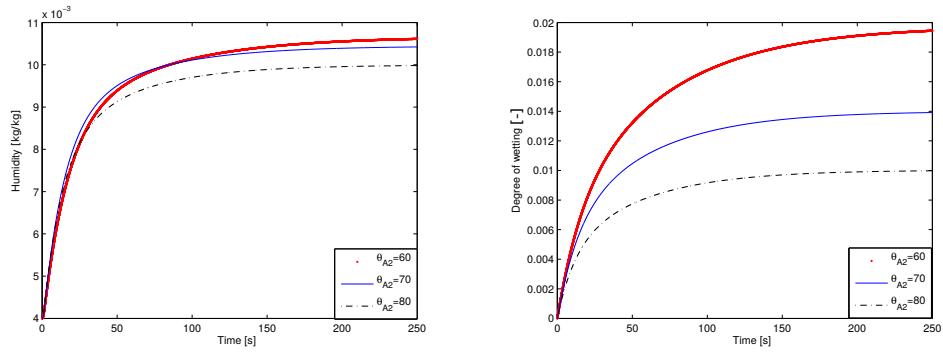


Figure 5.13: Simulation of air humidity and the degree of wetting for different values of θ_{A2} .

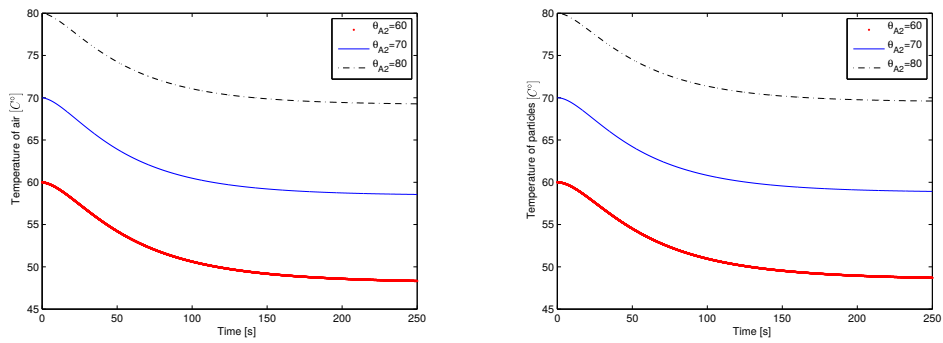


Figure 5.14: Simulation of the temperature of air and the temperature of particle for different values of θ_{A2} .

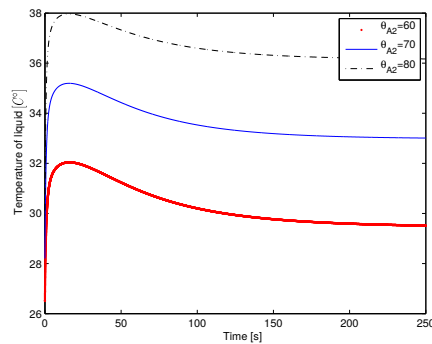


Figure 5.15: Simulation of the temperature of liquid for different values of θ_{A2} .

CHAPTER 5. NUMERICAL RESULTS

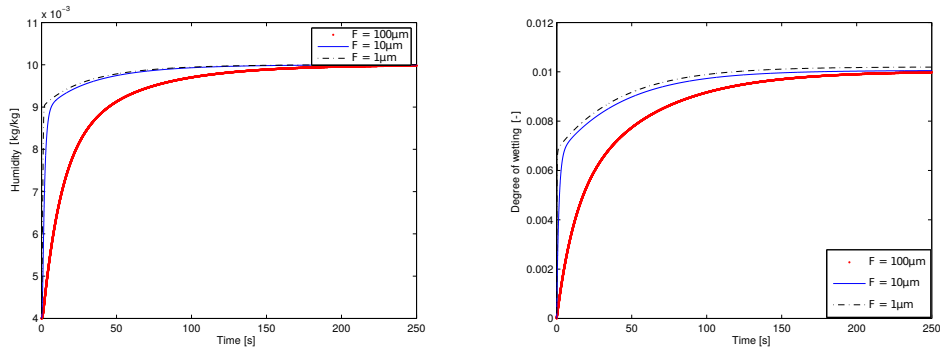


Figure 5.16: Simulation of air humidity and the degree of wetting for different values of F .

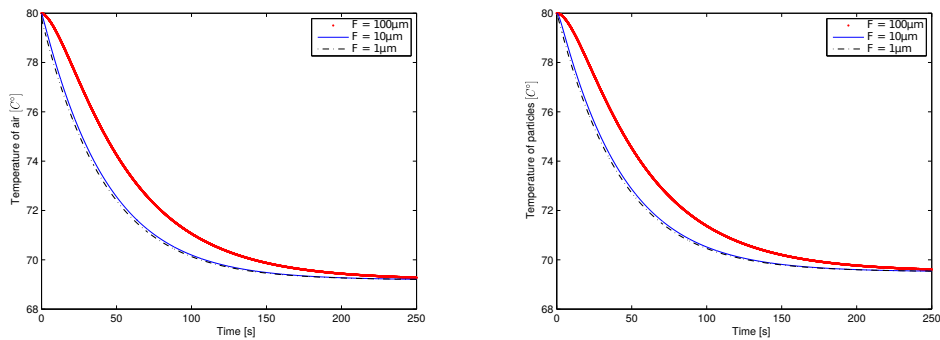


Figure 5.17: Simulation of the temperature of air and the temperature of particle for different values of F .

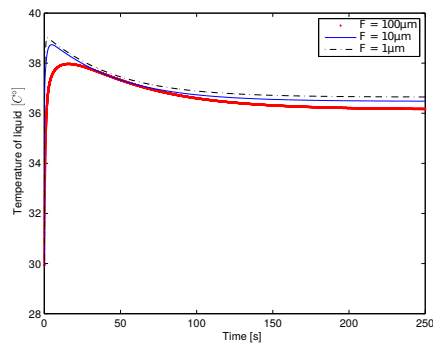


Figure 5.18: Simulation of the temperature of liquid for different values of F .

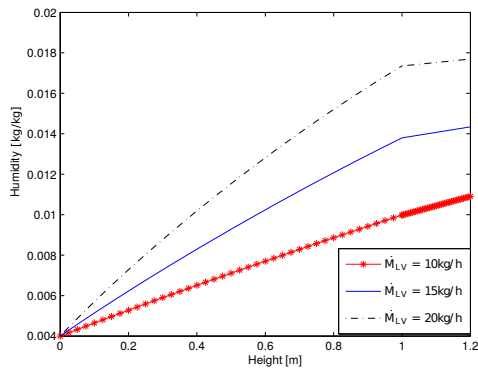


Figure 5.19: Simulation of air humidity with respect to the height for different values of \dot{M}_{LV}

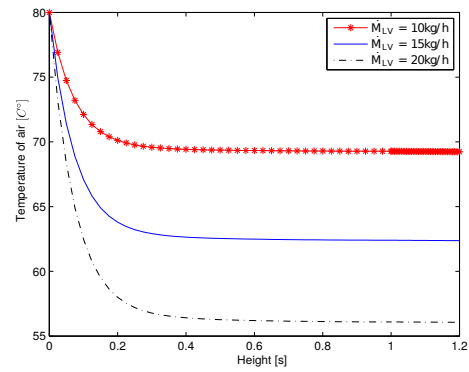


Figure 5.20: Simulation of air temperature with respect to the height for different values of \dot{M}_{LV}

CHAPTER 5. NUMERICAL RESULTS

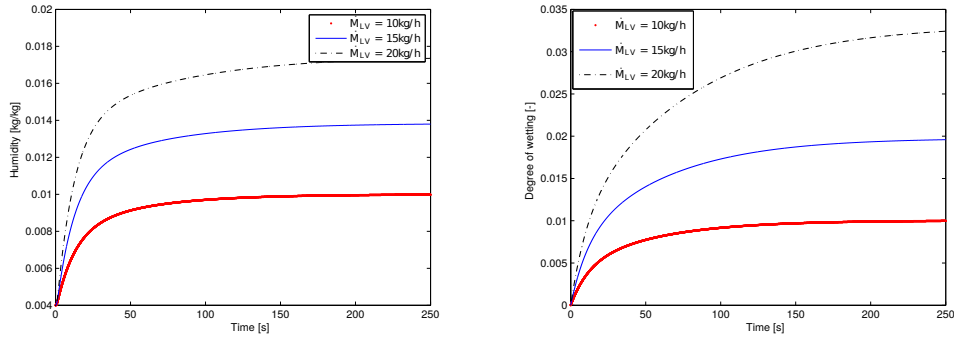


Figure 5.21: Simulation of air humidity and the degree of wetting for different values of \dot{M}_{LV} .

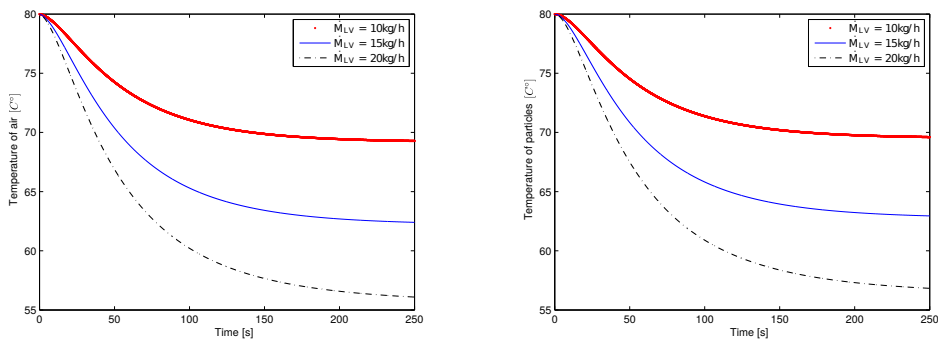


Figure 5.22: Simulation of the temperature of air and the temperature of particle for different values of \dot{M}_{LV} .

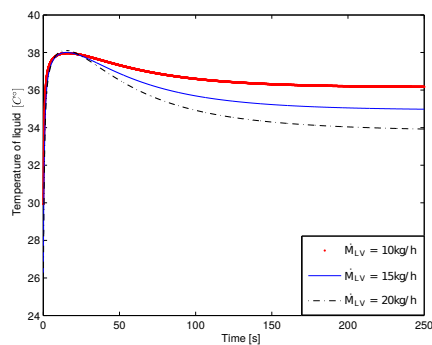


Figure 5.23: Simulation of the temperature of liquid for different values of \dot{M}_{LV} .

5.2. NUMERICAL RESULTS IN 2D

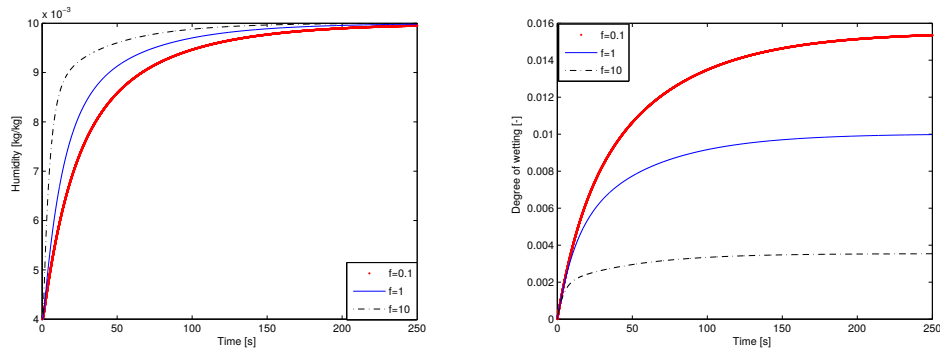


Figure 5.24: Simulation of air humidity and the degree of wetting for $F = 100 \mu\text{m}$ and different values of the heat transfer coefficient f .

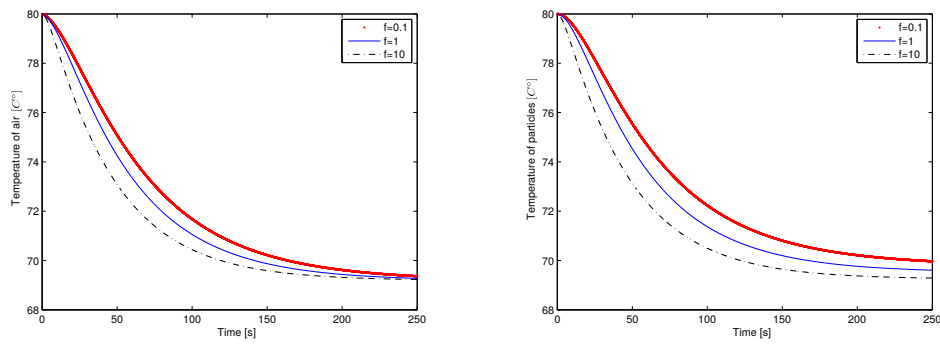


Figure 5.25: Simulation of air temperature and particle temperature for $F = 100 \mu\text{m}$ and different values of the heat transfer coefficient f .

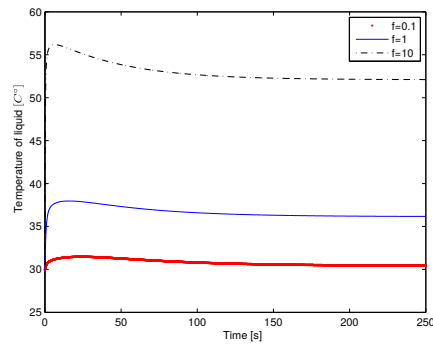


Figure 5.26: Simulation of the temperature of liquid for $F = 100 \mu\text{m}$ and different values of the heat transfer coefficient f .

CHAPTER 5. NUMERICAL RESULTS

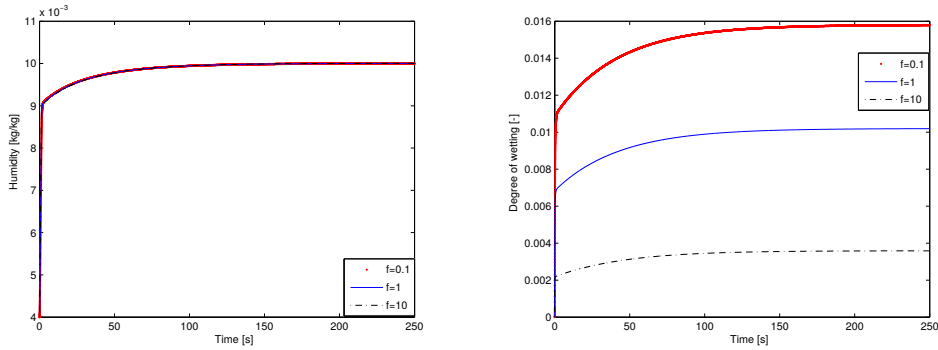


Figure 5.27: Simulation of air humidity and the degree of wetting for $F = 1 \mu m$ and different values of the heat transfer coefficient f .

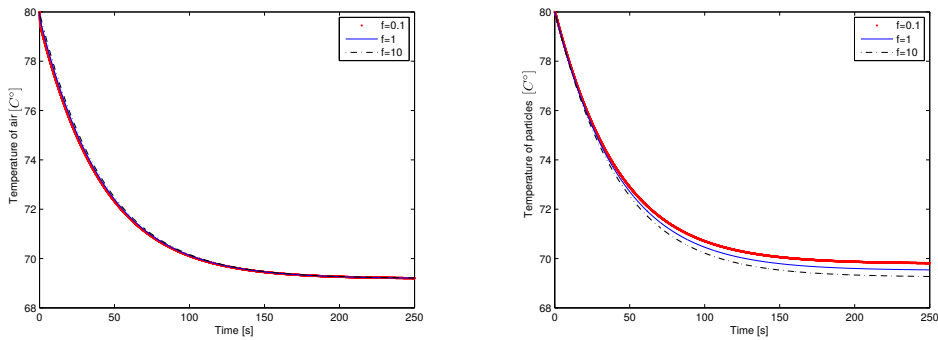


Figure 5.28: Simulation of air temperature and particle temperature for $F = 1 \mu m$ and different values of the heat transfer coefficient f .

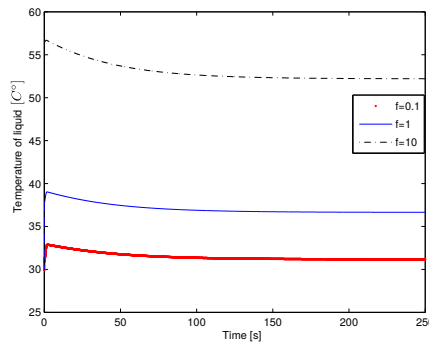


Figure 5.29: Simulation of the temperature of liquid for $F = 1 \mu m$ and different values of the heat transfer coefficient f .

5.2. NUMERICAL RESULTS IN 2D

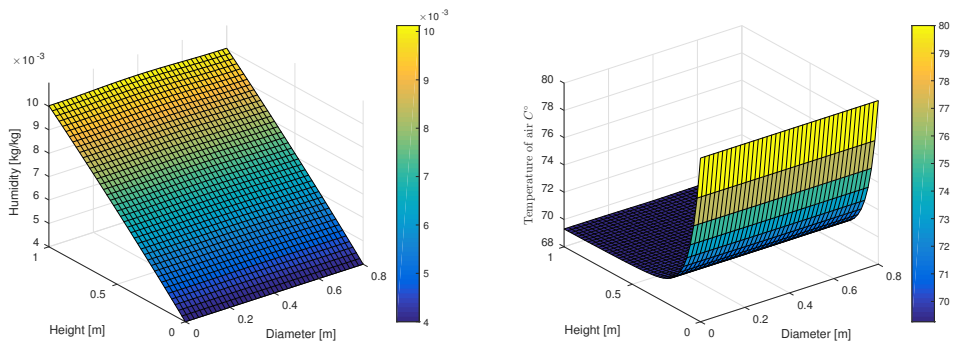


Figure 5.30: Simulation of air humidity and the temperature of air.

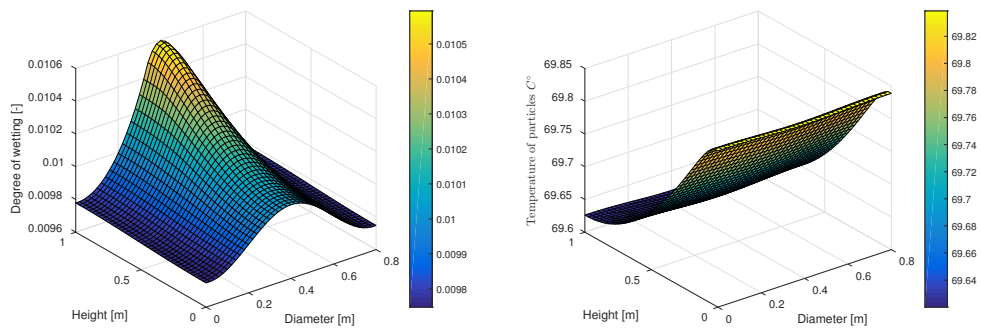


Figure 5.31: Simulation of the degree of wetting and the temperature of particles.

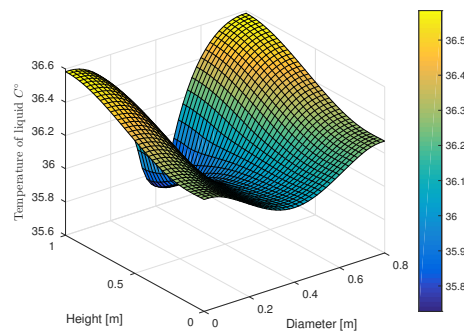


Figure 5.32: Simulation of the temperature of liquid.

CHAPTER 5. NUMERICAL RESULTS

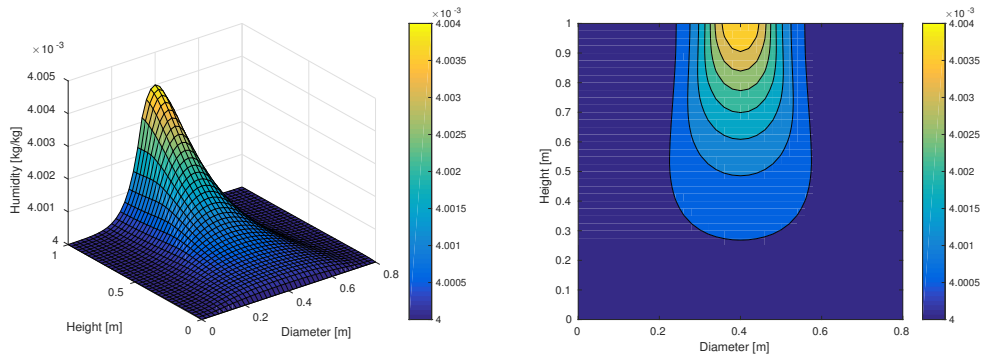


Figure 5.33: Simulation of air humidity at time $t = 0.1s$.

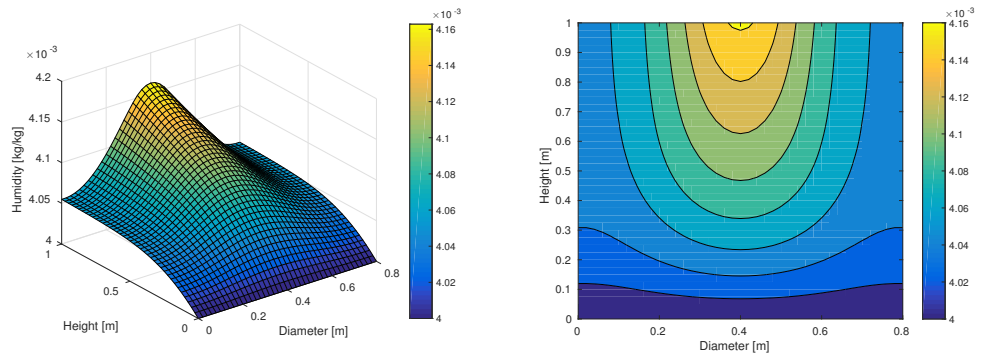


Figure 5.34: Simulation of air humidity at time $t = 1s$.

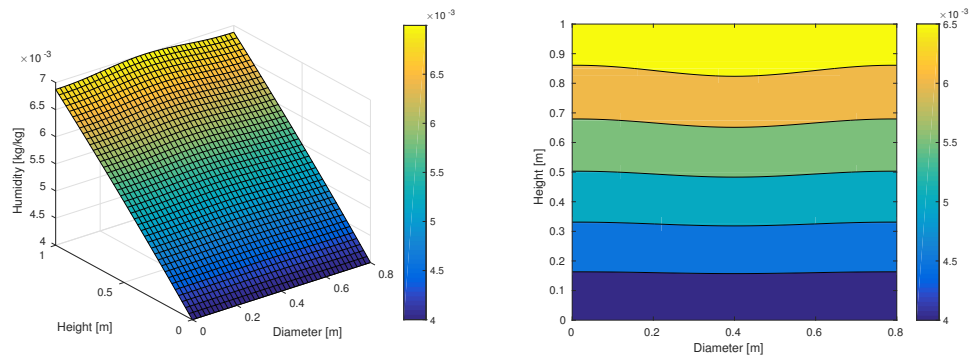


Figure 5.35: Simulation of air humidity at time $t = 10s$.

5.2. NUMERICAL RESULTS IN 2D

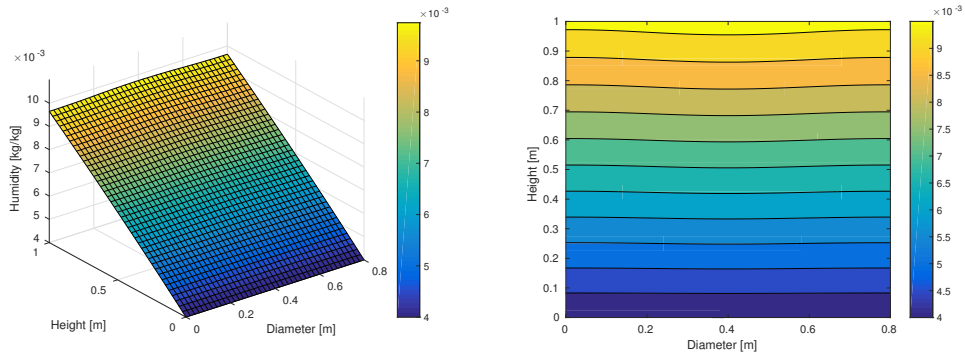


Figure 5.36: Simulation of air humidity at time $t = 50s$.

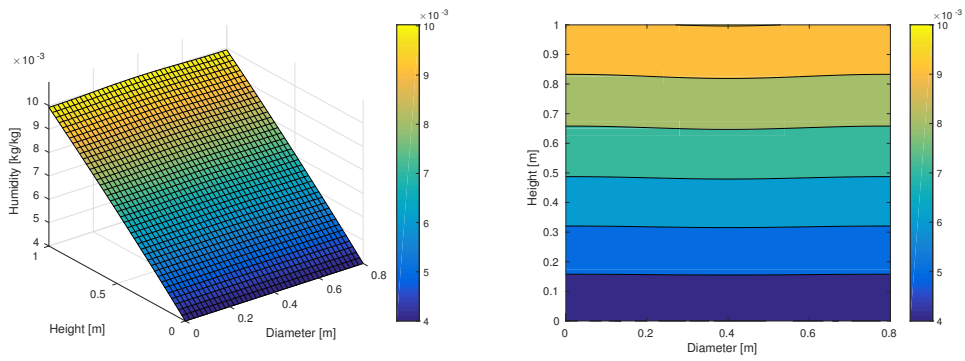


Figure 5.37: Simulation of air humidity at time $t = 100s$.

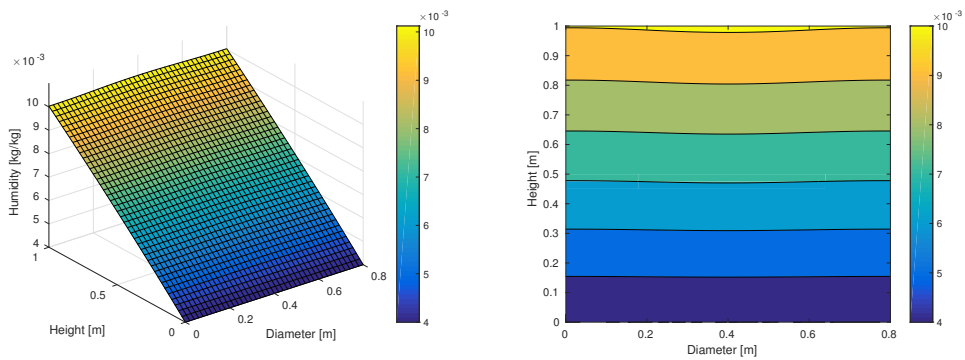


Figure 5.38: Simulation of air humidity at time $t = 250s$.

CHAPTER 5. NUMERICAL RESULTS

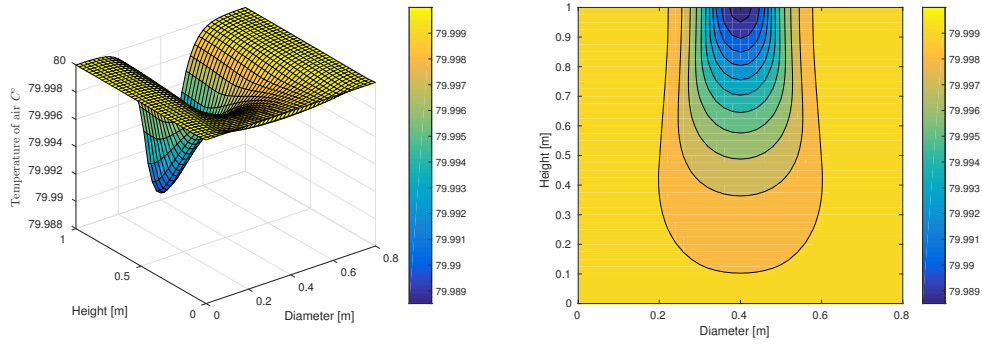


Figure 5.39: Simulation of air temperature at time $t = 0.1s$.

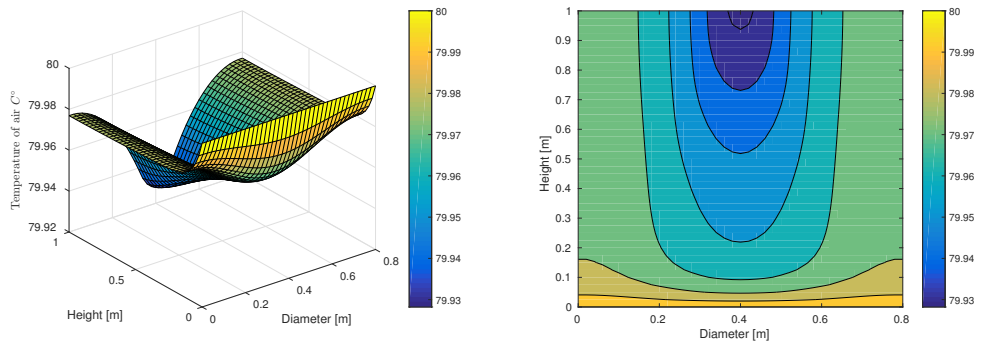


Figure 5.40: Simulation of air temperature at time $t = 1s$.

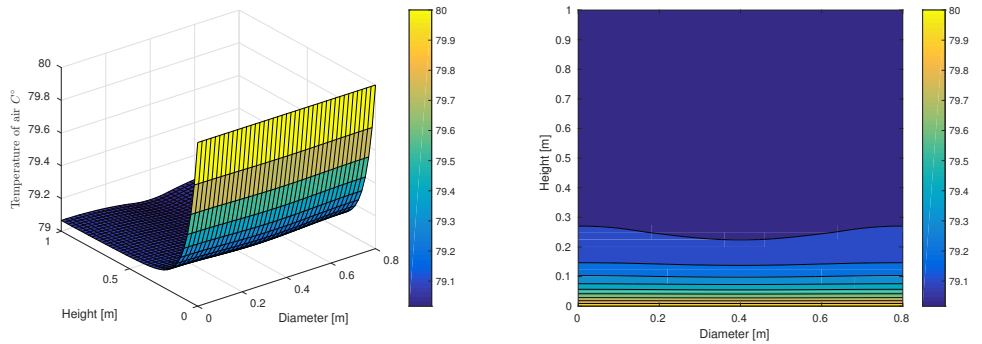


Figure 5.41: Simulation of air temperature at time $t = 10s$.

5.2. NUMERICAL RESULTS IN 2D

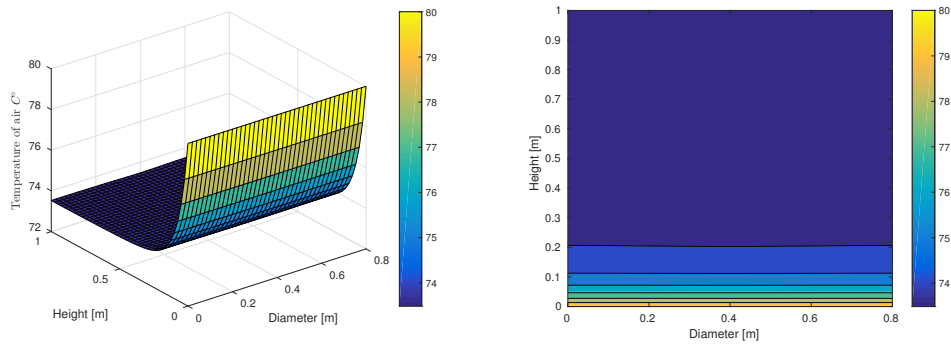


Figure 5.42: Simulation of air temperature at time $t = 50s$.

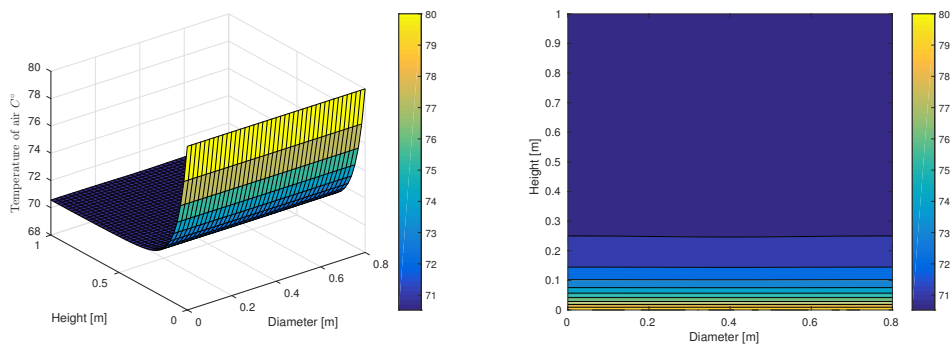


Figure 5.43: Simulation of air temperature at time $t = 100s$.

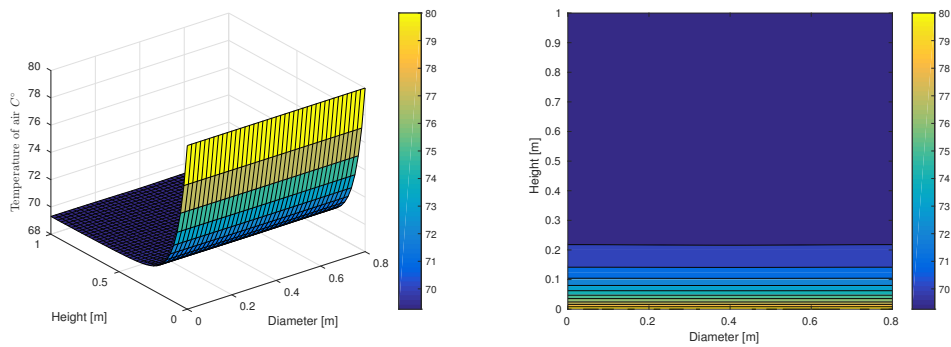


Figure 5.44: Simulation of air temperature at time $t = 250s$.

CHAPTER 5. NUMERICAL RESULTS

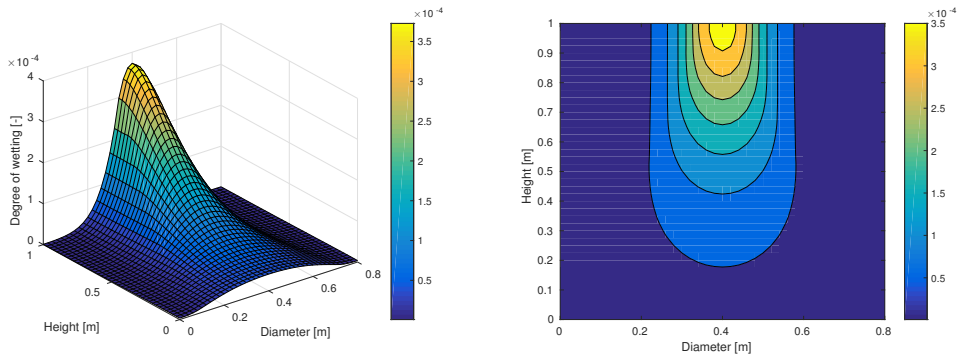


Figure 5.45: Simulation of the degree of wetting at time $t = 0.1s$.

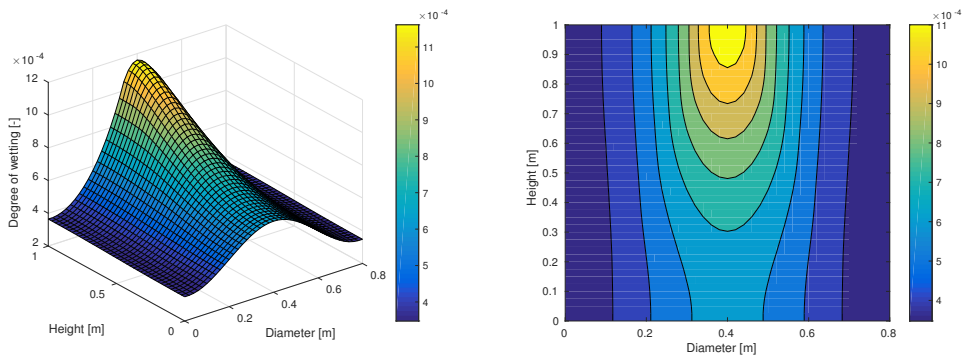


Figure 5.46: Simulation of the degree of wetting at time $t = 1s$.

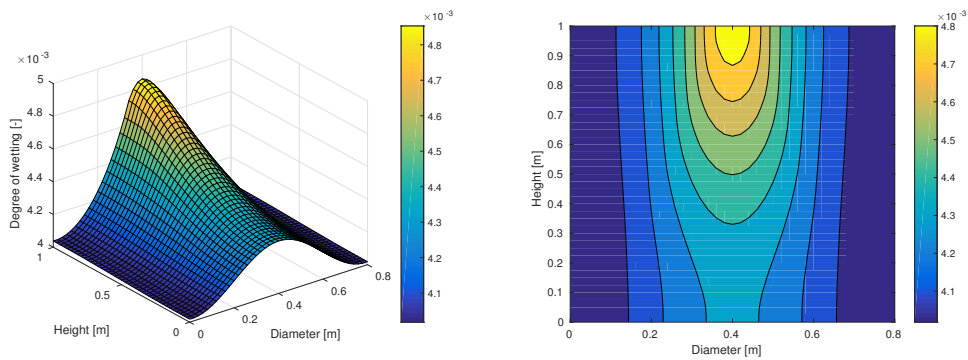


Figure 5.47: Simulation of the degree of wetting at time $t = 10s$.

5.2. NUMERICAL RESULTS IN 2D

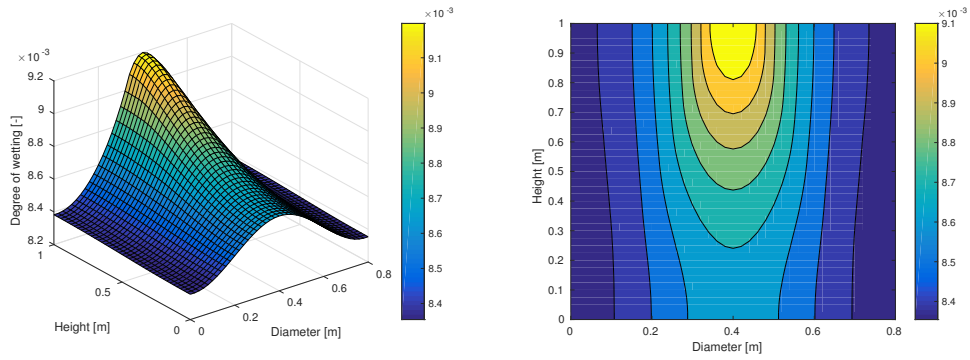


Figure 5.48: Simulation of the degree of wetting at time $t = 50s$.

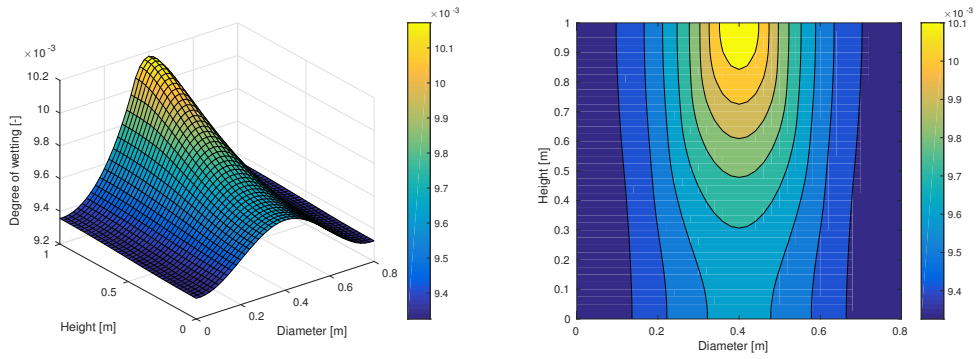


Figure 5.49: Simulation of the degree of wetting at time $t = 100s$.

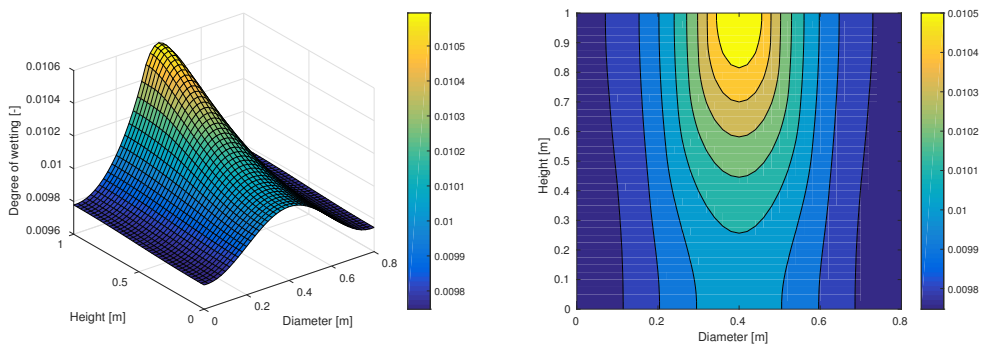


Figure 5.50: Simulation of the degree of wetting at time $t = 250s$.

CHAPTER 5. NUMERICAL RESULTS

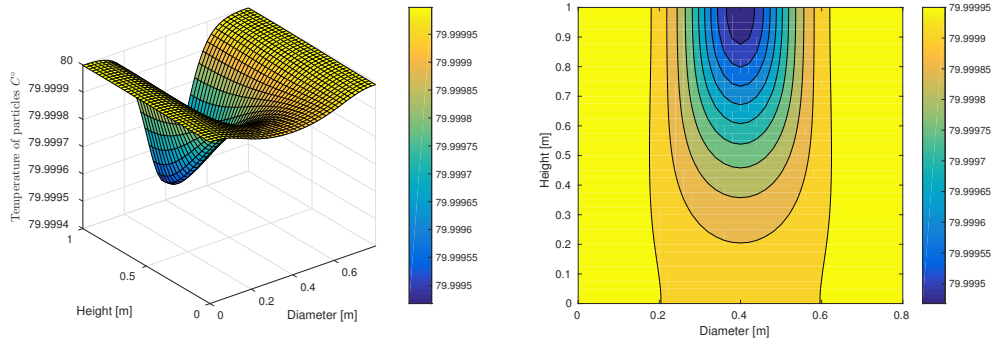


Figure 5.51: Simulation of the particle temperature at time $t = 0.1s$.

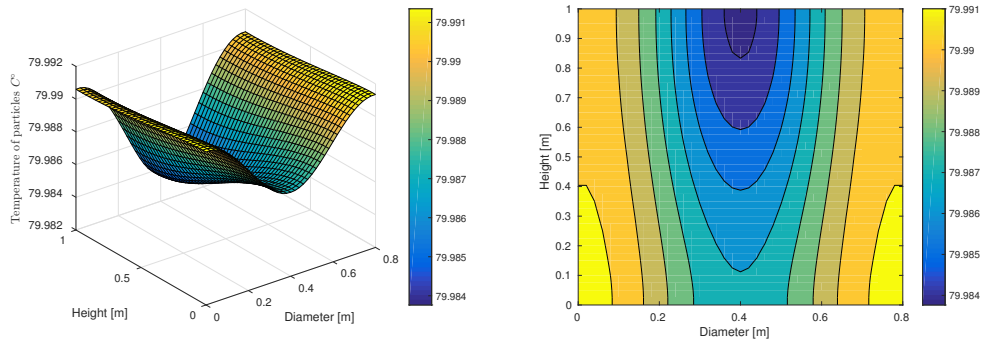


Figure 5.52: Simulation of the particle temperature at time $t = 1s$.

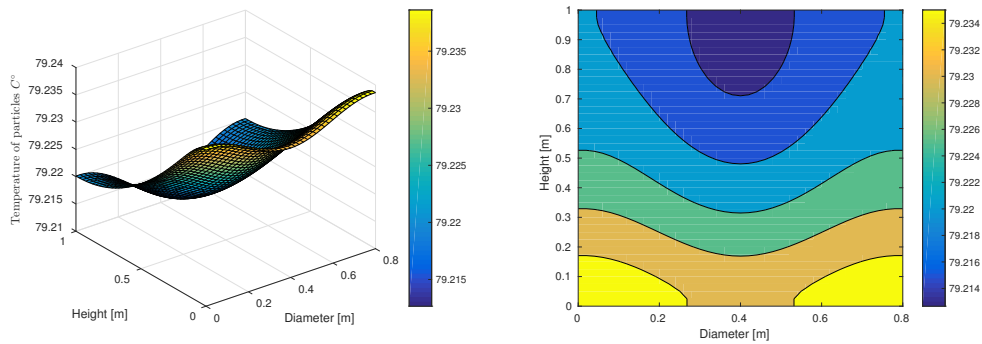


Figure 5.53: Simulation of the particle temperature at time $t = 10s$.

5.2. NUMERICAL RESULTS IN 2D

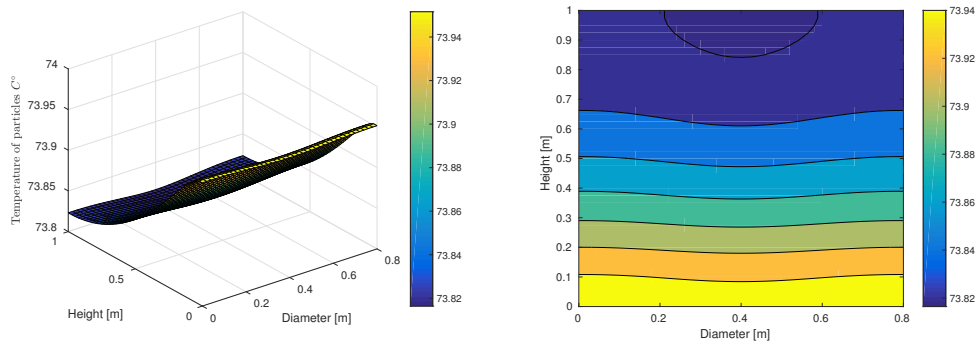


Figure 5.54: Simulation of the particle temperature at time $t = 50s$.

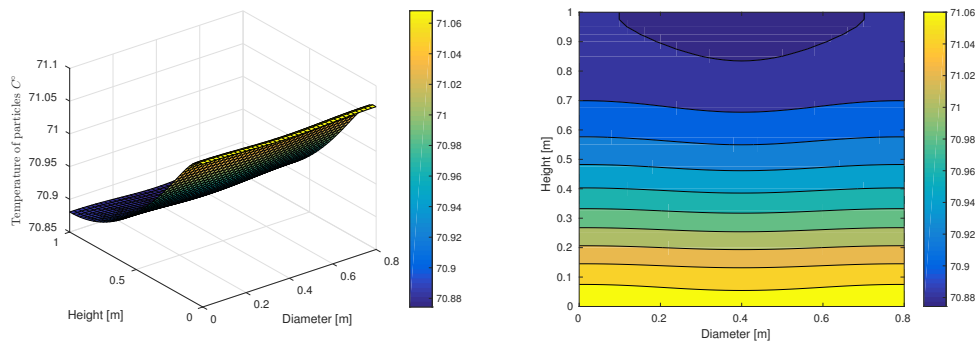


Figure 5.55: Simulation of the particle temperature at time $t = 100s$.

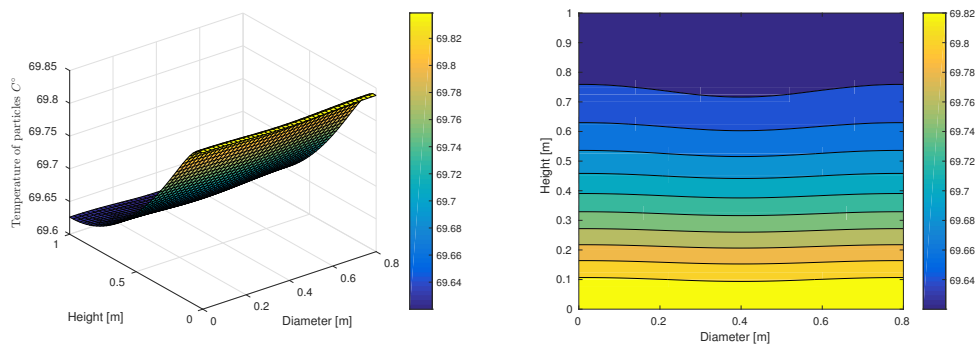


Figure 5.56: Simulation of the particle temperature at time $t = 250s$.

CHAPTER 5. NUMERICAL RESULTS

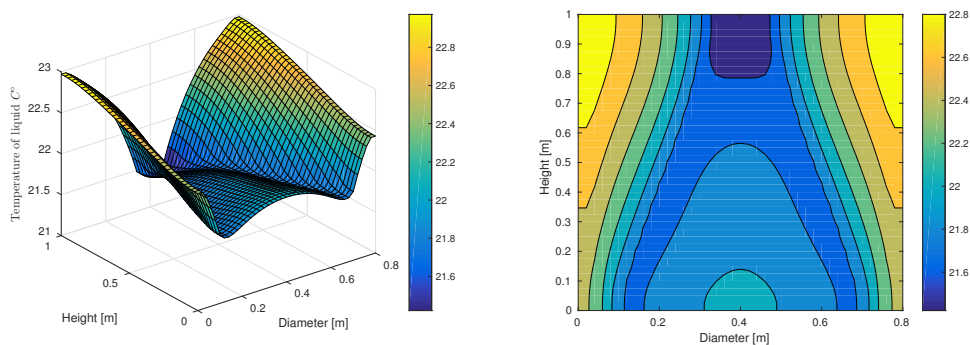


Figure 5.57: Simulation of the liquid film temperature at time $t = 0.1s$.

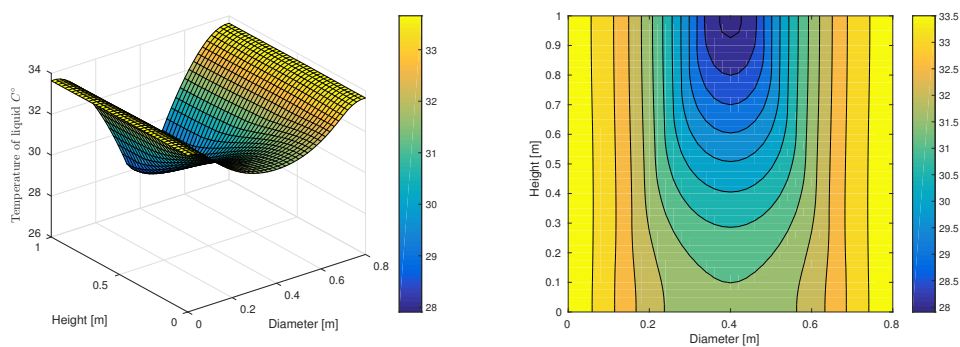


Figure 5.58: Simulation of the liquid film temperature at time $t = 1s$.

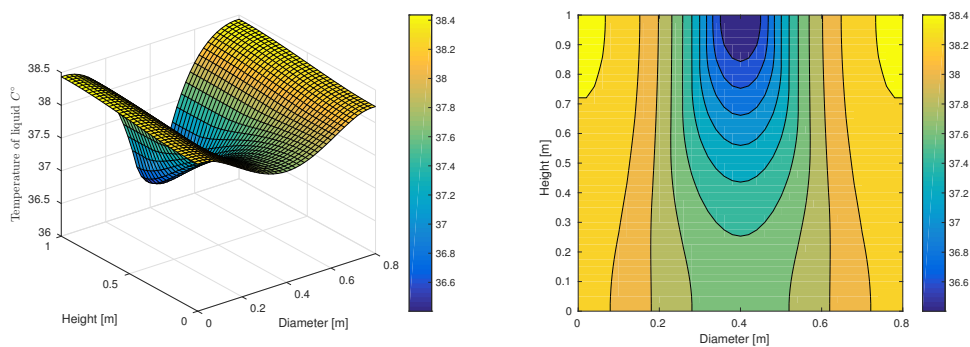


Figure 5.59: Simulation of the liquid film temperature at time $t = 10s$.

5.2. NUMERICAL RESULTS IN 2D

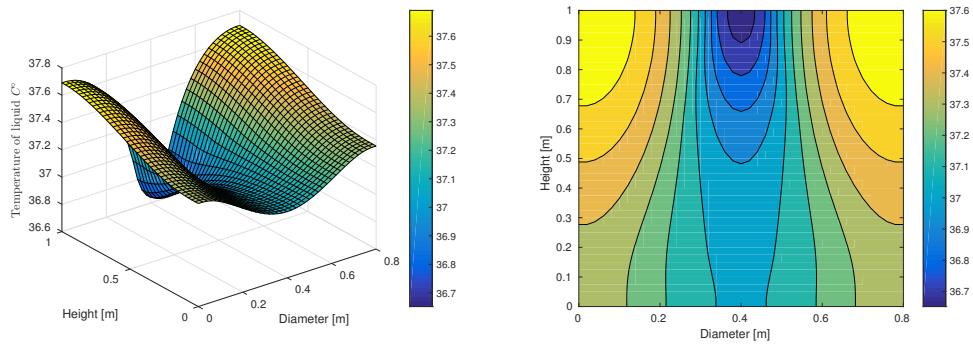


Figure 5.60: Simulation of the liquid film temperature at time $t = 50s$.

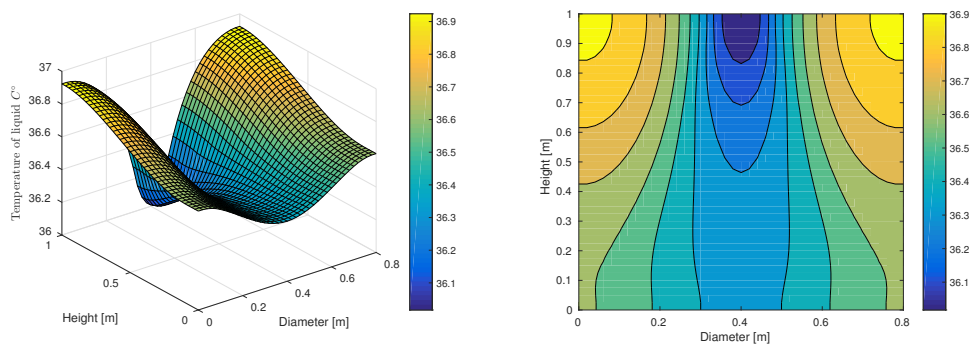


Figure 5.61: Simulation of the liquid film temperature at time $t = 100s$.

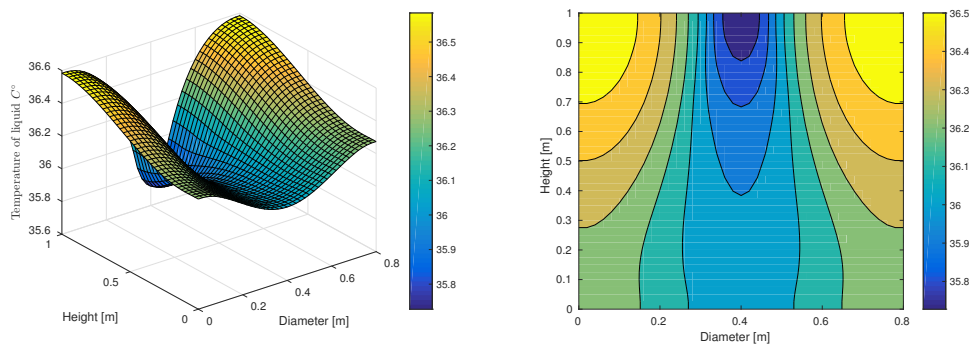


Figure 5.62: Simulation of the liquid film temperature at time $t = 250s$.

Chapter 6

Summary

In this thesis, a new study of the mass and heat transfer in a fluidized bed has been studied. An existing model was extended by adding two new partial differential equations related to the humidity and the temperature of the air. Also it was modified after taking the evaporation of the atomized droplets in region 1 into consideration. The derivation of the two models can be found in Chapter 2. The liquid spray model was also modified to match the new study. The arising semilinear partial differential equations were solved using the discontinuous Galerkin method. The numerical differentiation formulas (NDF) were applied to solve the resulting ordinary differential equations. Both methods were explained in Chapter 4. The numerical simulations for these equations were presented in Chapter 5, where the influence of the air mass flow rate, the temperature of the inlet air, the thickness of the liquid film, the liquid mass flow rate as well as the ratio of the heat transfer coefficient were presented in the uniform distribution for the 1D case. Also the two dimensional distribution of the humidity of air, the temperature of air, the degree of wetting, the temperature of the particles as well as the temperature of the liquid film in the non-uniform distribution of the liquid spray was presented.

To complete the work, another process called the spray drying process has been studied in Chapter 3. In this process we studied the change of the temperature of the droplet, the shrinkage of the droplet radius, the concentration of the droplet as well as the aggregation of the nano-particles inside a single droplet. This model can be also modified. In this model we assumed a constant thickness of the film on the particles surface while it is possible to consider different thicknesses according to how the particles are close to the nozzle.

Appendix A

Notations

A	surface area, m^2
A^*	specific surface area, m^2/m^3
C_p	specific heat capacity at constant pressure, $J/(kg\ K)$
d	diameter, m
D	dispersion matrix, m^2/s
dV	incremental volume, m^3
f	heat transfer ratio, (dimensionless)
F	liquid film thickness, m
g	gravitational acceleration, m/s^2
h	enthalpy, J
\dot{h}	enthalpy of the evaporation flow, J/s
H	height, m
h_{ad}	adhesion probability, (dimensionless)
Δh_v	specific heat of evaporation of water, J/kg
$\Delta h_{v,0}$	specific heat of evaporation of water at 0°C , J/kg
M	molecular mass, kg/mol
m	mass, kg
\dot{m}	mass flow, kg/s
\dot{M}	mass flow rate, kg/s
n	number density, $1/m^3$
P	pressure, Pa
q	area based heat, J/m^2
\dot{q}	area based heat flow, $J/(m^2\ s)$
R_A	specific gas constant for dry air, $J/(mol\ K)$
R	radius, m
S	length, m
t	time, s
T	temperature, K
V	velocity, m/s
X	mass fraction, (dimensionless)

APPENDIX A. NOTATIONS

Y humidity, (dimensionless)

Greek symbols

α heat transfer coefficient, $W/(m^2 K)$
 β mass transfer coefficient, m/s
 γ diffusivity, m^2/s
 δ_s contact angle, (dimensionless)
 ε porosity, m^3/m^3
 η dynamic viscosity, $kg/(m s)$
 η_{im} impingement efficiency, (dimensionless)
 θ temperature, K
 κ concentration, kg/m^3
 κ_0 initial concentration, kg/m^3
 $\dot{\kappa}$ concentration flow, $kg/(m^3 s)$
 λ thermal conductivity, $W/(m K)$
 ν kinematic viscosity, m^2/s
 ξ drag coefficient, (dimensionless)
 ρ density, kg/m^3
 ϕ degree of wetting, (dimensionless)
 ϕ_{dep} deposition efficiency, (dimensionless)
 ω local shrinkage rate of control volume, m/s

Subscripts

A air
ac acceleration
ad adhesion
agg aggregation
b binder
dep deposition
dr droplet
dr drag
eff effective
ev evaporation
gr gravity
in inflow
im impingement
L liquid
li lifting
nozz nozzle
out outflow
P particle

S	solid
sat	saturation
sd	single droplet
st	steam
tot	total
v	vapor

Dimensionless numbers

A.0.1 Dimensionless numbers

Archimedes number

$$Ar = \frac{d_p^3 g (\rho_p - \rho_A)}{\rho_A \nu_A^2}.$$

Nusselt number

$$Nu = \frac{\alpha L}{\lambda_A}.$$

Prandtl number

$$Pr = \frac{\eta C_p}{\lambda}.$$

Reynolds number

$$Re = \frac{d_p V_A}{\nu_A}.$$

Schmidt number

$$Sc = \frac{\nu_A}{D_V}.$$

Sherwood number

$$Sh = \frac{\beta d_p}{D_V}.$$

Spalding number

$$B = \frac{C_{pv}(T_A - T_d)}{\Delta h_V}.$$

Stokes number

$$St = \frac{\rho_{dr} V_{gas} d_{dr}^2}{18 \eta_A d_p}.$$

Biot number

$$Bi = \frac{\alpha L_c}{\lambda}.$$

Appendix B

Parameters for Heat and Mass Transfer in Fluidized Beds

B.0.2 Constants

Avogadro constant

$$N_A = 6.022140857 \cdot 10^{23} \text{ mol}^{-1}.$$

Boltzmann constant

$$\kappa_B = \frac{R}{N_A} = 1.38064852 \cdot 10^{23} \text{ J/K}.$$

Universal Gas constant

$$R = 8.3144598 \text{ J/(mol K)}.$$

Gravitational constant

$$g = 9.81 \text{ m/s}^2.$$

Molecular mass of air

$$M_A = 0.02896 \text{ kg/mol}.$$

Molecular mass of vapor

$$M_V = 0.01802 \text{ kg/mol}.$$

specific gas constant

$$R_A = 287.22 \text{ J/(kg K)}.$$

Specific heat of evaporation of water at 0 °C

$$\Delta h_{v,0} = 2500000 \text{ J/kg}.$$

Standard pressure

$$P = 101325 \text{ Pa}.$$

B.0.3 Values of parameters

The following parameters are taken from the Ph.D theses of Henneberg [36] and Heinrich [32].

- **Dry air**

Density of air

$$\rho_A = \frac{P}{R_A(\theta_A + 273.15)}.$$

Unit: $[kg/m^3]$

Specific heat capacity at constant pressure

$$\begin{aligned} C_{pA} &= A + B \cdot \theta_A + C \cdot \theta_A^2 + D \cdot \theta_A^3. \\ A &= +1006.256 \\ B &= +2.2120536 \cdot 10^{-2} \\ C &= +4.180195 \cdot 10^{-4} \\ D &= -1.521916 \cdot 10^{-7} \end{aligned} \tag{B.1}$$

Unit: $[J/(kg K)]$

Thermal conductivity

$$\begin{aligned} \lambda_A &= A + B \cdot \theta_A + C \cdot \theta_A^2 + D \cdot \theta_A^3. \\ A &= +24.5211 \cdot 10^{-3} \\ B &= +7.501414 \cdot 10^{-5} \\ C &= -2.593344 \cdot 10^{-8} \\ D &= +5.292884 \cdot 10^{-11} \end{aligned} \tag{B.2}$$

Unit: $[W/(m K)]$

Dynamic viscosity

$$\begin{aligned} \eta_A &= A + B \cdot \theta_A + C \cdot \theta_A^2 + D \cdot \theta_A^3. \\ A &= +1.705568 \cdot 10^{-5} \\ B &= +4.511012 \cdot 10^{-8} \\ C &= -8.766234 \cdot 10^{-12} \\ D &= -3.382035 \cdot 10^{-15} \end{aligned} \tag{B.3}$$

Unit: $[kg/(m s)]$

APPENDIX B. PARAMETERS FOR HEAT AND MASS TRANSFER IN FLUIDIZED BEDS

Kinematic viscosity

$$\nu_A = \frac{\eta_A}{\rho_A}.$$

Unit: $[m^2/(s)]$

Prandtl number

$$Pr_A = \frac{\eta_A C_{pA}}{\lambda_A}.$$

Unit: $[-]$

• **Water**

Density of water

$$\begin{aligned}\rho_L &= A + B \cdot \theta_L + C \cdot \theta_L^2. \\ A &= +1006 \\ B &= +0.26 \\ C &= -0.0022\end{aligned}\tag{B.4}$$

Unit: $[kg/m^3]$

Specific heat capacity at constant pressure

$$\begin{aligned}C_{pL} &= A + B \cdot \theta_L + C \cdot \theta_L^2 + D \cdot \theta_L^3. \\ A &= +4174.785 \\ B &= +1.785308 \cdot 10^{-2} \\ C &= -5.097403 \cdot 10^{-4} \\ D &= +4.216721 \cdot 10^{-5}\end{aligned}\tag{B.5}$$

Unit: $[J/(kg K)]$

Specific heat of evaporation of water

$$\begin{aligned}\Delta h_v &= A + B \cdot \theta_L + C \cdot \theta_L^2. \\ A &= +2500000 \\ B &= -2042.5 \\ C &= -3.8130\end{aligned}\tag{B.6}$$

Unit: $[J/kg]$

Saturation vapor pressure

$$\begin{aligned}
P_{sat}(\theta_L) &= \exp\left(A + \frac{B}{C + \theta_L}\right). \\
A &= +23.462 \\
B &= -3978.205 \\
C &= +233.349
\end{aligned}
\tag{B.7}$$

Unit: [Pa]

• Vapor

Adiabatic saturation humidity

$$Y_{sat}(\theta_L) = \frac{M_V}{M_A} \frac{P_{sat}}{P - P_{sat}}.$$

Unit: [kg/kg]

Specific heat of evaporation of vapor

$$\begin{aligned}
C_{pV} &= A + B \cdot \theta_L + C \cdot \theta_L^2 + D \cdot \theta_L^3. \\
A &= +1862 \\
B &= +2.858485 \cdot 10^{-1} \\
C &= +6.148483 \cdot 10^{-4} \\
D &= -2.060606 \cdot 10^{-7}
\end{aligned}
\tag{B.8}$$

Unit: [J/(kg K)]

Diffusion coefficient of water in air

$$D_V = \frac{2.252}{P} \left(\frac{\theta_A + 273.15}{273.15} \right)^{1.81}.$$

Unit: [m²/s]

B.0.4 Parameters calculations

Cross section surface of the Fluidized bed

$$A_{App} = \pi \left(\frac{d_{App}}{2} \right)^2.$$

APPENDIX B. PARAMETERS FOR HEAT AND MASS TRANSFER IN FLUIDIZED BEDS

volume of the Fluidized bed

$$V_{fb} = A_{App}H_{tot}.$$

Porosity

$$\varepsilon = \frac{V_{void}}{V_{fb}} = \frac{V_{void}}{V_{void} + V_P} = \left(\frac{18Re + 0.36Re^2}{Ar} \right)^{0.21}.$$

Number of particles

$$N_P = \frac{6(1 - \varepsilon)V_{fb}}{\pi d_p^3}.$$

Surface area of all particles

$$A_p = \frac{6(1 - \varepsilon)V_{fb}}{d_p}.$$

Schmidt number

$$Sc = \frac{\nu_A}{D_V}.$$

Sherwood number

$$Sh = 2 + 0.72\sqrt{Re}\sqrt[3]{Sc}.$$

Mass transfer coefficient

$$\beta = \frac{D_V Sh}{d_p}.$$

Nusselt number for laminar flow

$$Nu_{lam} = 0.664Pr^{1/3}Re_\varepsilon^{1/2},$$

where

$$Re_\varepsilon = \frac{Re}{\varepsilon}.$$

Nusselt number for turbulent flow

$$Nu_{turb} = 0.037 \frac{Pr Re_\varepsilon^{0.8}}{1 + 2.443 Re_\varepsilon^{-0.1} (Pr^{\frac{2}{3}} - 1)}.$$

Nusselt number

$$Nu = 2 + \sqrt{Nu_{lam}^2 + Nu_{turb}^2} (1 + 1.5(1 - \varepsilon)).$$

Lewis number

$$Le = \frac{\lambda_A}{C_p \rho_A D_V}.$$

For air-water mixture $Le \simeq 1 \Rightarrow Sh \simeq Nu$.

Heat transfer coefficient

$$\alpha = \frac{Nu \lambda_A}{d_p}.$$

B.1 Parameters

Parameters values in 2D for fluidized beds

Fluidized bed Parameters			
total height	H_{tot}	1.20	m
height of region 2	H_2	1	m
width	d_{App}	0.80	m
Bed material (beads)			
density	ρ_P	2471	kg/m^3
total mass	m_P	20	kg
diameter	d_P	1.16	mm
specific heat capacity	C_P	750	$J/kg K$
Liquid spraying			
mass flow rate	\dot{M}_L	10	kg/h
liquid inlet temperature	θ_{in}	20	$^{\circ}C$
Fluidization gas			
mass flow rate	\dot{m}_A	0.4	kg/s
inlet humidity	Y_{in}	0.004	kg/kg
inlet temperature	$\theta_{A,in}$	80	$^{\circ}C$
Other parameters			
heat transfer ratio	f	1	–
liquid film thickness	F	100	μm
dispersion in z -axis	D_z	0.055	m^2/s
dispersion in y -axis	D_y	0.55	m^2/s
Initial conditions for the computation			
humidity of air	Y_0	0.004	kg/kg
temperature of air	$\theta_{A,0}$	80	$^{\circ}C$
degree of wetting	ϕ_0	$1e - 8$	–
temperature of particles	θ_P	80	$^{\circ}C$
temperature of liquid film	θ_L	80	$^{\circ}C$

Parameters values for spray drying

mass fraction of solids	$X_{s,0}$	0.30	–
velocity of air	V_a	1.4	m/s
total mass of the droplet	$m_{tot,0}$	$4.3e - 6$	kg
specific heat capacity of the solids	$C_{p,s}$	750	$J/kg K$
humidity of air	Y_a	0.004	kg/kg
temperature of the inlet gas	θ_a	178	$^{\circ}C$
Initial conditions for the computation			
radius of the droplet	R_0	$1e - 3$	m
temperature of droplet	$\theta_{d,0}$	19	$^{\circ}C$

Bibliography

- [1] J. Beránek, K. Rose, and G. Winterstein. *Grundlagen der Wirbelschicht-Technik*. Buchreihe Verfahrenstechnik. Krausskopf, 1975.
- [2] W.H. Beyer. *CRC Standard Mathematical Tables: 28th Ed.* CRC Press, 1987.
- [3] R. Biswas, K.D. Devine, and J.E. Flaherty. Parallel, adaptive finite element methods for conservation laws. *Applied Numerical Mathematics*, 14(1-3):255–283, 1994.
- [4] J. Blumschein. Wärme- und Stoffübergang in der flüssigkeitsbedüsten Wirbelschicht. Diploma thesis, Otto von Guericke Universität Magdeburg, 2002.
- [5] G. Brenn. Concentration fields in evaporating droplets. *International Journal of Heat and Mass Transfer*, 48(2):395 – 402, 2005.
- [6] A. Bück, M. Peglow, M. Naumann, and E. Tsotsas. Population balance model for drying of droplets containing aggregating nanoparticles. *AIChE Journal*, 58(11):3318–3328, 2012.
- [7] A. Bück and E. Tsotsas. Agglomeration, in: Encyclopedia of food and health (Edited by: B. Caballero, P. Finglas, F. Toldrá). *Academic Press, Oxford*, 1:73 – 81, 2016.
- [8] J.C. Butcher. *Numerical Methods for Ordinary Differential Equations*. Wiley, 2008.
- [9] R. Butt. *Introduction to Numerical Analysis Using MATLAB®*. Infinity Science Series. Jones & Bartlett Learning, 2009.
- [10] E. Alberdi Celaya, J. J. Anza Aguirrezabala, and P. Chatzipantelidis. Implementation of an Adaptive BDF2 Formula and Comparison with the MATLAB Ode15s. *Procedia Computer Science*, 29(0):1014 – 1026, 2014. 2014 International Conference on Computational Science.
- [11] X.X. Cheng and R. Turton. The prediction of variability occurring in fluidized bed coating equipment. II. The role of nonuniform particle coverage as particles pass through the spray zone. *Pharmaceutical Development and Technology*, 5(3):323–332, 2000.
- [12] B. Cockburn, G.E. Karniadakis, and C.W. Shu. *Discontinuous Galerkin Methods: Theory, Computation and Applications*. Lecture Notes in Computational Science and Engineering. Springer Berlin Heidelberg, 2011.
- [13] B. Cockburn, A. Quarteroni, and Centro internazionale matematico estivo. *Advanced numerical approximation of nonlinear hyperbolic equations: lectures given at the 2nd session of the Centro Internazionale Matematico Estivo (C.I.M.E.) held in Cetraro, Italy, June 23-28, 1997*. Lecture notes in mathematics. Springer, 1998.

BIBLIOGRAPHY

- [14] B. Cockburn and C.-W. Shu. TVB Runge-Kutta Local Projection Discontinuous Galerkin Finite Element Method for Conservation Laws II: General Framework. *Mathematics of Computation*, 52:411–435, 1989.
- [15] B. Cockburn and C.-W. Shu. Runge-Kutta Discontinuous Galerkin methods for convection-dominated problems. *Journal of Scientific Computing*, 16(3):173–261, 2001.
- [16] N. Dalmaz, H. Onder Ozbelge, A. Nedim Eraslan, and Y. Uludag. Heat and mass transfer mechanisms in drying of a suspension droplet: A new computational model. *Drying Technology*, 25(2):391–400, 2007.
- [17] P. J. Davis and I. Polonsky. *Numerical Interpolation, Differentiation, and Integration, The Handbook of Mathematical Functions, with Formulas, Graphs, and Mathematical Tables*, ed. Milton Abramowitz and Irene A. Stegun, 1964. Dover Books on Mathematics. Dover Publications, 2012.
- [18] M. Dervedde, M. Peglow, and E. Tsotsas. Stochastic modeling of fluidized bed granulation: Influence of droplet pre-drying. *Chemical Engineering & Technology*, 34(7):1177–1184, 2011.
- [19] D.A. Di Pietro and A. Ern. *Mathematical Aspects of Discontinuous Galerkin Methods*. Mathématiques et Applications. Springer, 2011.
- [20] Dan E. Dorby., Dana M. Settell, John M. Baumann, Rod J. Ray, Lisa J. Graham, and Ron A. Beyerinck. A model-based methodology for spray-drying process development. *Pharmaceutical Innovation*, 4:133–142, 2009.
- [21] J.R. Dormand and P.J. Prince. A family of embedded Runge-Kutta formulae. *Journal of Computational and Applied Mathematics*, 6(1):19 – 26, 1980.
- [22] E.W. Gekeler. *Mathematische Methoden zur Mechanik: Ein Handbuch mit MATLAB®-Experimenten*. Springer-Lehrbuch Masterclass. Springer Berlin Heidelberg, 2010.
- [23] E.H. Georgoulis. Discontinuous Galerkin methods for linear problems: An introduction. volume 3, pages 91–126, 2011.
- [24] E.H. Georgoulis, E. Hall, and P. Houston. Discontinuous Galerkin methods for advection-diffusion-reaction problems on anisotropically refined meshes. *SIAM Journal on Scientific Computing*, 30(1):246–271, 2007.
- [25] N. Gerhard and S. Müller. Adaptive multiresolution discontinuous Galerkin schemes for conservation laws: multi-dimensional case. *Computational and Applied Mathematics*, pages 1–29, 2014.
- [26] V. Gnielinski. Wärme- und Stoffübertragung in Festbetten. *Chemie Ingenieur Technik*, 52(3):228–236, 1980.
- [27] B. Golman. Modeling of the drying kinetics of slurry droplet in spray drying. 11(2):1–7, 2011.
- [28] V.D. Goroshko, R.B. Rozenbaum, and O.M. Todes. Approximate laws of hydraulics of suspended layers and constrained fall. *Izv. Vuz. Neft i Gaz*, (1):125–131, 1958.

-
- [29] H. Groenewold and E. Tsotsas. Predicting apparent sherwood numbers for fluidized beds. *Drying Technology*, 17(7-8):1557–1570, 1999.
- [30] E. Hairer and G. Wanner. *Solving Ordinary Differential Equations II: Stiff and Differential - Algebraic Problems*. Springer Series in Computational Mathematics. Springer Berlin Heidelberg, 2013.
- [31] C.S. Handscomb, M. Kraft, and A.E. Bayly. A new model for the drying of droplets containing suspended solids after shell formation. *Chemical Engineering Science*, 64(2):228 – 246, 2009.
- [32] S. Heinrich. Modellierung des Wärme- und Stoffüberganges sowie der Partikelpopulationen bei der Wirbelschicht-Sprühgranulation. In *Verfahrenstechnisches Forschungsseminar im IVT, Otto-von-Guericke Universität Magdeburg*, 2000.
- [33] S. Heinrich, J. Blumschein, M. Henneberg, M. Ihlow, M. Peglow, and L. Mörl. Study of dynamic multi-dimensional temperature and concentration distributions in liquid-sprayed fluidized beds. *Chemical Engineering Science*, 58(2324):5135 – 5160, 2003.
- [34] S. Heinrich, M. Henneberg, M. Peglow, J. Drechsler, and L. Mörl. Fluidized bed spray granulation: Analysis of heat and mass transfers and dynamic particle populations. *Brazilian Journal of Chemical Engineering*, 22(2):181–194, 2005.
- [35] S. Heinrich and L. Mörl. Fluidized bed spray granulation : A new model for the description of particle wetting and of temperature and concentration distribution. *Chemical Engineering and Processing: Process Intensification*, 38(46):635 – 663, 1999.
- [36] M. Henneberg. *Untersuchung des Flüssigkeitseintrages auf die Temperaturverteilung in Gas/Feststoff-Wirbelschichten*. PhD thesis, Otto-von-Guericke University Magdeburg, 2004.
- [37] J.S. Hesthaven and T. Warburton. *Nodal Discontinuous Galerkin Methods: Algorithms, Analysis, and Applications*. Texts in Applied Mathematics. Springer, 2008.
- [38] J.R. Howard. *Fluidized beds: combustion and applications*. Applied Science Publishers, London, 1983.
- [39] H. Inaba, S. Husain, A. Horibe, and N. Haruki. Heat and mass transfer analysis of fluidized bed grain drying. *Memoirs of the Faculty of Engineering, Okayama University*, 41:52–62, 2007.
- [40] C.T. Kelley. *Iterative Methods for Linear and Nonlinear Equations*. Frontiers in Applied Mathematics. Society for Industrial and Applied Mathematics, 1995.
- [41] M.N. Levy, R.D. Nair, and H.M. Tufo. High-order Galerkin methods for scalable global atmospheric models. *Computers and Geosciences*, 33(8):1022–1035, 2007.
- [42] B.Q. Li. *Discontinuous Finite Elements in Fluid Dynamics and Heat Transfer*. Computational Fluid and Solid Mechanics. Springer London, 2006.

BIBLIOGRAPHY

- [43] K.C. Link. *Wirbelschicht-Sprühgranulation: Untersuchung der Granulatbildung an einer frei schwebenden Einzelpartikel*. Fortschrittberichte VDI / 3: Verfahrenstechnik. VDI-Verlag, 1997.
- [44] K.C. Link and E.-U. Schlünder. Fluidized bed spray granulation investigation of the coating process on a single sphere. *Chemical Engineering and Processing: Process Intensification*, 36(6):443–457, 1997.
- [45] F. Löffler. *Staubabscheiden*. Stuttgart: Thieme Verlag, 1988.
- [46] C. Macdonald. Constructing High-order Runge-Kutta Methods with Embedded Strong-Stability-Preserving Pairs. Master’s thesis, Acadia University, 2001.
- [47] T.-G. Malmström and Y. Zou. *Influence of outlet characteristics on free axial air jets*. Department for Building Services Engineering, KTH, Stockholm, Sweden, 1998.
- [48] M. Mezhericher, A. Levy, and I. Borde. Heat and mass transfer of single droplet/wet particle drying. *Chemical Engineering Science*, 63(1):12 – 23, 2008.
- [49] M. Mezhericher, M. Naumann, M. Peglow, A. Levy, E. Tsotsas, and I. Borde. Continuous species transport and population balance models for first drying stage of nanosuspension droplets. *Chemical Engineering Journal*, 210(0):120 – 135, 2012.
- [50] O. Molerus and K.-E. Wirth. *Heat Transfer in Fluidized Beds*. Chapman & Hall, 1997.
- [51] L. Mörl, S. Heinrich, and M. Peglow. Chapter 2 fluidized bed spray granulation. In M.J. Hounslow A.D. Salman and J.P.K. Seville, editors, *Granulation*, volume 11 of *Handbook of Powder Technology*, pages 21 – 188. Elsevier Science B.V., 2007.
- [52] Ch. Nagaiah. *Adaptive numerical simulation of reaction - diffusion systems*. PhD thesis, Otto-von-Guericke University Magdeburg, 2007.
- [53] Ch. Nagaiah, N. Suresh Kumar, A. Bück, and G. Warnecke. Parallel and high resolution numerical solution of concentration and temperature distributions in fluidized beds. *Computers & Chemical Engineering*, 52.
- [54] Ch. Nagaiah, G. Warnecke, S. Heinrich, and M. Peglow. Numerical simulation of temperature and concentration distributions in fluidized beds with liquid injection. *Chemical Engineering Science*, 62(6):1567 – 1590, 2007.
- [55] S. Nešić and J. Vodnik. Kinetics of droplet evaporation. *Chemical Engineering Science*, 46(2):527 – 537, 1991.
- [56] A.W. Nienow and P.N. Rowe. Particle growth and coating in gas-fluidized beds. *Fluidization*, pages 563–594, 1985.
- [57] Stanley Osher. Riemann solvers, the entropy condition, and difference approximations. *SIAM Journal on Numerical Analysis*, 21(2):pp. 217–235, 1984.
- [58] L. Papula. *Mathematik für Ingenieure und Naturwissenschaftler 2*. Ein Lehr- und Arbeitsbuch für das Grundstudium. Vieweg, 2007.

-
- [59] Kamlesh C. Patel and Xiao Dong Chen. Surface-center temperature differences within milk droplets during convective drying and drying-based Biot number analysis. *AIChE Journal*, 54(12):3273–3290, 2008.
- [60] M. Peglow. *Beitrag zur Modellierung von eigenschaftsverteiltern dispersen Systemen am Beispiel der Wirbelschicht-Sprühagglomeration*. PhD thesis, Otto-von-Guericke University Magdeburg, 2004.
- [61] S. Philipp. *Fluid Dynamics and Mixing of Solids and Gas in the Bottom Zone of Circulating Fluidized Beds*. Shaker Verlag GmbH, Germany, 2000.
- [62] P.J. Prince and J.R. Dormand. High order embedded Runge-Kutta formulae. *Journal of Computational and Applied Mathematics*, 7(1):67 – 75, 1981.
- [63] Doraiswami Ramkrishna. *Population balances: Theory and applications to particulate systems in engineering*. Academic press, 2000.
- [64] W.H. Reed and T.R. Hill. *Triangular mesh methods for the neutron transport equation*. Oct 1973.
- [65] H. Reichardt. *Gesetzmäßigkeiten der freien Turbulenz*. Beil. zu "Forschung auf dem Gebiete des Ingenieurwesens"; Ausg. B, Bd. 13, Mai/Juni 1942. VDI-Verlag, 1951.
- [66] D. Reppmann. *Experimentelle und theoretische Untersuchungen zur Eindüsung von Flüssigkeiten in eine Wirbelschicht*. PhD thesis, Otto-von-Guericke University Magdeburg, 1990.
- [67] F. Rieg, R. Hackenschmidt, and B. Alber-Laukant. *Finite Elemente Analyse für Ingenieure: Grundlagen und praktische Anwendungen mit Z88Aurora*. Carl Hanser Verlag GmbH & Company KG, 2014.
- [68] B. Riviere. *Discontinuous Galerkin Methods for Solving Elliptic and Parabolic Equations: Theory and Implementation*. Frontiers in Applied Mathematics. Society for Industrial and Applied Mathematics (SIAM, 3600 Market Street, Floor 6, Philadelphia, PA 19104), 2008.
- [69] A. Ryuichi, M. Nagase, and R. Vaillancourt. Behind and Beyond the MATLAB ODE Suite. *International Journal of Computer Mathematics*, 40(45):491 – 512, 2000.
- [70] F. Scala. *Fluidized Bed Technologies for Near-Zero Emission Combustion and Gasification*. Woodhead Publishing, 2013.
- [71] E.-U. Schlünder and E. Tsotsas. *Wärmeübertragung in Festbetten, durchmischten Schüttgütern und Wirbelschichten*. Stuttgart: Thieme Verlag, 1988.
- [72] G. Schuch. *Theoretische und experimentelle Untersuchungen zur Auslegung von Nassabscheiden*. Dissertation, Universität Karlsruhe, 1978.
- [73] P. Seydel, J. Blömer, and J. Bertling. Modeling particle formation at spray drying using population balances. *Drying Technology*, 24(2):137–146, 2006.
- [74] L. F. Shampine and M. W. Reichelt. The MATLAB ODE Suite. *SIAM J. Sci. Comput.*, 18(1):1–22, 1997.

BIBLIOGRAPHY

- [75] L.F. Shampine. *Numerical Solution of Ordinary Differential Equations*. Number Bd. 4 in Chapman & Hall mathematics. Taylor & Francis, 1994.
- [76] Chi-Wang Shu. Discontinuous Galerkin methods: general approach and stability, numerical solutions of partial differential equations. In *Advanced Courses in Mathematics CRM Barcelona, Pages*, pages 149–201, 2009.
- [77] Chi-Wang Shu. Discontinuous Galerkin method for time-dependent problems: Survey and recent developments. 157:25–62, 2014.
- [78] S. Sirca and M. Horvat. *Computational Methods for Physicists: Compendium for Students*. Graduate Texts in Physics. Springer Berlin Heidelberg, 2012.
- [79] J. Sloth, S. Kiil, A. Jensen, S. Klint Andersen, K. Jørgensen, He. Schiffter, and G. Lee. Model based analysis of the drying of a single solution droplet in an ultrasonic levitator. *Chemical Engineering Science*, 61(8):2701–2709, 2006.
- [80] P.G. Smith and A.W. Nienow. Particle growth mechanisms in fluidised bed granulation-I. the effect of process variables. *Chemical Engineering Science*, 38(8):1223–1231, 1983.
- [81] J. Smoller. *Shock waves and reaction-diffusion equations*. Grundlehren der mathematischen Wissenschaften. Springer-Verlag, 1983.
- [82] P. Solín. *Partial Differential Equations and the Finite Element Method*. Pure and Applied Mathematics: A Wiley Series of Texts, Monographs and Tracts. Wiley, 2005.
- [83] A. TenEyck. *Discontinuous Galerkin Methods for Approximating the Solutions to Problems in Nonlinear Elasticity*. Stanford University, 2008.
- [84] M. Trojosky. *Stoff- und Wärmetransportes in flüssigkeitsbedüsten Gas / Feststoff-Wirbelschichten*. PhD thesis, Otto-von-Guericke University Magdeburg, 1990.
- [85] E. Truckenbrodt. *Fluidmechanik: Elementare Strömungsvorgänge dichte veränderlicher Fluide sowie Potential- und Grenzschichtströmungen*. Fluidmechanik. Springer, 1980.
- [86] E. Tsotsas and A.S. Mujumdar. *Modern Drying Technology*. Modern Drying Technology. Wiley, 2014.
- [87] H. Uhlemann and L. Mörl. *Wirbelschicht-Sprühgranulation*. Springer Berlin Heidelberg, 2000.
- [88] W. P. M. van Swaaij and N. H. Afgan. *Heat And Mass Transfer In Fixed And Fluidized Beds*. Hemisphere, 1986.
- [89] F. Winkler. Verfahren zum Herstellen von Wassergas, December 28 1926. DE Patent 438,843.
- [90] S. Winter. *Discontinuous Galerkin Methods*. Bod Third Party Titles, 2008.
- [91] P. Wnukowski and F. Setterwall. The coating of particles in a fluidized bed (residence time distribution in a system of two coupled perfect mixers). *Chemical Engineering Science*, 44(3):493–505, 1989.

BIBLIOGRAPHY

- [92] Yan Xu and Chi-Wang Shu. Error estimates of the semi-discrete local discontinuous Galerkin method for nonlinear convection-diffusion and KdV equations. *Computer Methods in Applied Mechanics and Engineering*, 196(37-40):3805–3822, August 2007.
- [93] D. Zill. *A First Course in Differential Equations*. Cengage Learning, 2008.
- [94] Y. Zou. *Air jets in ventilation applications*. Bulletin no. 55, Royal Institute of Technology, ISSN 0284 - 141X., 2001.

Curriculum Vitae

Personal Information

Name	Yaser Ahmad Alkurdi
Date of birth	25.10.1981
Nationality	Palestinian
Place of birth	Damascus, Syria
Status	Married, two Children
Current job	Assistant Lecturer, Department of Mathematics Faculty of Science, Albaath University
E-mail	yaser.alkurdi@st.ovgu.de yaserkurdi81@yahoo.com.

Education

1999 - 2003	Bachelor in Mathematics (Very good), Department of Mathematics, Faculty of Science, Damascus University, Syria.
2003 - 2004	Diplom in Mathematics (Pure Algebra) (Very good), Department of Mathematics, Faculty of Science, Damascus University, Syria.
2005 - 2007	M.Sc. in Mathematics, Department of Mathematics, Faculty of Science, Damascus University, Syria.
2011 - 2016	PhD student, Institute for Analysis and Numerics, Faculty of Mathematics, Otto-von-Guericke University, Magdeburg, Germany.

Academic Honors

- Scholarship from the University of Albaath (Syria).

Work Experience

2003-2004 Lecturer. Faculty of Education, Damascus University

2005-2007 Teacher Instructor. Department of Mathematics,
Faculty of Science. Albaath University, Syria.

References

- Prof. Dr. Gerald Warnecke Institute für Analysis und Numerik (IAN),
Fakultät für Mathematik (FMA) ,
Otto-von-Guericke Universität Magdeburg,
Germany.
- Jun.-Prof. Dr.-Ing. Andreas Bück Institut für Verfahrenstechnik (IVT),
Fakultät für Verfahrens- und Systemtechnik (FVST)
Otto-von-Guericke Universität Magdeburg,
Germany.
- Prof. Dr. Muntajab Alhasan Department of Mathematics,
Faculty of Science, Albaath University,
Syria.